AMERICAN UNIVERSITY OF BEIRUT

DYE SENSITIZED SOLAR CELLS: DYES AND ANCHORING GROUPS

by
HAMSA MOUIN HILAL

A thesis
submitted in partial fulfillment of the requirements
for the degree of Master of Science
to the Department of Chemistry
of the Faculty of Arts and Sciences
at the American University of Beirut

Beirut, Lebanon
April 2018

AMERICAN UNIVERSITY OF BEIRUT

DYE SENSITIZED SOLAR CELLS: DYES AND
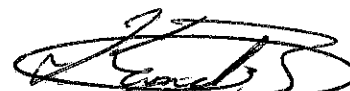ANCHORING GROUPS

by
HAMSA MOUIN HILAL

Approved by:

_____   _____
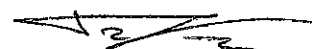Dr. Tarek Ghaddar, Professor   Advisor
Department of Chemistry

_____
Dr. Kamal Bouhadir, Professor   Member of Committee
Department of Chemistry

_____
Dr. Pierre Karam, Associate Professor   Member of Committee
Department of Chemistry

Date of thesis defense: April 30, 2018

AMERICAN UNIVERSITY OF BEIRUT

THESIS, DISSERTATION, PROJECT RELEASE FORM

Student Name:
_____Hilal_____Hamsa_____Mouin_____

Last   First   Middle

☑ Master's Thesis   ○ Master's Project   ○ Doctoral Dissertation

☐   I authorize the American University of Beirut to: (a) reproduce hard or electronic copies of my thesis, dissertation, or project; (b) include such copies in the archives and digital repositories of the University; and (c) make freely available such copies to third parties for research or educational purposes.

☑   I authorize the American University of Beirut, to: (a) reproduce hard or electronic copies of it; (b) include such copies in the archives and digital repositories of the University; and (c) make freely available such copies to third parties for research or educational purposes after:

One ---- year from the date of submission of my thesis, dissertation, or project.

Two ---- years from the date of submission of my thesis, dissertation, or project.

Three ☑ years from the date of submission of my thesis, dissertation, or project.

_____10-05-2018_____

Signature   Date

ACKNOWLEDGMENTS

First and foremost, I would like to offer my sincere gratitude to my advisor, Dr. Tarek Ghaddar, who has guided and supported me with patience and knowledge, not only throughout this thesis, but throughout all my years at AUB. I attribute this level of my master's degree to his encouragement and efforts.

Second, I would like to thank my committee members, Dr. Pierre Karam and Dr. Kamal Bouhadir, for proofreading my thesis and providing valuable comments.

This work was achieved by using the facilities of the Central Research Science Laboratory (CRSL) at AUB. I am thankful to all its friendly staff that helped me throughout my research work.

Next, I would like to thank all my friends at AUB who made this journey a memorable one. I consider myself grateful to have met them and proud to have them as friends. Special thanks go to my roommate and best friend, Rita Douaihy, for all her support, care, and the great memories she has left for me.

To my wonderful parents and adorable sisters Hoda, Haifa, and Hana, thank you for encouraging me in all of my pursuits and inspiring me to follow my dreams. This thesis, and all that I have achieved, wouldn't have been possible without your continuous and unparalleled love.

Last but not least, I am particularly indebted to my fiancé, Raja, whose love is the greatest gift of my life and whose commitment, support, and patience are true models for all. Thank you for inspiring me to grow and succeed.

AN ABSTRACT OF THE THESIS OF

<u>Hamsa Mouin Hilal</u>   for   <u>Master of Science</u>
                                        <u>Major:</u> Chemistry

Title: <u>Dye Sensitized Solar Cells: Dyes and Anchoring Groups</u>

Dye-sensitized solar cells (DSSCs) have attracted much attention due to their relatively low cost, acceptable conversion efficiency and ease of fabrication. Several attempts were made in order to increase the light-harvesting efficiency of solar cells mainly the engineering of panchromatic dyes (sensitizers). One of the main functional moieties in a sensitizer is the anchoring group; the group that functions as the adsorption site of the dye to the semi-conductor. In the chemical literature many examples of anchoring groups have been proposed, ranging from carboxylic and phosphonic acids to pyridyl *N*-oxide, pyridine, and azoles. In an attempt to investigate the effect of different anchoring groups on the performance of DSSCs, we present the synthesis of two different dyes T181 and T182 with pyridine and pyridine oxide anchoring groups, respectively. Moreover, the pyridine-based dye T181, which binds to the Lewis-acid sites of TiO_2 was co-sensitized with commercial dyes YD2 and DB having carboxylic acid anchoring groups, which bind to the Brønsted-acid sites of TiO_2 in order to increase the efficiencies of DSSCs by enhancing the light harvesting efficiency and reducing unwanted recombination reactions. An increase in the total cell efficiency was seen for the T181-DB and T181-YD2 co-sensitized cells in two different iodine-based and cobalt-based electrolytes. The difference in enhancement between the T181-DB and T181-YD2 DSSCs was due to different total dye loading in the co-sensitized films. In the T181-DB cell the amount of adsorbed T181 and DB was equal to the sum of the dyes' loadings found in the non-co-sensitized films, unlike the T181-YD2 one where less of T181 was adsorbed due to non-complementary sizes of the two dyes. In the cobalt-based electrolyte system, more enhanced photocurrent and photovoltage of the two co-sensitized cells were seen compared to the iodine-based electrolyte system because of the effect of the extended linker fragment in T181, which is more effective with the cobalt electrolyte in comparison to the iodine electrolyte. The remarkable increases in photocurrent and photovoltage were mainly attributed to the increase in dye coverage resulting in a blocking behavior at the TiO_2/electrolyte interface. This behavior highly affected the co-sensitized DSSCs' electron lifetimes and total efficiencies.

CONTENTS

ILLUSTRATIONS

x

TABLES

CHAPTER I

INTRODUCTION

Nowadays, the world's energy requirements are supplied by fossil fuels which are promptly depleting. In addition, the use of fossil fuels is provoking major environmental hazards such as global warming, pollution, climate change, resource depletion, acid rain, ozone layer depletion, and many other serious outcomes.[1] Moreover, the greenhouse gas emissions from fossil fuels have significantly increased which may lead to disastrous health consequences. Therefore, it is necessary to make a suitable conversion to the consumption of renewable fuels and avoid the use of nonrenewable and finite resources for energy supply.[2] Along with its environmental and health advantages, renewable energy is also able to provide economic development, help reduce poverty, and implement employment opportunities.[3] Additionally, the increasing global population and economic growth are contributing to an increase in energy demand, which also requires the employment of renewable energy resources that meet the expansion of global energy needs in a climate-friendly approach.[4,5] Renewable energy resources can be divided into three major groups of geothermal, planetary, and solar energy. Geothermal energy is the energy exploited from the heat in the core of the earth. Additionally, planetary energy is represented by the tidal power of the tides on the coast which is an effect of the gravitational forces between the planets and the moon.[6] However, solar energy or energy from the sun is the biggest source of renewable energy. The amount of solar energy reaching the surface of the earth each year is greatly larger than the basic energy demand of the globe, hence, greater than all the fossil energy reserves.[7,8] Solar energy can be used directly; through the utilization of the

incident solar radiation or indirectly; when natural processes transform this solar energy into other forms of energy like wind or biomass.[9] One of the numerous technologies adopted in order to harvest solar energy directly from incident insolation was the field of photovoltaics; it is concerned with the production of electricity from electromagnetic radiation.[10] Electricity generation by solar photovoltaics has been growing at a fast rate in the past decades; the PV market has showed a yearly growth of 33% per year since 1997.[11,12] This fast growth is due to the attractiveness of PV solar cells; they are environmental-friendly having an inexhaustible source of energy which is the sun, they are free of chemical or noise pollution, and they have a competitive price compared to the traditional energy sources.[13]

A. Brief History of Photovoltaics:

Today's conventional solar cells which are called first generation solar cells are based on silicon. The PV market is mostly dominated by mono and polycrystalline silicon due to the element's natural abundance in earth's surface, its low toxicity, and its efficient manufacturing technology.[14] Crystalline silicon used in solar cells called "solar grade" silicon (SGS) is of an intermediate purity level, it is supplied to the PV industry as a by-product of the microelectronic industry in order to avoid the high cost of the purifying process which causes a dependence on the electronic industry and an increase in the price of silicon.[15,16] A crystalline silicon solar cell is constituted of 3 layers; the n-type layer, the p-type layer, and the pn-junction which is the connection between the p and n layers. The n-type layer works as the anode; it is doped with group V elements and has extra electrons. The p-type layer works as the cathode; it is doped with group III elements and has a lack of electrons forming "holes".[14] In the pn-junction, each photon

generates an electron-hole pair by the excitation of electrons from the valence to the conduction band. Accordingly, different potentials are developed in the anode and cathode which induces an electron flow and generates electricity.[17] Subsequently, second generation solar cells were exhibited and they were the main competitors of crystalline silicon solar cells; they are based on thin-film technologies and they include, for example, amorphous silicon, CIGS, and CdTe.[18,19,20] Thin-film technologies are considered a competitive class of photovoltaics due to their numerous advantages which involve a low production cost due to their uncomplicated manufacture process, a broad range of applications, an attractive appearance, and the use of less materials and flexible substrates.[21] Amorphous silicon (a-Si) is the most incorporated thin-film technology. Despite the fact that it has efficiencies lower than crystalline silicon (c-Si), it shows a lower temperature coefficient for power loss and a slightly lower cost.[22] However, second generation solar cells have a major drawback, they utilize non-abundant raw material which causes an increase in the final product price due to the unavailability of cheap raw material.[23] The approach of third generation solar cells is to increase the device efficiency along with using thin-film technologies and abundant, non-toxic, and low-cost raw material.[24] First and second generation solar cells are mostly based on single junction devices limited by the Shockley-Queisser limit which can be circumvented by using multiple junction devices or third generation solar cell devices. Those are aimed to produce electricity at a competitive price compared to traditional solar cells along with achieving a higher efficiency and a better performance.[25]

B. Dye Sensitized Solar Cells:

Dye sensitized solar cells, which are part of the third generation solar cells, have brought noticeable recognition being an alternative to the low-priced production of photovoltaic energy.[26] They are a rising photovoltaic technology with an attempt of increasing the efficiency of solar devices along with providing major advantages like having a low cost compared to other photovoltaic devices, using environmental-friendly raw material, having different design options like transparency and showing several color ranges.[27] In other PV solar cells, light absorption and charge transfer are performed by the semiconductor, however, in DSSCs light absorption is carried out by the dye which then injects an electron to the conduction band of the semiconductor at the interface.[28] In 1991, a seminal paper by O'Regan and Grätzel demonstrated that a film of TiO_2 deposited on a dye-sensitized solar cell increases the available surface area for dye attachment acting as a mesoporous photoanode; this approach dramatically enhanced the dye absorption as well as the energy conversion efficiency to 7% approximately allowing DSSCs to become significant competitors to other solar cells.[29,30]

1. Device Structure and Working Principle:

A typical dye-sensitized solar cell is composed of two glass plates coated with a transparent conductive oxide layer (TCO). The first glass sheet is the working electrode or anode where a mesoporous oxide layer composed of a network of TiO_2 (anatase) nanoparticles sintered together to establish good electronic conduction is deposited. The dye or sensitizer is adsorbed on the surface of this wide band-gap semiconductor TiO_2.[31] This glass plate is joined to a second glass plate which acts as the

counter electrode or cathode coated by a catalyst which is usually platinum. An

electrolyte is injected between the two glass plates through holes in the counter

electrode which are then sealed.[32] Light absorption is carried out by the dye molecules

which causes an excitation of the dye to directly inject an electron to the semiconductor.

This electron reaches the TCO and passes through an outer circuit to the other TCO

plate or counter electrode. After the dye is left in the excited state, it restores back its

ground state by an electron from the electrolyte which results in the oxidation of the

latter.[33]

2. *Electron Transfer Processes in DSSCs:*

The electron transfer processes in a dye-sensitized solar cell as well as the

energy levels based on the dye, the semiconductor TiO_2, and the electrolyte I^-/I^{3-} are

shown in Scheme 1. Reaction 0 shows an excitation of an electron in the dye molecule

from the ground state D to an excited state D* due to light radiation. After the electron

reaches the excited state of the dye, it undergoes an ultrafast electron injection to the

conduction band of TiO_2 (Reaction 2).[34] The time scale for this injection process is said

to be in femtoseconds which is significantly faster than the excited state decay of the

dye to its ground state (Reaction 1). Normally, the rate constant for electron injection is

about 100 times larger than that of electron decay.[35] Higher electron injection increases

the energy of the Fermi level of TiO_2 (E_F) resulting in an increase in the open-circuit

voltage of a DSSC, however, this will lead to a decrease in the driving force for electron

injection or the energy difference between the excited state of the dye and the acceptor

states in TiO_2 and a decrease in the overlap between the two states thus, a decrease in

electron injection efficiency and the short-circuit current of the device.[36] Furthermore,

5

electron injection can occur not only from the dye singlet but also from the triplet excited state. Triplet states are formed by the intersystem crossing from the singlet states; they have a longer lifetime than singlet states but a lower energy.[37] Fast electron injection requires strong electronic coupling of the dye LUMO orbital to the conduction band states of the metal oxide semiconductor and a large density of states in TiO_2 energetically accessible from the dye's excited state.[38] Moreover, the energy of the conduction band in TiO_2 relative to the excited state of the dye is dependent on the presence of certain additives in the electrolyte. For example, basic electrolytes having low Li^+ and high TBP (*tert*-butylpyridine) concentrations increase the potential of the conduction band leading to a higher V_{OC} but reduces the driving force for electron injection thus, decreasing the photocurrent.[39] Furthermore, a carboxylic acid anchoring group in a dye sensitizer holds labile protons which are capable of lowering E_C promoting the driving force and energetics for electron injection.[40] After the electron injection from the dye's excited state to the conduction band of TiO_2, the dye is in its oxidized state and has to be reduced back to it ground state by an electron donor in the electrolyte (Reaction 3).[41]

semiconductor   dye   electrolyte   counterelectrode
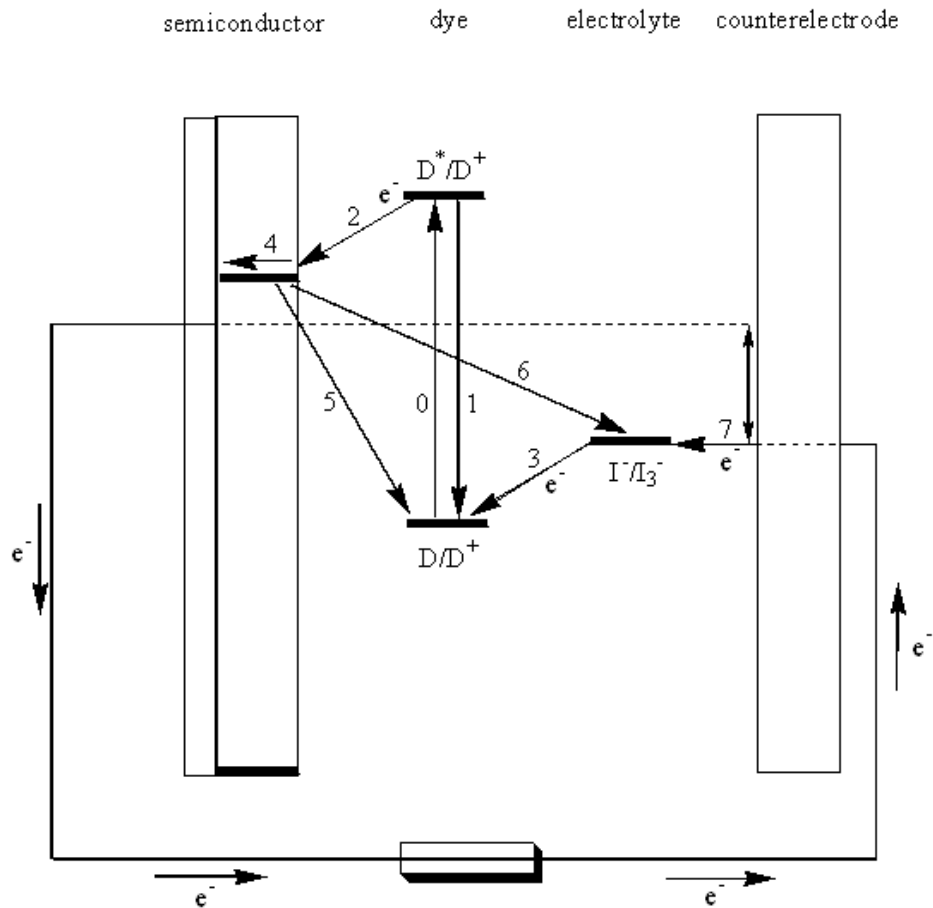
0: $D + h\upsilon \rightarrow D^*$ (photoexcitation)
1: $D^* \rightarrow D + h\upsilon'$ (emission)
2: $D^* \rightarrow D^+ + e^-CB$ (TiO$_2$ injection)
3: $2D^+ + 3I^- \rightarrow 2D + I_3^-$ (regeneration of the oxidized dye)
7: $I_3^- + 2e^- \rightarrow 3I^-$ (regeneration of I$^-$)
5: $D^+ + e^-(TiO_2) \rightarrow D$ (recombination with the oxidized dye)
6: $I_3^- + 2e^-(TiO_2) \rightarrow 3I^-$ (recombination with the electrolyte species)

Scheme 1: The basic electron transfer processes in a DSSC indicated by the numbers 0-7. The energy levels in a DSSC based on the dye, the electrolyte I$^-$/I$_3^-$, and the semiconductor TiO$_2$

The regeneration efficiency shows the efficiency of regeneration of the

oxidized dye by an electron from the electrolyte rather than by an electron in TiO$_2$.[42]

Dye regeneration by a redox species in the electrolyte increases the lifetime of charges that are photogenerated; it also plays a role in completing the electric circuit.[43] It is required that the rate of dye reduction by the redox species, most commonly the iodine/iodide redox couple, in the electrolyte to exceed that of the charge recombination of electrons injected in the semiconductor for efficient dye regeneration to occur.[44] Additionally, the kinetics of dye regeneration are influenced by various factors. The most apparent factor is the reliance on the iodide concentration which can alter the effectiveness of regeneration.[45] Moreover, an increase in the viscosity of the electrolyte which is usually adopted to enhance the device's long-term stability by lowering the electrolyte's volatility leads to a delay in regeneration.[46] Furthermore, the cation of the iodine salt in the electrolyte influences the kinetics of regeneration, for example, the cations Li^+ and Mg^{2+} which have the ability to adsorb on the surface of TiO_2 induce a faster regeneration however, a much slower regeneration is observed with TBA^+ ions. This is because of the presence of a higher iodide concentration near the surface of the semiconductor when positive charge is adsorbed on it.[47] Besides, the dye sensitizer of a DSSC plays a major role in altering the kinetics of regeneration; dyes with bulky alkyl groups are found to have a slower regeneration rate due to the nonpolar shielding and steric effects around the oxidized metal center.[48] Moreover, some studies involve the use of low bandgap sensitizers having a smaller ground state oxidation potential in order to reduce the free energy loss and enhance the durability of the device.[49] However, dyes showing less positive oxidation potentials tend to result in low regeneration kinetics increasing the kinetic competition with electron recombination.[50] In contrast, faster regeneration kinetics are reported for dyes having higher oxidation potentials decreasing the ability for recombination losses.[51] After an electron is injected from the excited state

of the dye to the conduction band of the semiconductor TiO_2 and the ground state of the

dye is restored by an electron donation from the electrolyte, electrons are expected to

transfer from the conduction band of TiO_2 to the conductive substrate inducing a

photocurrent in the outer circuit of the device.[52] However, electron transport in

mesoporous TiO_2 is concentration dependent thus, electron transport occurs by diffusion

since the main driving force for electron transport appears to be the gradient in electron

concentration.[53] Moreover, the electron diffusion coefficient is found to be dependent on

the light intensity which is explained by the trapping and detrapping of electrons in

localized states present below the conduction band from which they need thermal

activation to escape.[54] The traps that are involved in electron transport are situated on

the surface of TiO_2 called surface states.[55] An increase in TiO_2 particle size decreasing

the roughness factor causes a decrease in trap state density thus increasing the diffusion

coefficient.[56] Furthermore, the presence of Li^+ ions in the electrolyte embeds into TiO_2

under open-circuit conditions leading to an increased trap density close to the surface

generating an increase in the electron lifetime thus a decrease in the diffusion

coefficient.[57] The electron transported to the conductive substrate of the working

electrode then to the outer circuit inducing a current in the device is accordingly

transferred to the counter electrode. There, triiodide is reduced back to iodide by gaining

2 electrons from the counter electrode in electrolytes containing the I^-/I_3^- redox species

(Reaction 7).[58] The counter electrode ought to be catalytically active in order to provide

a fast reaction and low overpotential. An overpotential η is required to drive the latter

reaction at a specific current density J which contributes to a charge transfer resistance

($R_{CT} = \eta/J$) that functions as a series resistance in the solar cell. Therefore, lower R_{CT}

values at the counter electrode signify higher exchange current densities at the interface

electrolyte/counter electrode implying a higher catalytic activity.[59] To catalyze the

regeneration reaction of the electrolyte, platinum is deposited on the counter electrode

however, low Pt loadings are required to keep the counter electrode transparent. A weak

counter electrode has a negative effect on the current-voltage characteristic curve of a

DSSC by reducing the fill factor.[60]

3. Loss Mechanisms in DSSCs:

Besides the pathway of electron transfer processes, loss reactions are also

present which include the recombination of injected electrons in the TiO_2 with the

oxidized dye or with certain acceptors in the electrolyte indicated by the two reactions 5

and 6.[61] The oxidized dye may be reduced by the charge recombination of electrons

residing in the conduction band of the metal oxide on a time scale ranging from

nanoseconds to milliseconds. The recombination reaction kinetics have been

documented to be dependent on the electron density in the conduction band or the trap

states of TiO_2.[62] The increased electron density in TiO_2 results in the packing of the

deepest electron traps which contributes in an increased electron diffusion coefficient.[63]

Moreover, the application of a potential or an increase in the cell voltage accelerates the

kinetics of the recombination reaction developing a dependence on the device operating

conditions thus, limiting the efficiency of regeneration.[64] Other than the dependence of

the kinetics of recombination on the electron density, they are also found to be

dependent on TiO_2 and the dye sensitizer employed.[65] The location of the HOMO

orbital of the dye sensitizer affects the recombination reaction; the farther it is from the

metal oxide surface, the higher the barrier of recombination.[66] Another kind of

recombination reaction is the recombination of electrons in TiO_2 with acceptors present

in the electrolyte which has been studied by measuring the response of a solar cell under an open-circuit potential (V_{OC}).[67] Recombination can take place at the interface between TiO_2 and the electrolyte or at the portion of the conducting substrate in contact with the electrolyte however, the second case is restrained by placing a blocking layer of the metal oxide on the conducting substrate.[68] The open-circuit potential in a solar cell is dependent on the electron concentration in TiO_2 therefore, the recombination of electrons with acceptors in the electrolyte can alter V_{OC}. Moreover, the rate of electron transfer from the electrode to the electrolyte balances the rate of electron transfer from the dye to TiO_2 affecting the electron concentration in the semiconductor under open-circuit potential conditions.[69] The recombination reaction rate increases as the concentration of triiodide ions in the electrolyte increases.[70] Also, additives in the electrolyte have the ability to suppress the reaction between the electrons in TiO_2 and triiodide, such as TBP which shifts the conduction band edge towards a negative potential.[71] They reduce the recombination rate by adsorbing on the surface of TiO_2 and hindering the approach between the electrons and acceptors on the surface or by blocking the reduction sites.[72] Furthermore, certain co-adsorbers that are added to the dye solution can reduce recombination and shift the conduction band edge towards a negative potential.[73] Dye sensitizers can also influence the recombination of electrons; several dyes with hydrophobic chains acquire a blocking effect which reduces the recombination reaction rate while other dyes increase the rate of recombination reaction by increasing the concentration of triiodide ions near the dye or by binding of the iodine to the dye.[74,75]

4. Quantification parameters of the performance of DSSCs:

The overall conversion efficiency (η) of a solar cell is given by the maximum power output obtained by a solar cell (P_{max}) over the total power of the incident light (P_{in}).

$$\eta = \frac{P_{max}}{P_{in}}$$

However, the maximum power (P_{max}) is defined as the product of the maximum phtotovoltage (V_{max}) and the maximum photocurrent (J_{max}).

$$P_{max} = V_{max}J_{max}$$

The open-circuit potential of a solar cell (V_{OC}) is described as the potential when the device's terminals are disconnected from any external load i.e. at zero current. It is the difference between the semiconductor's quasi-Fermi level and the redox level. Furthermore, the short-circuit current of a solar cell (J_{SC}) is described as the current measured when the voltage across the device is zero. It is strongly affected by the alignment of energy of the dye/TiO_2/electrolyte interface, the electron traps, and the dye's HOMO-LUMO bandgap. Moreover, the fill factor (FF) of a solar cell which can adopt values between 0 and less than 1 is illustrated as the ratio of the maximum power (P_{max}) over the V_{OC} and J_{SC}.

$$FF = \frac{P_{max}}{V_{oc}J_{sc}}$$

It is associated with the series resistance where a reduced series resistance commonly contributes to a larger fill factor. Hereby, the efficiency of a solar cell can be concluded as

$$\eta = \frac{J_{SC} V_{OC}\, FF}{P_{in}}$$

The incident photon-to-current conversion efficiency (IPCE) which is another measurement of the performance of a solar cell is determined as the short-circuit current under monochromatic illumination generated in the external circuit divided by the photon flux that hits the solar cell.

$$IPCE = \frac{J_{SC}(\lambda)}{e^{\Phi}(\lambda)} = 1240\,\frac{J_{SC}(\lambda)[Acm^{-2}]}{\lambda[nm]P_{in}(\lambda)[Wcm^{-2}]}$$

e represents the elementary charges[76]

5. Components of DSSCs:

a. <u>Electrolyte:</u>

In an electrochemical device, the material that supplies pure ionic conductivity between the negative and the positive electrodes is the electrolyte. It is an indispensable component in a dye sensitized solar cell being a medium for the transportation of charge carriers or ions between the two electrodes and continuously regenerating the oxidized dye.[77] The electrolyte and its interaction with the interfaces of the electrodes influence the fill factor (FF), the photocurrent density (J_{SC}), and the photovoltage (V_{OC}) affecting accordingly the efficiency of a solar cell. In order to be used in DSSCs, the electrolyte ought to have several crucial aspects.[78] First, the electrolyte must have a suitable redox potential in a way that permits the regeneration of the dye and itself and the transport of the charge carriers between the working and counter electrodes. Second, it should ensure high conductivity through rapid diffusion of charge carriers to generate good interfacial contact between the counter electrode and the mesoporous metal oxide

semiconductor thus, the evaporation of the solvent in liquid electrolytes should be reduced to avoid its loss. Third, the electrolyte must not provoke the desorption or degradation of the sensitizer and it should acquire a long-term stability. Finally, the iodide/triiodide redox couple's concentration must be optimized since the latter displays a color, reducing the light absorption and leading to a reaction with the electrons injected in TiO_2. Moreover, the electrolyte must not reveal a notable absorption in the range of visible light for the sake of prevailing significant absorption by the dye sensitizer.[79] In the circuit of a DSSC, the TiO_2 film is responsible for the transport of the electrons, whereas the holes are carried through the hole transport material or the electrolyte. The main role of the electrolyte is the regeneration of the oxidized dye and itself for example, the dye's regeneration reaction for the typical iodide/triiodide redox electrolyte is the following[80]

$$2D^+ + 3I^- \rightarrow 2D + I_3^-$$
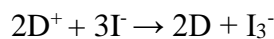
Then, the regenerative cycle is achieved by the reduction of I_3^- back to I^- by the following reaction that takes place on the counter electrode by the help of a catalyst which is usually platinum[60]

$$I_3^- + 2e^- \rightarrow 3I^-$$
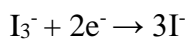
At the counter electrode, a charge transfer resistance (R_{CT}) is generated due to the charge transfer reaction which requires an overpotential (η) to be driven at a certain current density (J). The catalytic activity at the counter electrode ensures a fast regeneration reaction and low overpotential where $R_{CT} = \eta/J$. The performance of a solar cell is negatively affected by decreasing the fill factor if a poor counter electrode is present in a DSSC.[81] Moreover, the regeneration reactions are dependent on the

transport of the redox mediator between the working and counter electrodes in a DSSC in addition, the transport capacity is reflected by two significant parameters; the conductivity and diffusivity.[82] Electrolytes used in DSSCs can be classified into 3 major categories: liquid electrolytes, quasi-solid electrolytes, and solid-state conductors. In this section, our discussion will be limited to liquid electrolytes which are the most broadly used transport media in DSSCs having various advantages over other kinds of electrolytes such as; low viscosity, high conductivity, and uncomplicated preparation leading to an increase in the conversion efficiency.[83] In general, liquid electrolytes are supposed to have low viscosity for the aim of reducing the charge transfer resistance, to maintain physical and chemical stability, and be in a suitable solvent which dissolves the electrolyte and the different additives present while avoiding the dissociation of the adsorbed sensitizer.[84] The three main components of liquid electrolytes are the solvent, the ionic conductor, and the additives.

i. Electrolyte Solvent:

In a dye sensitized solar cell device, the solvent of an electrolyte should meet certain general requirements for it to be eligible for the proper function of the cell: (i) a broad electrochemical window to prevent the degradation of the electrolyte in the range of the working potentials of the anode and the cathode and adequate chemical stability in the dark and under light; (ii) a melting point less than -20°C and a boiling point higher than 100°C to avoid the evaporation of the electrolyte specially in an outdoor environment; (iii) a high dielectric constant that ensures sufficient solubility and full dissociation of the electrolyte salts and proper solubility of the redox mediator; (iv) low viscosity which guarantees high diffusion coefficients of the redox mediators and

significant conductivity of the liquid electrolyte; (v) inertness to the sensitized dye and to the TiO$_2$-dye bond; (vi) weak solubility towards the sealing materials and the electrodes; (vii) insignificant light absorption; (viii) low toxicity and a reduced price.[85] Generally, polar organic solvents and ionic liquids are the two types of electrolyte solvents that meet the general requirements and are suitable for dye sensitized solar cells. Since it is difficult for a single solvent to meet all the above-mentioned requirements, sometimes mixed solvents are used in order to achieve a good device performance.[86] Acetonitrile is believed to be an excellent polar organic solvent owing to its low viscosity, admirable chemical stability, and efficient solubilizing ability. However, it possesses a low boiling point of 82°C and serious toxicity restricting its use for industrial solar cells. Acetonitrile is favorable for laboratory analysis attaining a high conversion efficiency due to its decreased mass-transport limitations also, mixtures of nitrile compounds are employed for the sake of increasing the boiling point to reduce evaporation and cell sealing difficulties. Other than acetonitrile, various electrolyte solvents have been investigated such as nitriles, esters, lactones, and others where most of them contributed in designing stable and highly efficient DSSC devices.[87] The more basic the solvent is or the stronger its electron donating capacity; the lower the number of surface-bound protons and the more negatively charged the surface of TiO$_2$ is. This will lead to a decrease in the driving force for the transfer of electrons from the oxidized sensitizer to the semiconductor which results in a reduced J_{SC} and an increase in the potential difference between the elevated flatband potential (V_{fb}) and the electrolyte's redox potential which causes a larger V_{OC}.[88] Liquid electrolytes that are constituted solely of ions are called ionic liquids or salts in their liquid states. Room-temperature ionic liquids have been employed in electrolytes of DSSCs in view of their exceptional

features such as thermal and chemical stability, analogous nonflammability, adjustable

viscosity, strong ionic conductivity, and intensely reduced vapor pressure decreasing

leakage and evaporation.[89] The most commonly exploited and efficient electrolytes for

electrochemical cells in general and DSSCs in specific are the imidazolium-based ionic

liquids yet, other ionic liquids have also been used as solvents for the electrolytes of

DSSCs like sulfonium, ammonium, pyridinium, and many more.[90] The nature of the

cations and anions that make up ionic liquids determine the device's

photoelectrochemical properties. Moreover, the choice and grouping of cations and

anions controls the performance of a DSSC. For example, while utilizing imidazolium

iodides; smaller cations showed higher triiodide diffusion coefficients leading to larger

photocurrents whereas, bigger cations exhibited larger photovoltages.[91,92] The

drawbacks of pure ionic liquids are the low ion mobility and high viscosity which

reduce the diffusion coefficient of triiodide and limit the restoration of the oxidized

sensitizer.[93] On the other hand, in low viscosity ionic liquids; low temperature limits

triiodide diffusion and high temperature promotes recombination reactions that limit the

device's performance.[94] Therefore, in the aim of reducing their mass-transport

limitations, ionic liquids are sometimes diluted with an organic solvent such as

acetonitrile although it tends to have a high volatility, or high viscosity imidazolium

iodides are mixed with low viscosity ionic liquids.[95] Despite their drawbacks, ionic

liquids are a promising alternative to the highly volatile organic solvents acting as

electrolyte solvents for DSSCs.[96]

ii. <u>Redox Couples:</u>

As previously discussed, the electrolyte or rather the reduced state of its redox couple is responsible for the regeneration of the oxidized dye back to its ground state, and then the couple's oxidized state gets reduced again at the counter electrode. Regarding reaction kinetics, the donation of electrons from the reduced electrolyte state to the oxidized dye should be faster than the electron transfer from TiO_2 to the oxidized dye for the aim of reducing recombination losses and improving the efficiency of dye regeneration.[87] Furthermore, the formation of the reduced redox state by the reduction of the oxidized state at the counter electrode is supposed to be fast enough to wrap up the electrochemical cycle and supply adequate couple sources in a minimal overpotential. The energy level of the redox species is required to be as close as it could be to the D^+/D energy level for the sake of increasing the photovoltage of the device however, it is crucial to preserve a sufficient driving force for the quantitative regeneration of the dye.[97] The iodide/triiodide redox couple adheres to the above standards by possessing an appropriate redox potential providing fast dye regeneration along with slow electron recombination. At the same time, I_3^-/I^- has long-term stability, high conductivity, good solubility, and a beneficial ability of penetration into the mesoporous TiO_2 film.[98] Due to its advantages, the iodide/triiodide redox couple has been the most utilized paradigm primarily introduced by Grätzel in 1991.[29] Iodine binds with iodide in solution to form triiodide in the following equilibrium reaction

$$I_2 + I^- \overset{K_1}{\leftrightarrow} I_3^- \; ; \; K_1 \approx 10^7 \; M^{-1}$$
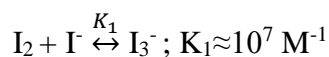
Although other polyiodide species may be formed if the iodine concentration is high, only triiodide is significant in DSSCs.[99] At the counter electrode, a two-electron

reaction takes place where, according to it, the electrolyte's redox potential (E_{redox}) is determined by the Nernst equation

$$E_{redox} = E^{0'} + \frac{RT}{2F} ln \frac{[I_3^-]}{[I^-]^3}$$

$E^{0'}$: formal potential, F: Faraday constant, R: gas constant, T: absolute temperature[100]

The difference of potential between $E^{0'}$(D$^+$/D) and $E^{0'}$(I$_3^-$/I$^-$) is about 0.75 V; it is utilized to drive the forward reactions in a DSSC device. A potential loss of a few hundred millivolts [$E^{0'}$(I$_2^-$/I$^-$) - $E^{0'}$(I$_3^-$/I$^-$)] is present in a DSSC where the driving force for the regeneration of the sensitizer is provided by the difference between $E^{0'}$(I$_2^-$/I$^-$) and $E^{0'}$(D$^+$/D).[101] In order to rapidly regenerate the oxidized dye sensitizer, the concentration of iodide and the diffusion rate are required to be sufficiently high. For example, a 30 mM concentration of triiodide is enough in a nonviscous solvent like acetonitrile but in a viscous solvent, a higher triiodide concentration is required. This is because the triiodide transport to the counter electrode may be a rate-determining step owing to a low iodide concentration or a high solvent viscosity.[102] The cations that are associated with the I$^-$/I$_3^-$ anions in the electrolyte influence the electrolyte's properties and the DSSC's photovoltaic performance. The cations' type and concentration in the electrolyte alter the TiO$_2$ conduction band edge's position. For example, the conduction band of TiO$_2$ shifts to a lesser energy as the concentration of cations increases.[47] Furthermore, for the sake of establishing electroneutrality in the TiO$_2$ film, the transport of electrons is strongly associated with the diffusion of ions therefore, the electron transport in the mesoporous oxide layer is considerably affected by the cations in the electrolyte.[57] For instance, when the electrolyte contains LiI, the Li$^+$ cations bearing a

small radius have the ability to deeply enter into the mesoporous layer of TiO_2 where they form an ambipolar Li^+-e^- leading to an increase in the electrons' transport speed and an enhancement in the photocurrent of the device.[103] However, the small radius of the cations negatively influences the open-circuit voltage of a DSSC by binding to triiodide and causing recombination losses. Accordingly, an increase in the radius of the cations shifts the potential of the conduction band negatively which increases the photovoltage but decreases the photocurrent.[104] Apart from the cation size, the charge density of the cations also influences the performance of DSSCs due to recombination losses and shifts in energy bands.[105] Even though the I^-/I_3^- redox couple demonstrates an impressive performance in dye sensitized solar cells, it still reveals several unfavorable features such as the acute corrosiveness of iodine towards various sealing materials which increases the difficulty in assembling and sealing DSSCs with large areas and decreases their long-term stability, the high vapor pressure of iodine which triggers a problem in device encapsulation, the absorption of visible light by I_3^- and other polyiodide species lowering the photocurrent of the device, and sometimes a loss in the photovoltage of the device is induced due to the gap between the redox potential of I^-/I_3^- and that of certain sensitizers.[106] Earlier, the traditional I^-/I_3^- redox couple was mainly employed in most of the studies on dye sensitized solar cells. Since 2010, the field of development of contemporary redox mediators has received noticeable attention and the number of articles about new redox couples has been enormous.[107] Using a new Co-complex-based electrolyte, the group of Grätzel reported a solar cell with an efficiency of 12.3% in 2011.[108] Co-complex one-electron redox systems are usually noncorrosive, nonvolatile, lightly colored, and have a tunable potential by the modification of their ligands.[109] However, electrolytes with such redox couples exhibit recombination losses

20

of TiO$_2$ conduction band electrons and mass transport limitations that go back to the large size of the Co complex. For the sake of overcoming these detriments, different research groups investigated the Co-complex-based electrolyte. One group found out that the use of TiO$_2$ films with larger porosity helps in increasing the diffusion which is usually slower for cobalt-based electrolytes within the mesoporous titania film.[110] Another group showed that the structure of Co complexes has a large effect on the recombination kinetics thus on the performance of DSSCs.[111] Recently, Mathew and Grätzel used a Co(II/III) redox shuttle in conjugation with a panchromatic porphyrin dye (SM315) to develop a device with 13% efficiency.[112] Furthermore, a study was done by Song and coworkers on porphyrin-based sensitizers using a cobalt-based electrolyte system, which showed increased efficiencies of DSSCs compared to an iodine-based electrolyte system especially with sensitizers bearing bulky electron donors. Those proved to be more efficient with cobalt electrolytes.[113] Therefore, cobalt-complex mediators are currently the most competent redox couples for DSSCs. Other than Co-based redox shuttles, the thiolate/ disulfide (T$^-$/T$_2$) organic redox couple proved to be successful for DSSCs where T$^-$ symbolizes the 1methyl-1-H-tetrazole-5-thiolate anion. The latter redox couple achieved a very high efficiency DSSC compared to DSSCs with other organic redox couples.[114] The T$^-$/T$_2^-$ redox couple exhibited a better performance compared to other organosulfur-based redox couples although an improvement of the long-term stability is needed.[115] Another metal-based redox couple used in DSSCs was the Cu(I)/Cu(II) redox mediator. A conversion efficiency of 7% was reached by assembling a DSSC using the latter redox couple in combination with an organic dye sensitizer.[116]

iii. <u>Additives:</u>

Additives are substantial constituents of liquid electrolytes found to optimize the photovoltaic performance of DSSCs. Adding a small amount of additives manages to improve the potential of the redox couple, the surface states of the semiconductor, the recombination kinetics, the conduction band edge shifting, and the photovoltaic parameters of a DSSC.[117] Grätzel et al. primarily used 4-*tert*-butyl pyridine or TBP as an electrolyte additive which resulted in a significant enhancement of the open-circuit potential of a DSSC.[118] After that, derivatives and analogues of pyridine, benzimidazole, quinoline, and other nitrogen-containing compounds were investigated as additives in liquid electrolytes. As a result of developing a similar impact on DSSCs compared to TBP, nitrogen-containing heterocyclic compounds became the most commonly utilized additives in DSSCs.[119] The electron recombination rate was reduced by approximately 1 to 2 orders of magnitude due to the addition of pyridine derivatives or TBP to the liquid electrolyte in a solar cell. Furthermore, such additives caused an impressive increase in the open-circuit potential of a DSSC which was mainly attributed to the negative shift of the conduction band edge of the semiconductor film towards a higher energy level and the longer lifetimes of electrons in the conduction band.[120,121,122] Raman measurements and surface analysis of the TiO_2 semiconductor showed that TBP binds to the surface of TiO_2 and probably also to iodine or the sensitizer molecules. Adversely, adding an unnecessary amount of additives may negatively affect a solar cell and result in a poor photovoltaic performance.[123] Lithium (Li^+) or guanidinium (G^+) ions are part of a different class of regularly used additives. These additives are also able to boost the performance of DSSCs, but they acquire a contrasting mechanism from that of nitrogen-containing heterocyclic compounds.[124] Numerous studies on Li^+ additives demonstrated

that they shift the conduction band edge towards a lower energy as a result of the adsorption of Li^+ cations on the surface of TiO_2. This causes an increased electron injection from the D* energy level to the conduction band of the semiconductor leading to an enhancement in the photocurrent of the device.[39] Furthermore, the addition of G^+ cations displayed a significant improvement in the photocurrent of the DSSC device due to an increase in the electron injection. Also, when G^+ ions were adsorbed on the surface of TiO_2 along with the N3 dye they formed a compact monolayer of dye which caused a reduction in the dark current thus, a remarkable enhancement of the device's photovoltage and a significant increase in the conversion efficiency.[125] The addition of G^+ cations also developed an advancement in the V_{OC} because of the slower recombination kinetics and the downward shift in the conduction band edge of TiO_2.[126] As previously discussed, heterocyclic nitrogen-containing additives and cation additives bear completely opposite functions concerning the energy level of the semiconductor. Nevertheless, both differing kinds of additives are concurrently used in electrolytes.[124] This argument is required to reinforce the DSSC device's performance by retrieving both benefits from both kinds of electrolyte additives, i.e., the shifting of the conduction band to a higher energy leading to an increase in the photovoltage of the device as well as the blocking of the surface of TiO_2 resulting in the reduction of recombination losses thus, an increase in the photocurrent of the device.[127] For instance, electrolytes containing both Li^+ cations and TBP provided a significant device performance which was proved to be better that electrolytes with one kind of additives.[128] As explained earlier, the electrolyte's performance depends on the properties of the solvent, the ionic conductor, and the additives. The interactions between those constituents and the

electrolyte's interaction with electrodes and dye sensitizers determines the performance of an electrolyte in a DSSC device.

b. Dye Sensitizer:

Being one of the most essential parts of a dye-sensitized solar cell, a dye sensitizer must display certain crucial characteristics. Its absorption spectrum must cover the entire visible region and part of the near-infrared region as well. Also, the excited state of the dye should be higher in energy than the conduction band of the semiconductor for the aim of ensuring efficient electron transfer from the dye's excited state to the semiconductor's conduction band.[129] Moreover, to provide effective dye regeneration, the oxidized state level of the sensitizer should be lower in energy than the redox potential of the electrolyte. The molecular structure of the dye should be optimized or certain co-adsorbers should be added for the sake of reducing unfavorable dye aggregation. Furthermore, the dye sensitizer should maintain electrochemical, thermal, and photo stability.[130] Most importantly, the dye must possess a suitable anchoring group able to bind it to the surface of TiO_2. Dye sensitizers are usually metal complexes or organic dyes. Metal complexes, particularly ruthenium complexes, have been extensively investigated for their application in DSSCs since they have favorable electrochemical properties and a broad absorption spectrum.[65] Organic dyes are considered as alternatives to ruthenium complexes because they demonstrate numerous alternatives. First, their molecular structures can be seen in diverse forms and can be effortlessly synthesized. Second, organic dyes possess higher molar extinction coefficients compared to metal complexes which make them more attractive for thin film solar cells. Third, organic dyes are cheaper than metal complexes and they have

suitable environmental characteristics. Finally, organic dyes have showed improved

efficiencies compared to the efficiencies of ruthenium complexes.[131] As previously

discussed, the anchoring group is the most significant part of the dye sensitizer since it

is employed to bind the dye to the surface of the semiconductor and to promote the

injection of electrons to the conduction band of TiO_2. Historically, carboxylic acid and

cyanoacrylic acid groups have been the most commonly used anchoring groups in

DSSCs.[132] Usually, carboxylic acid anchors are used in transition metal complexes due

to their metal-to-ligand charge transfer and cyanoacrylic acid anchors are used in

organic D-π-A dyes. These anchoring groups possess an excellent electron withdrawing

capability which makes them act as electron acceptors.[133] Subsequently, intramolecular

charge transfer is advanced towards the region of the dye close to the TiO_2 substrate

from the donor region. Certain studies investigated the insertion of a phenyl moiety

between the adsorber and the acceptor group which resulted in an improvement of the

DSSC's efficiency compared to the normal D-π-A structure. This gain in the

performance was attributed to the decrease of back electron transfer from the

semiconductor to the sensitizer.[134] Scheme 2 shows the structure of a sensitizer, DN-

F05, possessing a cyanoacrylic acid anchoring group.
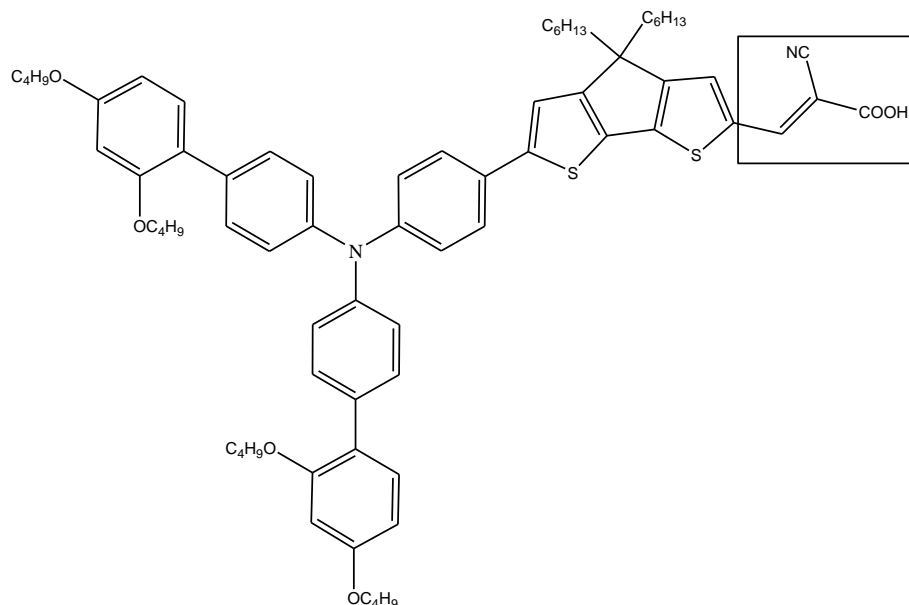
Scheme 2: Structure of DN-F05 dye

In a class of carbazole-based organic dyes, pyridine was utilized as an anchoring group by Ooyama et al. in 2011.[135] Devices containing a pyridyl anchor as well as a triarylamine donor showed comparable efficiencies to those containing a traditional carboxylate anchor. The anchoring site for the pyridyl anchor on the surface of TiO_2 is different from the anchoring site of the carboxylate anchor. FTIR spectroscopy was used to study the anchoring mode of pyridyl on TiO_2 where a new IR band at 1615 cm^{-1} was detected and assigned to the coordination complex between TiO_2 and the pyridyl ring. The strong coordination bond was suggested to be formed between the Lewis-acid sites of TiO_2 and the pyridine ring resulting in efficient electron injection owing to the good electronic communication and a large red-shift in the absorption peak of the dye sensitizer. Moreover, the maximum amounts of dyes containing a pyridyl anchor adsorbed on the surface of TiO_2 were about half that of dyes containing a

carboxylate anchor because there are less Lewis-acid sites than Brønsted-acid sites used for the adsorption of carboxylate anchors.[135,136] Since pyridyl groups adsorb on the Lewis-acid sites of TiO_2 and carboxylate groups adsorb on the Brønsted-acid sites of TiO_2, a synergetic effect was possible where a carboxylate anchor was incorporated with a pyridyl-based dye NI7 resulting in a higher overall conversion efficiency.[137] Another study using a pyridyl-based dye incorporated a bulky trithiophenyl-triarylamine group forming a dye TTC-105 having a decreased conversion efficiency due to the decrease in the dye loading amount and an increase in the charge recombination rate.[138] The structures of NI7 and TTC-105 are shown in scheme 3.
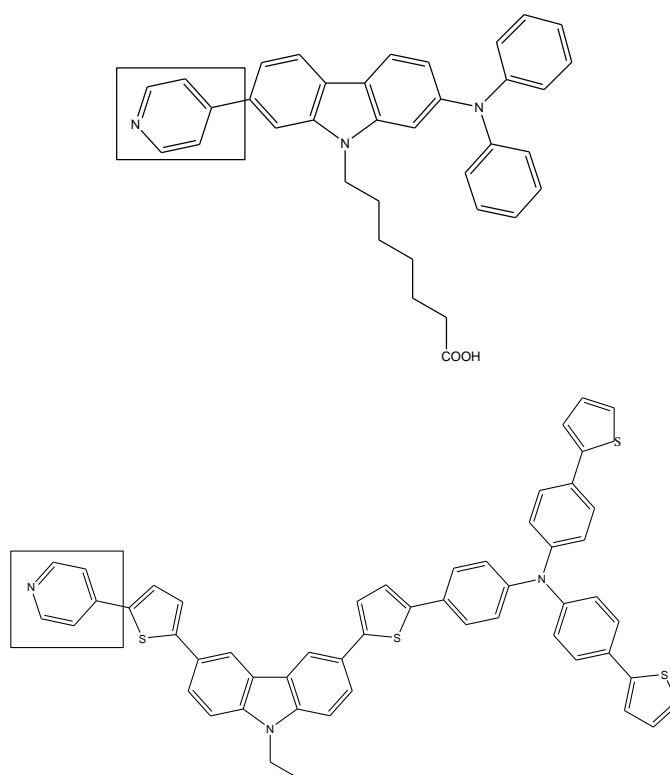
Scheme 3: Structures of NI-7 and TTC-105 respectively

Other than cyanoacrylic acid, carboxylic acid, and pyridine, many other anchoring groups have been investigated in the studies of anchoring groups for dye sensitizers. Phosphonic acid is an extensively studied anchor due to its superior anchoring stability and its immensely high adsorption strength compared to carboxylic acid.[139] However, the tetrahedral geometry of the phosphoryl center and the conjugation loss remarkably decrease the charge transfer rate of phosphonic acid.[140] The performance of the phosphonate anchor in DSSCs devices is considered moderate and acceptable.[141] The latter binds to TiO$_2$ through the phosphoryl oxygen and it also allows other anchoring modes like hydrogen bonding due to the presence of three oxygen atoms.[142] Scheme 4 shows a dye 4-O having a phosphonate anchoring group.
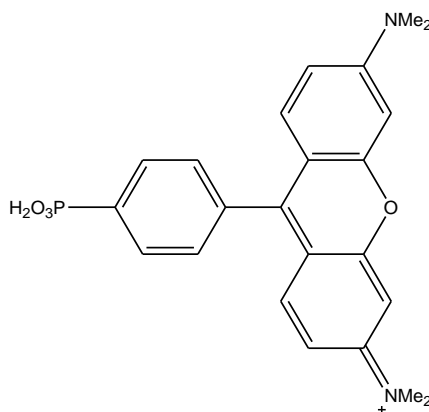
Scheme 4: Structure of 4-O dye

Pyridine-N-oxide was also implemented as an anchoring and electron acceptor. An acceptable conversion efficiency was reached while utilizing pyridine-*N*-oxide-based dyes. Pyridine-N-oxides are thought to bind to the Brønsted-acid sites of TiO$_2$ similar to cyanoacrylic and carboxylic acid.[143] Scheme 5 shows a dye WL102 having a pyridine-*N*-oxide anchoring group.
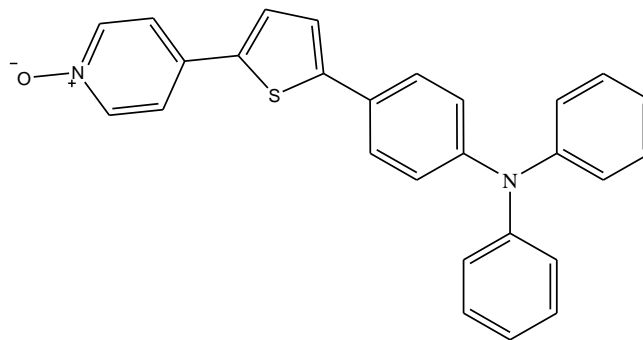
Scheme 5: Structure of WL102 dye

A great deal of diverse anchoring groups has been explored in the study of dye sensitizers for dye-sensitized solar cells. Those were sulfonic acid, boronic acid, nitro, catechol, hydroxamate, acetylacetonate, and many others. The exploration and understanding of these different types of anchoring substituents is contributing to further development of dye-sensitized solar cells and to an improvement in their performance and efficiency.[144]

C. Electrochemical impedance spectroscopy (EIS) studies:

EIS is a powerful steady-state technique used in evaluating the electrochemical processes in a DSSC. It evaluates the current response upon the application of an AC voltage as a function of frequency. EIS experiments are carried out by applying an AC potential $V(\omega,t)$ with a certain frequency range ($f=\omega/2\pi$) and then, measuring the current $I(\omega,t)$ of the electrochemical system. EIS data are usually demonstrated in the form of Nyquist plots where the imaginary impedance Z'' is plotted against the real impedance

Z' for different values of the angular frequency ω. A typical Nyquist plot and a DSSC circuit model of a dye sensitized solar cell system are presented in Scheme 6 below.
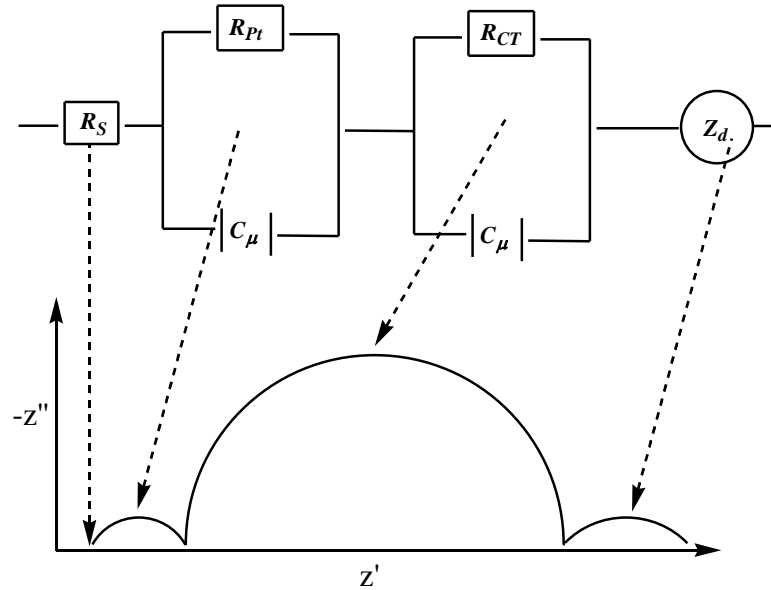
Scheme 6: A typical Nyquist plot of a DSSC and the equivalent circuit that is used for the fitting of the data

The onset of the first semicircle on the x-axis represents the series resistance (R_S) in a DSSC device. The semicircle in the high frequency region (left semicircle) represents the charge transfer resistance and the double layer capacitance (R_{Pt} and C_μ) at the counter electrode. The semicircle at the middle frequency region represents the charge transfer resistance of the electron recombination (R_{CT}) and the chemical capacitance at the TiO$_2$ interface (C_μ). The semicircle at the lowest frequency is associated to the diffusion of the triiodide ions in the electrolyte (Z_d). All of the electrical elements can be obtained by fitting the EIS spectra using an equivalent DSSC circuit as shown in Scheme 6. Moreover, the electron lifetime (τ) corresponds to the product of the charge transfer resistance and the chemical capacitance: $\tau = R_{CT}.C_\mu$. An increase in the charge transfer resistance of the electron recombination (R_{CT}) corresponds to a decrease in the recombination processes in a DSSC. Moreover, an upward or a downward voltage shift

in the capacitance at the TiO$_2$ interface (C$_\mu$) represents an upward or downward shift in the quasi-Fermi level of TiO$_2$ with respect to the redox Fermi level, respectively.

D. Aim of the work:

In 2011, Harima et at. reported on new efficient dyes bearing a pyridine anchoring group.[135,137] Those dyes were proved to bind to the Lewis-acid sites of TiO$_2$ by the same research group later in 2013, where the pyridine-based dye NI4 was co-sensitized with a carboxylic acid-based dye 4CT and the latter showed no effect on the amount of adsorbed NI4 on the surface of TiO$_2$. However, when co-sensitizing 2 carboxylic acid-based dyes NI2 and 4CT, the Bronsted-acid sites were occupied with 4CT which prevented the adsorbtion of NI2 on them.[136] In 2014, Arakawa and coworkers co-sensitized Black dye with a dye having a pyridine anchoring group and displayed an increase in the short-circuit current of this co-sensitized device which was due to an increase in the light absorption in the blue region of the spectrum where the pyridine-based dye absorbs.[145,146] In a different study conducted by Sun and coworkers in 2013, a dye having a pyridine-*N*-oxide anchoring group was sensitized in a DSSC and showed a significant conversion efficiency, although its binding site on TiO$_2$ was not determined.[143] Inspired by the studies mentioned earlier on pyridine and pyridine oxide based sensitizers, we designed and synthesized two new dyes T181 and T182 bearing pyridine and pyridine-*N*-oxide anchoring groups respectively and studied their photovoltaic performance and anchoring sites on the semiconductor TiO$_2$. Both dyes had similar molecular structures with large donor groups which are believed to decrease the charge recombination in DSSCs with cobalt-based electrolyte systems. In addition, T181 which was proven to bind to the Lewis-acid sites of TiO$_2$, was co-sensitized with two commercially available dyes YD2 and DB having carboxylic acid anchoring groups

using two electrolyte systems; iodine and cobalt. This approach shall contribute to an increase in the total dye loading amount due to the binding of T181 to the Lewis-acid sites of TiO_2 while conserving the loading amount of the co-sensitized carboxylic acid dye. Moreover, the short-circuit current and open-circuit voltage of the co-sensitized DSSCs are expected to increase resulting in the enhancement of the solar cells' efficiencies.

CHAPTER II

EXPERIMENTAL METHODS AND INSTRUMENTATION

A. Materials:

Chemicals were purchased from Sigma-Aldrich and were used as supplied. TiO_2 colloids were purchased from Dyesol (Australia). Dyenamo Blue and YD2 dyes were purchased from Dyenamo (Sweden). Fluorine-doped transparent conducting oxide films that are deposited on glass (SnO_2:F) "Tec15" and "Tec8" were purchased from Pilkington (USA). TiO_2 colloids 30NR-D and WER2-O were purchased from Dyesol (Australia).

B. Instrumentation:

The NMR spectra (^{1}H and ^{13}C) were measured on a Bruker AM 500 MHz spectrometer. UV-vis spectra were recorded on a Jasco V-570 UV/vis/NIR. Steady state emission spectra were measured on a JobinYvon Horiba Fluorolog-3 spectrofluorometer. The electrochemical setup consisted of a three-electrode cell, with a platinum rod as the working electrode, a Pt wire ~ 1 mm diameter as the counter electrode, and Ag/Ag^+ (10 mM $AgNO_3$) as the reference electrode. The electrochemical measurements were performed in 0.1 TBAPF$_6$ in DMF, and Fc/Fc^+ standard (0.69 vs NHE in DMF) was used as an internal reference. Electrochemical impedance spectra of the DSSCs were performed with CH Instruments 760B (USA). The obtained impedance spectra were fitted with the Z-view software (v2.8b, Scribner Associates Inc.). The spectra were performed in the frequency range 0.1 Hz - 105 Hz with oscillation

potential amplitudes of 10 mV at RT under open circuit conditions at different light levels. IPCE% spectra were recorded using a Newport 74000 Cornerstone™ monochromator. Photocurrent vs. Voltage characteristics were measured with a Keithley 2400 source meter and a solar simulator illuminated by a Xenon arc lamp (Oriel) through an AM1.5 simulation filter (ScienceTech). The irradiated area of the cell was 0.5 x 0.5 cm with a 0.6 x0.6 cm black mask.

C. Electrolytes:

The iodine electrolyte used in the YD2 study was composed of 2 M DMII, 0.5 M TBP, 0.1 M GuSCN, 0.05 M LiI, 0.05 M I_2 in ACN and that used in the DB study was composed of 2 M DMII, 0.2 M TBP, 0.1 M GuSCN, 0.05 M LiI, 0.05 M I_2 in ACN. The cobalt electrolyte used in the YD2 study was composed of 0.25 M Co(II), 0.06 M Co(III), 0.1 M $LiClO_4$ and 0.6 M TBP and that used in the DB study was composed of 0.25 M Co(II), 0.06 M Co(III), 0.1 M $LiClO_4$ and 0.2 M TBP.

D. Computational Methods:

Calculations were carried out using Gaussian 03.[147] Geometries were optimized using the 6-31G* basis set with (B3LYP) in water (C-PCM algorithm).[148]

E. Synthesis:

1. Synthesis of T181 dye:

a. Preparation of 4-dihexyl-4H-cyclopenta[2,1-b:3,4-b']dithiophene:

In a nitrogen-degassed dimethyl sulfoxide, a mixture of 4H-cyclopenta[2,1-b:3,4-b']dithiophene (3.36 g, 18.88 mmol), potassium hydroxide (3.17 g, 56.63 mmol),

and 1-iodo hexane (12.01 g, 56.63 mmol) was stirred at room temperature for 24 hours then water was added. Then, the crude product was extracted into diethyl ether for 3 times. The organic layer was washed with an aqueous solution of ammonium chloride and water then dried with anhydrous sodium sulfate. Finally, the product was filtered and the solvent was removed under reduced pressure. The product was purified by column chromatography with hexane as the eluting solvent. The main band was collected and the solvent was removed by reduced pressure to get 4,4-dihexyl-4H-cyclopenta[2,1-*b*:3,4-*b'*]dithiophene as a pure solid (5.6 g, 89% yield). ^{1}H NMR (500 MHz, Chloroform-*d*) δ 7.08 (d, 2H), 7.00 (d, 2H), 1.69 (d, *J* = 552.0 Hz, 4H), 1.45 – 1.37 (m, 8H), 1.30 – 1.18 (m, 8H), 0.80 (t, 4H).

b. Preparation of 2,6-dibromo-4,4-dihexyl-4H-cyclopenta[2,1-b:3,4-b']dithiophene:

To prepare 2,6-dibromo-4,4-dihexyl-4H-cyclopenta[2,1-*b*:3,4-*b'*]dithiophene, 4,4-dihexyl-4H-cyclopenta[2,1-*b*:3,4-*b'*]dithiophene (2 g, 5.78 mmol) was dissolved in tetrahydrofuran at 0 °C under nitrogen and kept for 15 minutes. Then, *N*-bromosuccinimide (2.06 g, 11.56 mmol) was added and the reaction was warmed to room temperature and stirred in the dark for 24 hours then water was added. The crude product was extracted into dichloromethane then washed with water. The organic layer was dried over anhydrous sodium sulfate. Finally, the product was filtered and the solvent was removed under reduced pressure. The product was purified by column chromatography with hexane as the eluting solvent. The main band was collected and the solvent was removed by reduced pressure to get a yellow colored 2,6-dibromo-4,4-dihexyl-4H-cyclopenta[2,1-*b*:3,4-*b'*]dithiophene (1.7g, 59% yield). ^{1}H NMR (500 MHz,

Chloroform-*d*) δ 6.86 (s, 2H), 1.68 (t, 4H), 1.27 – 1.17 (m, 8H), 1.16 – 1.03 (m, 8H), 0.79 (t, 4H).

c. <u>Preparation of T181 dye:</u>

In a nitrogen-degassed medium of dioxane:tetrahydrofuran:water 5:1:1, a mixture of 2,6-dibromo-4,4-dihexyl-4H-cyclopenta[2,1-*b*:3,4-*b*']dithiophene (0.4 g, 0.6 mmol), 4-pyridinylboronic acid (0.09 g, 0.73 mmol), 2',4'-dibutoxy-*N*-(2',4'-dibutoxy-[1,1'-biphenyl]-4-yl)-*N*-(4-(4,4,5,5-tetramethyl- 1,3,2-dioxaborolan-2-yl)phenyl)-[1,1'-biphenyl]-4-amine (0.58 g, 0.72 mmol), triphenylphosphine (0.08 g, 0.29 mmol), potassium carbonate (1.35 g, 9.77 mmol), and palladium acetate (12 mg, 0.05 mmol) was stirred under reflux for 48 hours. The product was extracted into dichloromethane and washed with water. Then, the organic layer was dried over anhydrous potassium carbonate and the product was filtered and the solvent was removed under reduced pressure. The product was purified by column chromatography with hexane:ethyl acetate as the eluting solvent and the main band was collected. Finally, the solvent was removed under reduced pressure to get an orange compound **T181** (141.7 mg, 21% yield). ^{1}H NMR (500 MHz, Acetone) δ 8.41 (dd, *J* = 4.5, 1.6 Hz, 2H), 7.71 (s, 1H), 7.53 (d, *J* = 8.7 Hz, 2H), 7.48 (dd, *J* = 4.5, 1.6 Hz, 2H), 7.40 (d, *J* = 8.7 Hz, 4H), 7.38 (s, 1H), 7.16 (d, *J* = 8.4 Hz, 2H), 7.03 (d, *J* = 2.1 Hz, 3H), 7.03 (d, *J* = 8.7, 6.6 Hz, 3H), 6.53 (d, *J* = 2.4 Hz, 2H), 6.48 (dd, *J* = 8.4, 2.4 Hz, 2H), 3.92 (t, *J* = 6.4, 3.5 Hz, 4H), 3.92 (t, *J* = 6.4, 3.5 Hz, 4H), 1.63 (quin, 4H), 1.63 (quin, 4H), 1.37 (sext, *J* = 22.6, 15.1, 7.5 Hz, 4H), 1.37 (sext, *J* = 22.6, 15.1, 7.5 Hz, 4H), 1.20 – 1.00 (m, *J* = 63.1 Hz, 10H), 0.84 (t, *J* = 22.2, 7.4 Hz, 6H), 0.84 (t, *J* = 22.2, 7.4 Hz, 6H), 0.67 (t, *J* = 7.0 Hz, 6H). APPI MS (*m/z*): calculated for $C_{72}H_{86}N_2O_4S_2$ [M + H^{+}][+], 1107.6; found, 1108.1. [13]C

NMR (126 MHz) δ 160.57, 157.87, 153.03, 151.22, 148.67, 146.70, 146.43, 142.43, 141.66, 141.14, 138.28, 134.74, 131.64, 131.25, 130.17, 127.35, 126.54, 126.13, 125.24, 125.08, 124.78, 124.32, 123.97, 123.95, 119.88, 105.87, 101.40, 68.28, 67.90, 31.95, 31.66, 19.83, 19.81, 14.23, 14.17, 1.61. MALDI-TOF MS (m/z): calculated for $C_{65}H_{64}N_4O_4S_3$, 1061.4; found, 1061.3.

2. Synthesis of T182 dye:

A mixture of **T181** (50 mg, 0.045 mmol) and *meta*-chloroperoxybenzoic acid (*m*CPBA) (24 mg, 0.14 mmol) was dissolved in chloroform and stirred while heating for 24 hours. The reaction was then diluted with chloroform and stirred for 15 minutes. The product was washed with a solution of potassium carbonate then with water. After that, the organic layer was dried over anhydrous potassium carbonate where the product was filtered, and the solvent was dried under reduced pressure. The product was purified by column chromatography with hexane:ethyl acetate as the eluting solvent and the main band was collected. Finally, the solvent was removed under reduced pressure to get a red compound **T182** (30 mg, 59.3% yield). ^{1}H NMR (500 MHz, Acetone) δ 7.97 (dd, J = 7.4 Hz, 2H), 7.59 (s, 1H), 7.52 (d, 2H), 7.50 (dd, 2H), 7.39 (d, J = 8.7 Hz, 4H), 7.36 (s, 1H), 7.15 (d, J = 8.4 Hz, 2H), 7.02 (d, J = 8.6 Hz, 4H), 7.00 (d, 1H), 6.52 (d, J = 2.4 Hz, 2H), 6.47 (dd, J = 8.4, 2.4 Hz, 2H), 3.91 (t, J = 6.4, 3.0 Hz, 4H), 3.90 (t, J=6.4, 3.0 Hz, 4H), 1.63 (quin, 4H), 1.58 (quin, 4H), 1.39 (sex, J = 15.1, 7.5 Hz, 4H), 1.34 (sex, J = 15.1, 7.5 Hz, 4H), 1.18 – 1.00 (m, J = 65.4 Hz, 10H), 0.85 (t, J = 7.4 Hz, 6H), 0.80 (t, J = 7.4 Hz, 6H), 0.66 (t, J = 7.0 Hz, 6H). MALDI-TOF MS (*m/z*): calculated for $C_{72}H_{86}N_2O_5S_2$ [M + H$^+$]$^+$, 1123.6; found, 1124.1.

F. Solar Cell Fabrication:

Dye sensitized solar cells were fabricated using standard procedures. A compact titania layer (Ti-Nanoxide BL/SP, Solaronix, Switzerland) was first spin-coated to the cleaned "TEC15" conductive glass, followed by the treatment with 40 mM TiCl$_4$ aqueous solution at 70 °C for 30 min. A 4 µm was then was printed by the doctor blade method from a diluted TiO$_2$ paste (60% TiO$_2$ Dyesol 30NRD, 34% terpineol and 6% ethyl cellulose), followed by a scatting layer (4 µm) of Dyesol WER2-O TiO$_2$ paste. Next, the electrodes were sintered at 500 °C for 60 min, followed by treatment with 40 mM TiCl$_4$ aqueous solution at 70 °C for 30 min. The films were further heated at 500 °C for 60 min before sensitizing with 0.2 mM YD2 or 0.03 mM DB with 0.2 mM T181 in 1:1:1 THF/acetonitrile/*tert*-butanol mixture. The counter electrodes were fabricated by applying a 2-3 µl/cm^2 of 5 mM H$_2$PtCl$_6$ in 2-propanol to the "Tec8" FTO glass, followed by heating in an oven at 400 °C for 20 minutes. Cell assembly was performed by sealing the counter electrode to the TiO$_2$ electrode with a 25 µm Surlyn (Dupont) spacer at ~ 100 °C for 3 mins. The corresponding electrolyte was introduced through two small holes, previously drilled through the counter electrode, which were then sealed with Surlyn.

CHAPTER III

RESULTS AND DISCUSSION

A. Synthesis and Characterization:

The synthesis of the two new dyes T181 and T182 was successful using the procedure shown in synthetic Schemes 7 and 8 below. While T181 possesses a pyridine anchoring group, T182 possesses a pyridine oxide anchoring group where the nitrogen in the ring is coordinated to an oxygen atom. In order to synthesize T181, 4H-cyclopenta[2,1-*b*:3,4-*b'*]dithiophene was substituted by two hexyl groups. This substitution was essential to prevent other unwanted reactions and to derivatize the dye by alkyl groups. Alkyl groups are believed to decrease recombination between TiO_2 and the electrolyte by reducing their contact with each other. The second step was the bromination of position 2 and 2' of the thiophene rings for subsequent Suzuki coupling on these sites. Finally, the synthesis of T181 was completed by two simultaneous Suzuki coupling reactions. Moreover, the synthesis of T182 was accomplished by the reaction of T181 with *m*-CPBA which oxidizes the nitrogen atom of the pyridine ring. The structures of the dyes were confirmed by NMR and mass spectrometry.
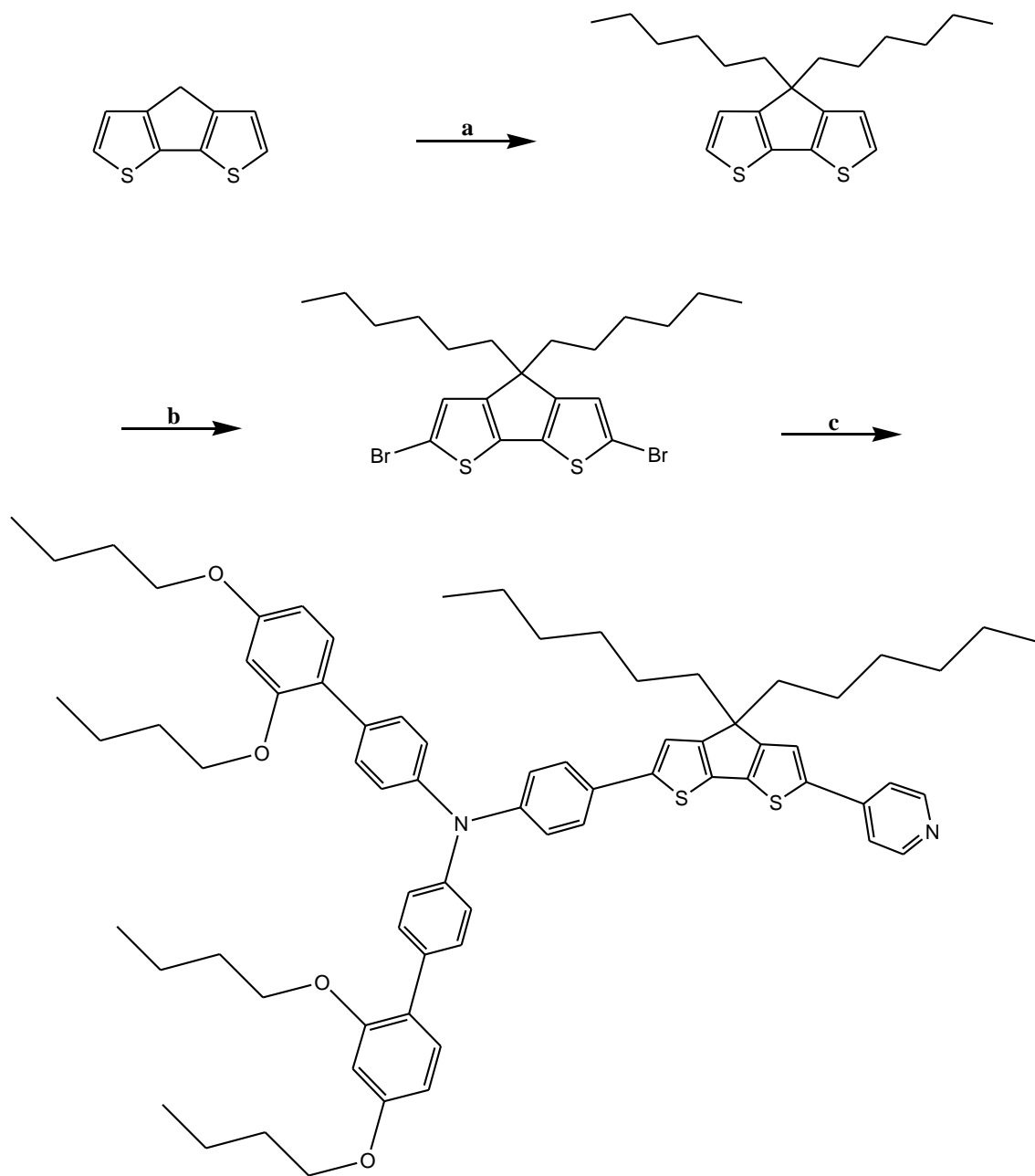
Scheme 7: The synthetic scheme of T181where (a) dimethyl sulfoxide, KOH, 1-iodohexane; (b) NBS, THF; (c) $C_5H_6BNO_2$, $C_{52}H_{66}BNO_2$, triphenyl phosphine, potassium carbonate, palladium acetate, dioxane:THF:H_2O
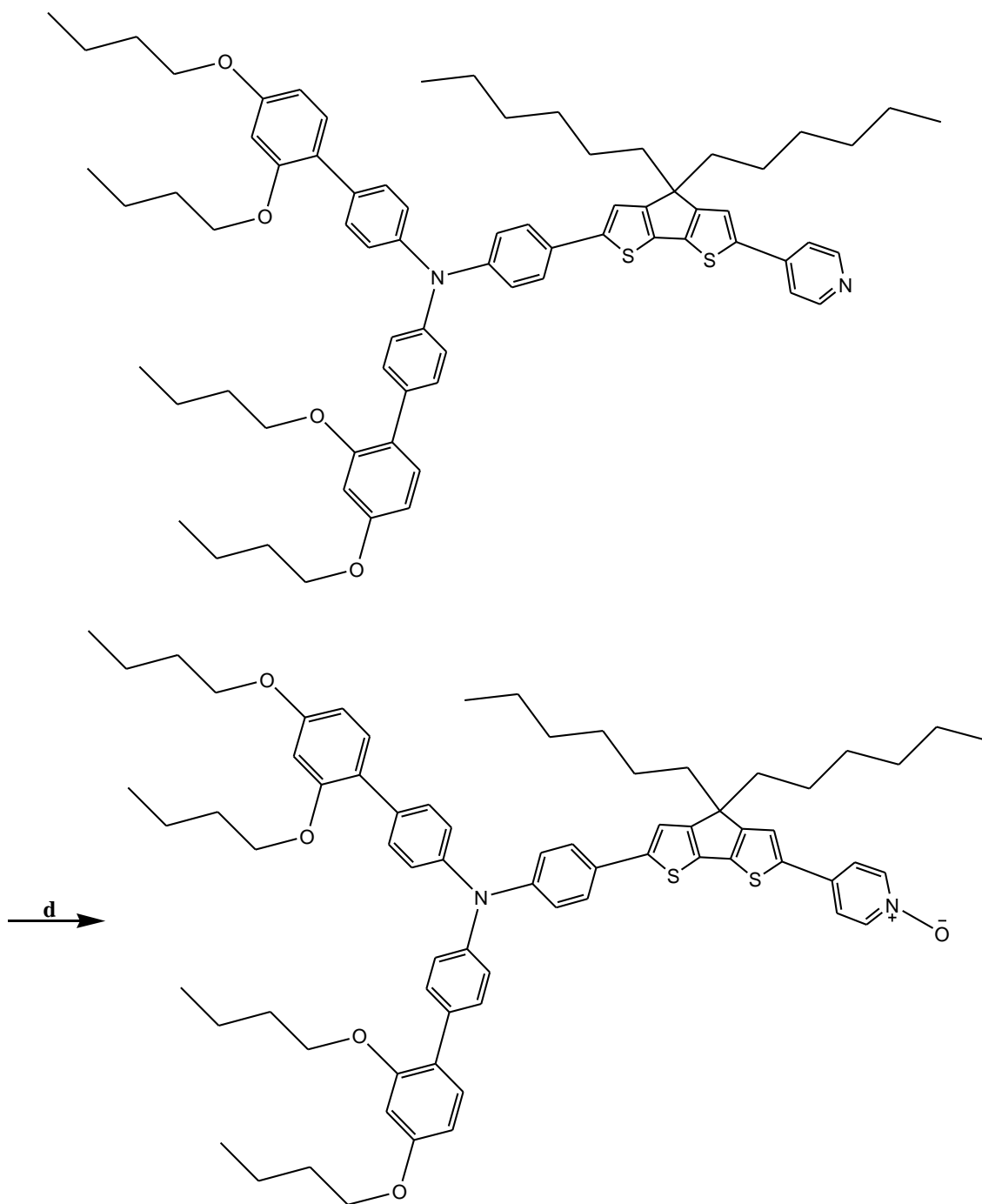
Scheme 8: The synthetic scheme of T182 where (d) *m*-CPBA, chloroform

Furthermore, the two dyes were characterized by UV/Vis and emission spectroscopy. The UV/Vis spectra of T181 and T182 are shown in Figure 1 below.
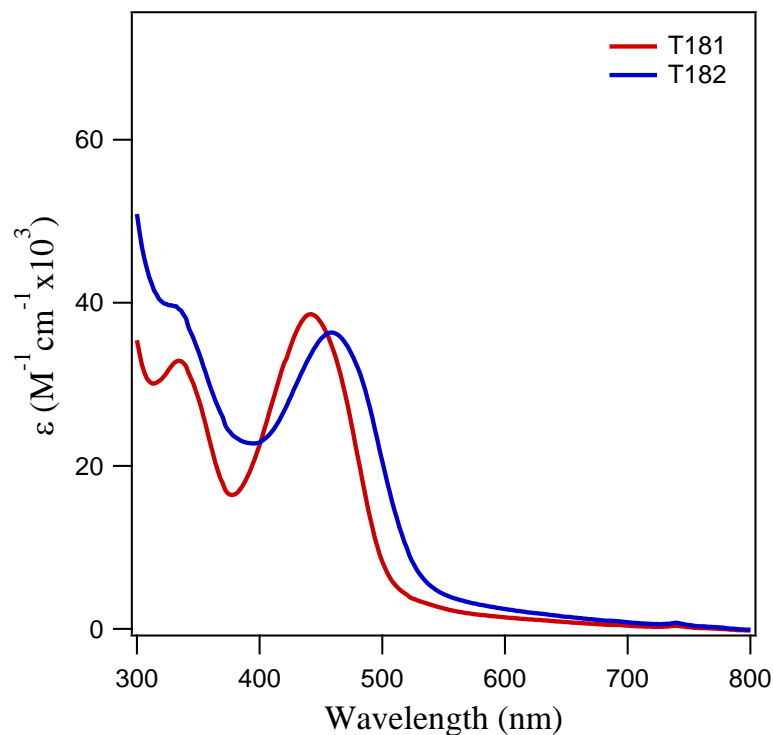
Figure 1: The absorbance spectra of T181 and T182 dyes in THF

The UV/Vis spectrum of T181 shows peaks at 334 nm ($\varepsilon = 32900$ M^{-1} cm^{-1}) and at 442 nm ($\varepsilon = 38600$ M^{-1} cm^{-1}). Likewise, the UV/Vis spectrum of T182 is red-shifted as expected and shows peaks at 336 nm ($\varepsilon = 39000$ M^{-1} cm^{-1}) and at 460 nm ($\varepsilon = 36300$ M^{-1} cm^{-1}). The emission spectra of T181 and T182 are shown in Figures 2 and 3 respectively. The emission maximum of T181 was seen at 538 nm at an excitation wavelength of 460 nm whereas, that of T182 was seen at 566 nm at an excitation wavelength of 480 nm.
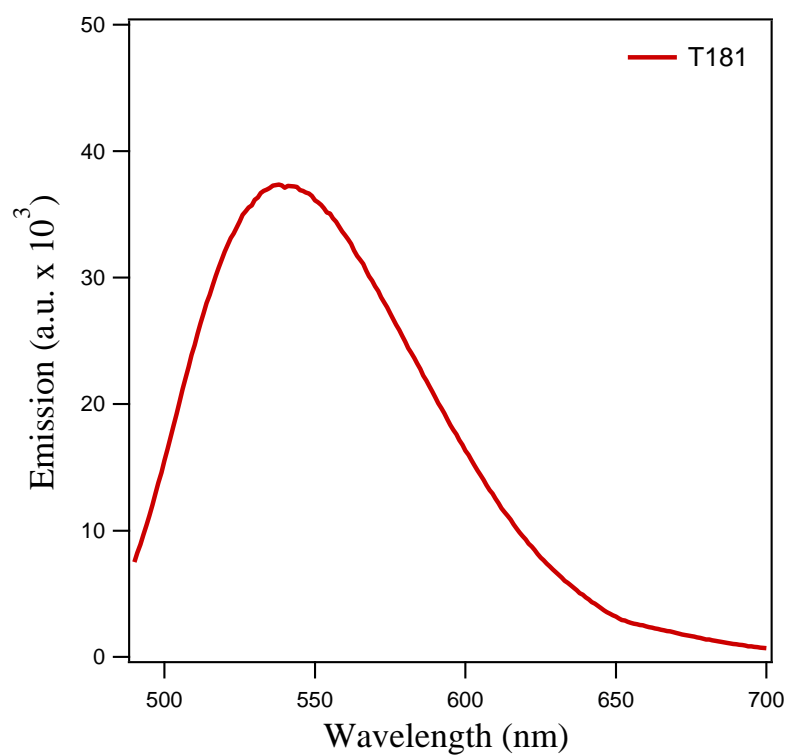
Figure 2: The emission spectrum of T181 dye in THF (λ_{ex}= 460 nm)
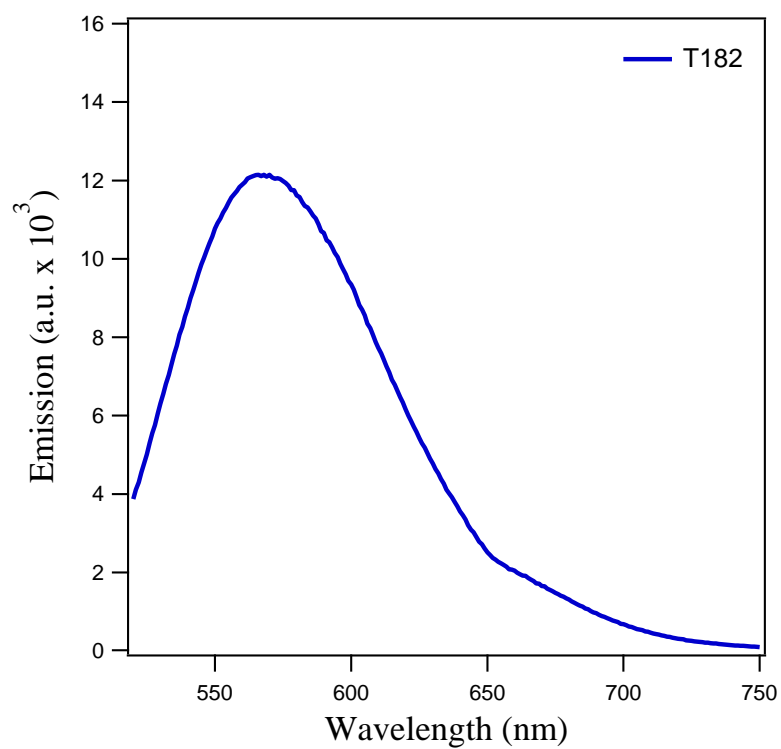
Figure 3: The emission spectrum of T182 dye in THF (λ_{ex}= 480 nm)

From the intersection of the absorbance and the emission curves of T181 and T182, the E_{0-0} was calculated to be 2.422 eV and 2.296 eV for T181 and T182, respectively. Furthermore, differential pulse voltammetry measurements were performed in order to evaluate the redox potential of the two dyes (T181 and T182). The measurements were carried out at a scan rate of 100 mV.s^{-1} using dimethyl formamide as a solvent where Ag/Ag^{+} was used as a reference electrode and platinum as a counter electrode. The differential pulse voltammograms of T181 and T182 are shown in Figure 4 (a,b) below.
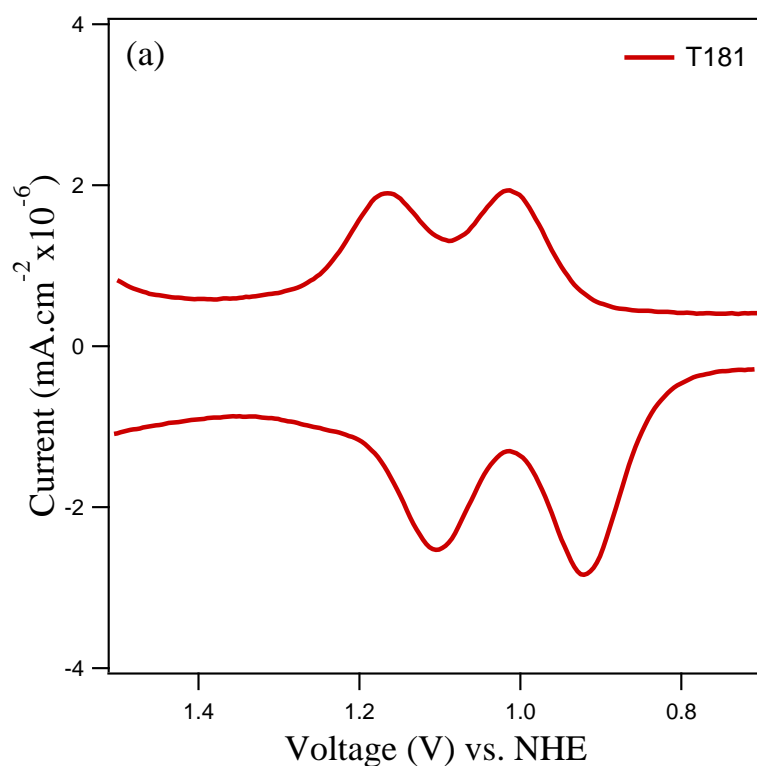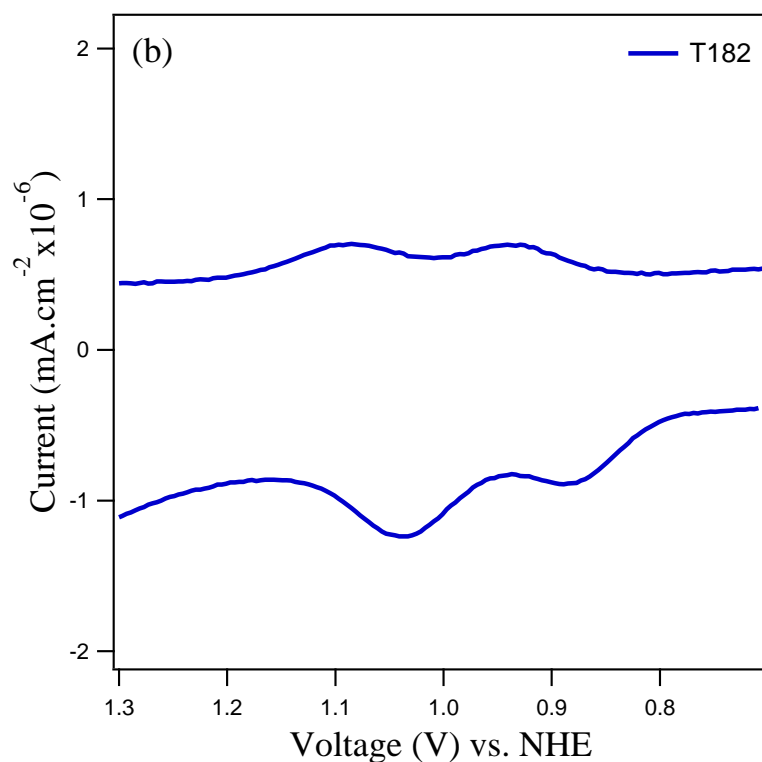
Figure 4: Differential pulse voltammograms of (a) T181 dye in DMF and (b) T182 dye in DMF obtained at a scan rate of 100 mV.s^{-1} vs. Ag/Ag$^+$ using Pt as a counter electrode

The measurements obtained from differential pulse voltammetry were normalized in contrast to ferrocene/ferrocenium used as a reference vs. NHE (Fc/Fc$^+$ 0.69 V vs. NHE in DMF). The E$_{ox}$ of T181 and T182 were approximated to be 1.00 V and 1.04 V vs. NHE, respectively. In order to calculate the excited state potential (E$^*_{ox}$) of the two dyes, the bandgap energy (E$_{0-0}$) was subtracted from the measured redox potential (E$_{ox}$). The values obtained from the absorbance and emission spectra and differential pulse voltammetry are summarized in Table 1 below.

Table 1: The spectra and electrochemistry results for T181 and T182 dyes

Dye	Abs. (λ in nm) ε (10^4 M^{-1}.cm$^-$	Em. (λ in nm)	E_{ox} (V vs. NHE)	$E_{ox}^* = E_{ox} - E_{0-0}$ (v vs. NHE)
T181	334, 442 3.3, 3.9	538	1.00	- 1.42
T182	336, 460 3.9, 3.6	566	1.04	- 1.26

B. Determination of the Binding Sites:

For the aim of studying the binding sites on TiO$_2$ of the anchoring groups of T181 and T182 dyes, FT-IR spectroscopy was performed on T181 and T182 powder as well as T181 and T182 adsorbed on TiO$_2$. The different FT-IR spectra are shown in Figures 5 and 6 below.
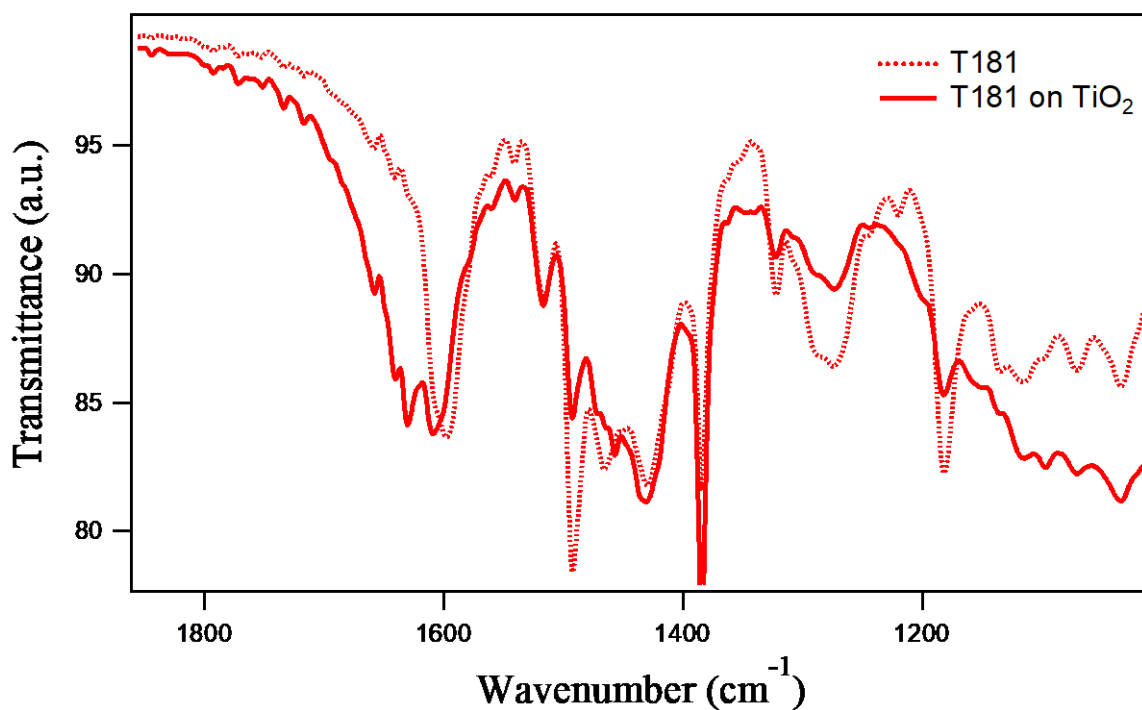
Figure 5: FT-IR spectra of T181 powder and T181 adsorbed on TiO$_2$
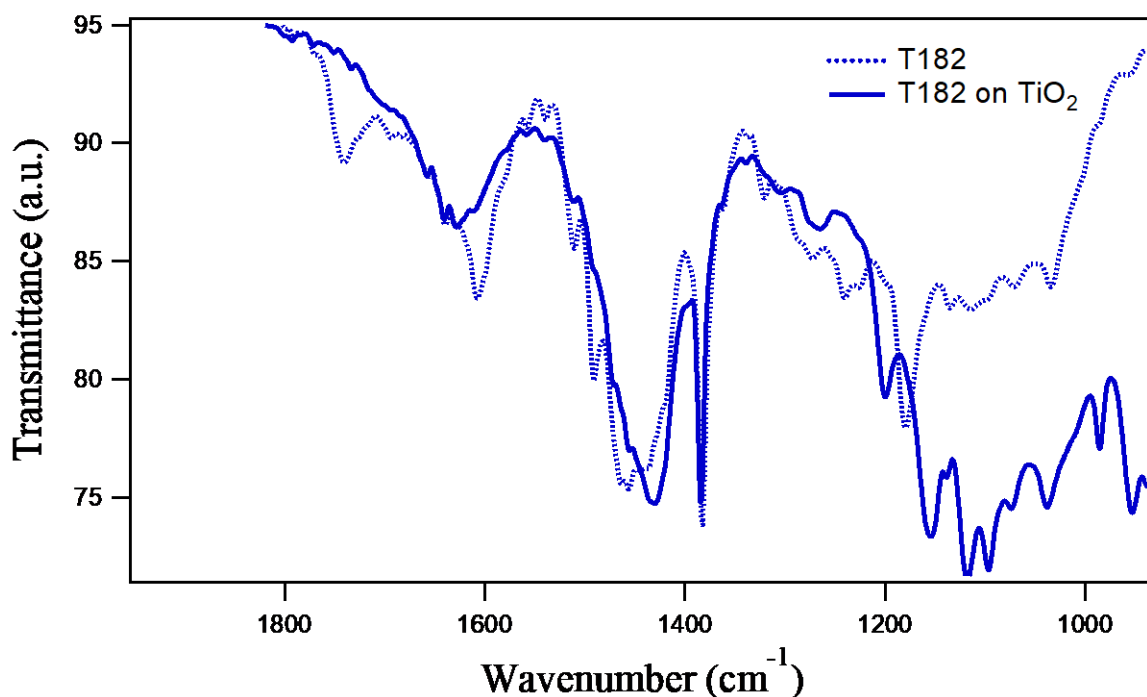
Figure 6: FT-IR spectra of T182 powder and T182 adsorbed on TiO_2

As shown in Figure 5, T181 powder has a peak at 1595 cm^{-1} close to 1580 cm^{-1} which was ascribed to a breathing mode of the pyridine ring. When T181 was adsorbed on TiO_2, the peak at 1595 cm^{-1} was shifted to a higher energy side. An intense peak observed at 1610 cm^{-1} in the spectrum of T181 adsorbed on TiO_2, along with other peaks at a higher wavenumber, indicated that the pyridine ring of T181 was adsorbed on the Lewis-acid sites of TiO_2 through a coordinate bond. Similar results were previously seen in a study done by Harima and coworkers on the dye NI4 having a pyridine anchoring group that binds to the Lewis-acid sites of TiO_2. The FTIR spectrum of NI4 adsorbed on TiO_2 showed an intense peak at 1614 cm^{-1} indicating the coordinate bonding of the pyridine ring to the Lewis-acid sites on TiO_2.[136] However, in Figure 6,

while T182 powder showed a peak at 1606 cm^{-1} which can also be assigned to one of the breathing modes of a pyridine ring, no significant peak indicating adsorption on Lewis-acid sites of TiO_2 was seen in the spectrum of T182 adsorbed on TiO_2. The latter only showed shifts in the peaks' positions already present in the spectrum of T182 powder. This indicates that the pyridyl anchoring group of T181 clearly binds to the Lewis-acid sites of TiO_2 however, there was no clear peak indicating the binding of T182 on the surface of TiO_2. Furthermore, to precisely specify the sites of adsorption of T181 and T182 on TiO_2, 6 µm electrodes of TiO_2 were dipped in 0.2 mM solutions of T181, T182, and T181 mixed with T182 in THF:EtOH for 24 hours. The UV/Vis spectra of the dyes adsorbed on TiO_2 films are shown in Figure 7 below.
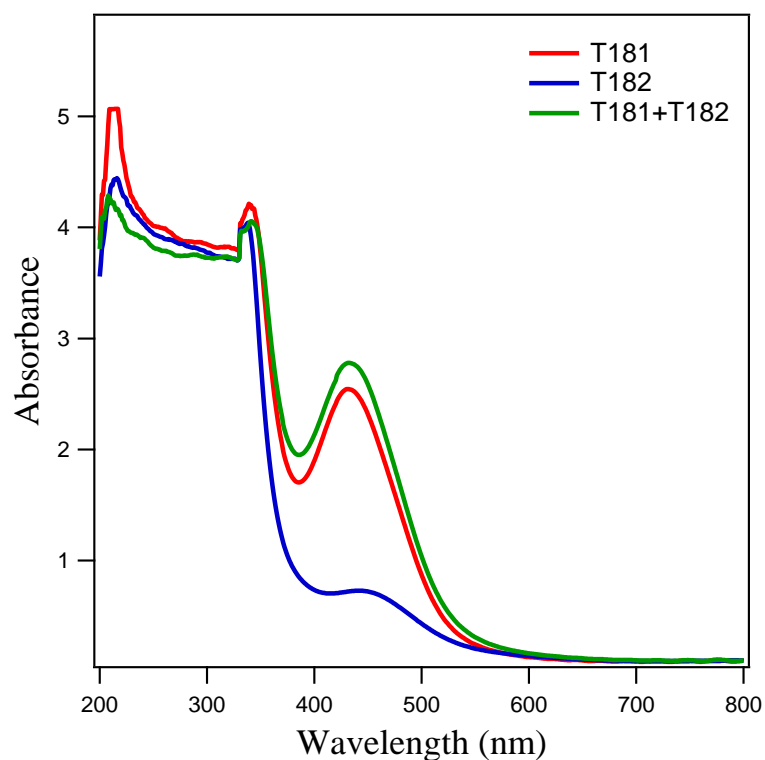
Figure 7: The absorbance spectra of TiO$_2$ films of T181, T182, and T181-T182

Later, the dye-adsorbed TiO$_2$ electrodes were soaked in an alkaline solution in THF:EtOH:H$_2$O for a couple of minutes to allow the desorption of the dye molecules. Then, the absorbance spectra of the desorbed solutions were measured as a function of wavelength in order to calculate the dye loading amounts from the maximum absorbance of the curves. The absorbance spectra of desorbed TiO$_2$ films of T181, T182, and T181 mixed with T182 are shown in Figure 8 below. Table 2 shows the calculated dye loading amounts of T181 and T182 in the 3 different electrodes.
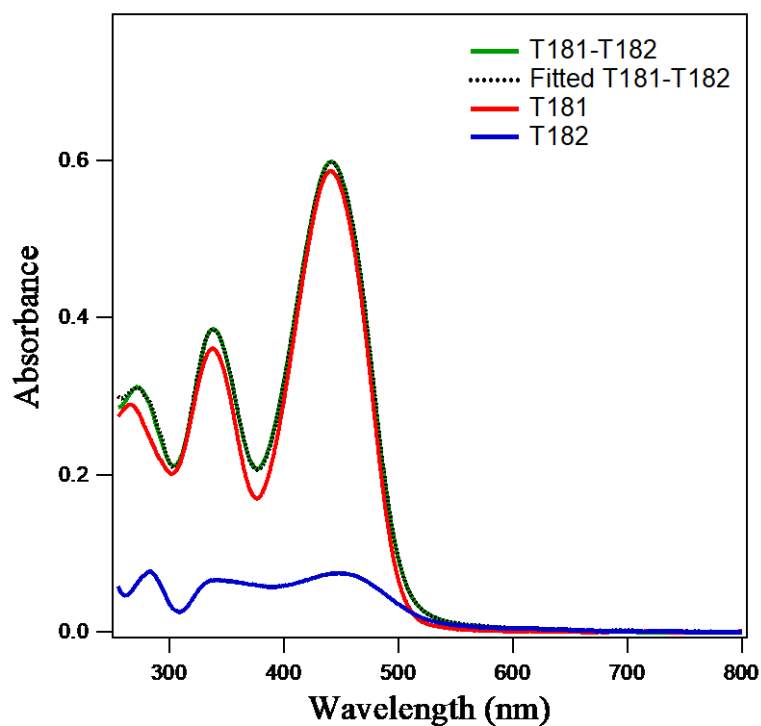
Figure 8: The absorbance spectra of desorbed TiO$_2$ films of T181, T182, and T181-T182

Table 2: The dye loading amounts of T181 and T182 in pure and co-adsorbed TiO$_2$ films

Dye concentration in solution	n_{T181} (mol)	n_{T182} (mol)	Total dye loading amount (mol)
T181 (0.2 mM)	1.5 ($\pm$ 0.1) x 10^{-7}	0	1.5 ($\pm$ 0.1) x 10^{-7}
T182 (0.2 mM)	0	0.2 ($\pm$ 0.1) x 10^{-7}	0.2 ($\pm$ 0.1) x 10^{-7}
T181 (0.2 mM) + T182 (0.2 mM)	1.4 ($\pm$ 0.1) x 10^{-7}	1.8 ($\pm$ 0.1) x 10^{-8}	1.6 ($\pm$ 0.2) x 10^{-7}
TiO$_2$ colloid 18NR-T; TiO$_2$ film thickness= 6.0 $\pm$ 0.5 μm; TiO$_2$ electrode area= 2.56 cm^2			

For the sake of calculating the percentage of adsorption of T181 and T182 in the co-sensitized electrode, the experimental values of the co-sensitized T181 and T182 were fitted along with the spectra of T181 and T182 of the desorbed solutions. The coefficients adsorbed T181 and T182 were calculated from the graph and found to be 0.908 for T181 and 0.877 for T182, Figure 8. These coefficients which were close to 1 suggest that when T181 and T182 were co-sensitized together, the two dyes did not compete for the same site or else the sum of the two coefficients would be less than 1 designating the decrease in the dye loading amount of each dye. The dye loading amounts shown in Table 2 showed that T181 was adsorbed on TiO_2 in a higher proportion than T182. However, when the two dyes were co-sensitized together, the dye loading amounts weren't significantly decreased which implied that T181 and T182 did not compete for the same adsorption site.

C. Dye Loading Measurements:

T181 bearing a pyridine anchoring group that binds to the Lewis-acid sites of TiO_2 is expected to be an efficient co-sensitizer with dyes that adsorb to the Brønsted-acid sites of TiO_2 like the ones having carboxylic acid anchoring groups. In order to verify the previous hypothesis, T181 was co-sensitized with two commercial dyes having a carboxylic acid anchoring group which were chosen to be YD2 and Dyenamo Blue (DB) having the structures shown in Scheme 9 below.

(a)

(b)
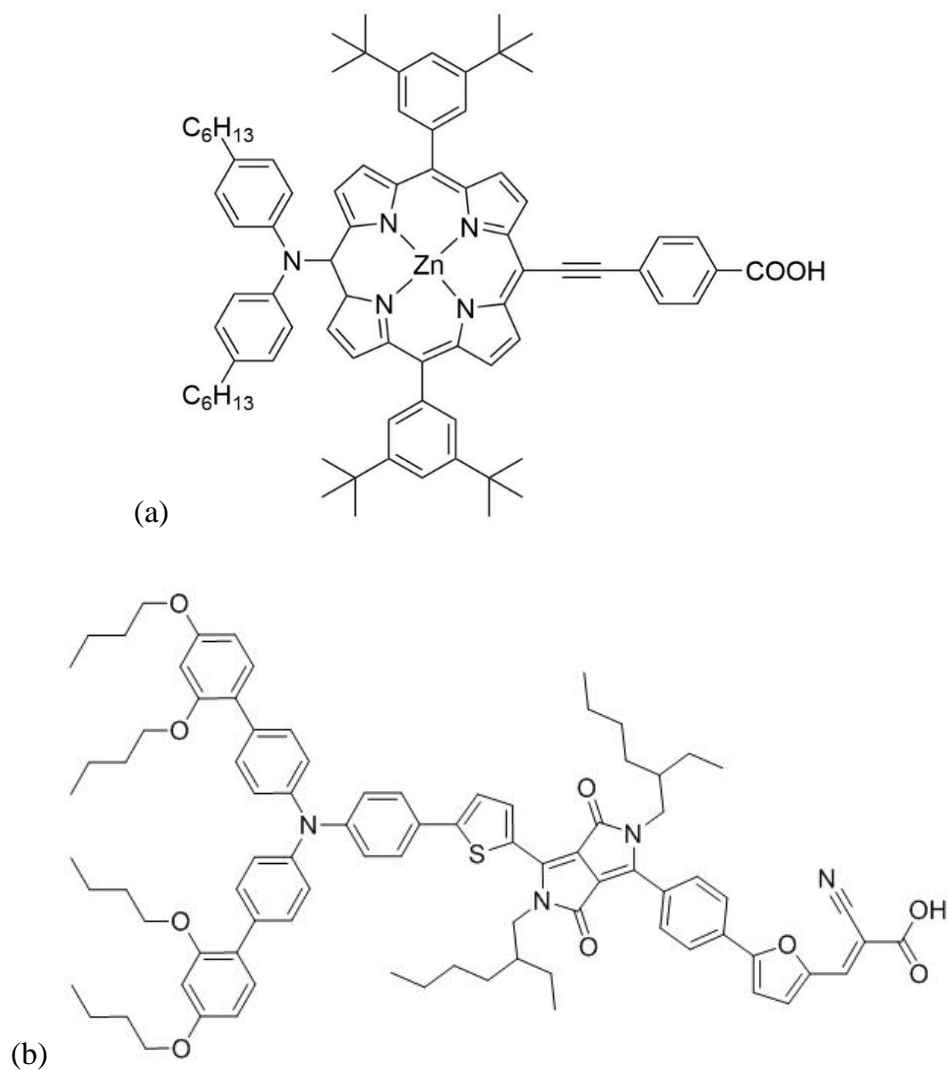
Scheme 9: The molecular structures of (a) YD2 dye and (b) DB dye

To study the dye loading amounts of DB co-sensitized with T181, 4 μm TiO$_2$ electrodes were immersed in 0.2 mM solution of T181, 0.03 mM solution of DB, and T181 mixed with DB having the same concentrations in THF:EtOH for 24 hours. The UV/Vis spectra of the dyes adsorbed on TiO$_2$ films are shown in Figure 9 below.
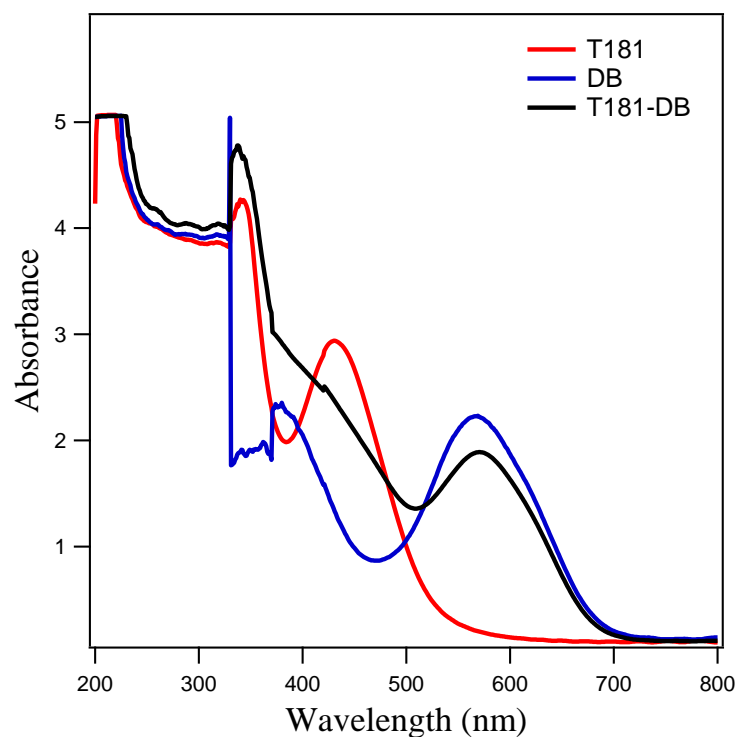
Figure 9: The absorbance spectra of TiO$_2$ films of T181, DB, and T181-DB

As performed earlier, the dye-adsorbed TiO$_2$ electrodes were dipped in an alkaline solution in THF:EtOH:H$_2$O for a couple of minutes to allow the desorption of the dye molecules. Then, the absorbance spectra of the desorbed solutions were measured as a function of wavelength in order to calculate the dye loading amounts from the maximum absorbance of the curves. The absorbance spectra of desorbed TiO$_2$ films of T181, DB, and T181 mixed with DB are shown in Figure 10 below. Table 3 shows the dye loading amounts of T181 and DB in the 3 different electrodes.

Figure 10: The absorbance spectra of desorbed TiO$_2$ films of T181, DB, and T181-DB

Table 3: The dye loading amount of T181 and DB in pure and co-adsorbed TiO$_2$ films

Dye concentration in solution	n_{T181} (mol)	n_{BD} (mol)	Total dye loading amount (mol)
T181 (0.2 mM)	6.6 ($\pm$ 0.1) x 10^{-8}	0	6.6 ($\pm$ 0.1) x 10^{-8}
BD (0.03 mM)	0	8.5 ($\pm$ 0.3) x 10^{-8}	8.5 ($\pm$ 0.3) x 10^{-8}
T181 (0.2 mM) + BD (0.03 mM)	6.6 ($\pm$ 0.1) x 10^{-8}	8.6 ($\pm$ 0.3) x 10^{-8}	15.2 ($\pm$ 0.4) x 10^{-8}
TiO$_2$ colloids 30 NR-D, TiO$_2$ film thickness= 3.8 $\pm$ 0.5 µm; TiO$_2$ electrode area= 2.56 cm^2			

The experimental values of the co-sensitized T181 and DB were fitted along with the spectra of T181 and DB of the desorbed solutions. The coefficients of adsorbed

T181 and DB were calculated from the graph and found to be 1.000 for T181 and 1.023 for DB. These coefficients which are both close to 1 show that the two dyes did not compete for the same adsorption site. The dye loading amounts for the co-sensitized film of T181-DB were measured as 6.6×10^{-8} mol for T181 and 8.6×10^{-8} mol for DB.

In a second study, YD2 having a different structure than DB was co-adsorbed with T181. The UV/Vis spectrum of YD2 is shown in Figure 11 below.
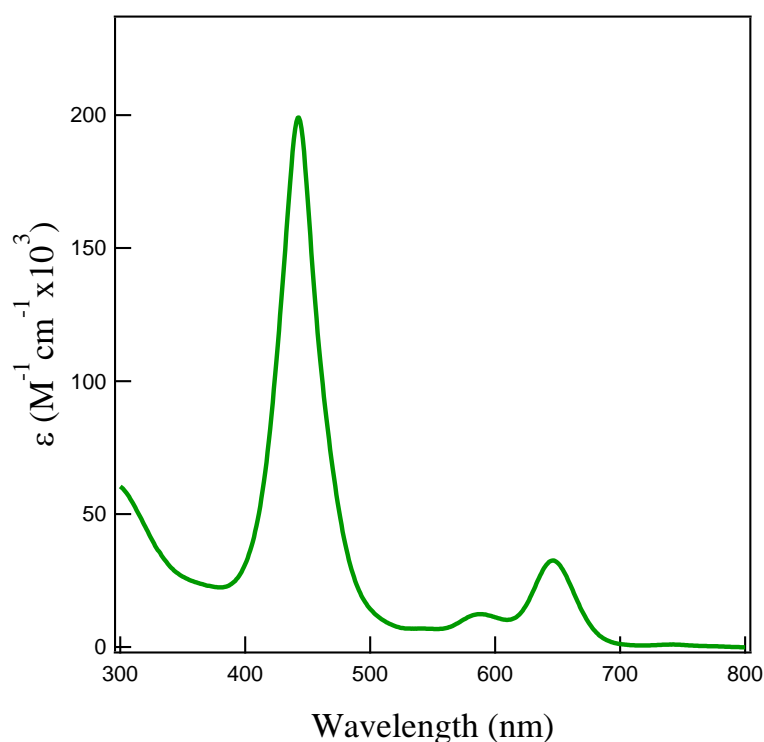
Figure 11: The absorption spectrum of YD2 in THF

The UV/Vis spectrum of YD2 shows 2 maxima at 442 nm ($\varepsilon = 199,000$ M^{-1}.cm^{-1}) and at 646 nm ($\varepsilon = 33,000$ M^{-1}.cm^{-1}), Figure 11. 8 µm TiO$_2$ electrodes were immersed in 0.2 mM solutions of T181, YD2, and T181 mixed with YD2 in THF:EtOH

for 24 hours. The UV/Vis spectra of the dyes adsorbed on TiO_2 films are shown in Figure 12 below.
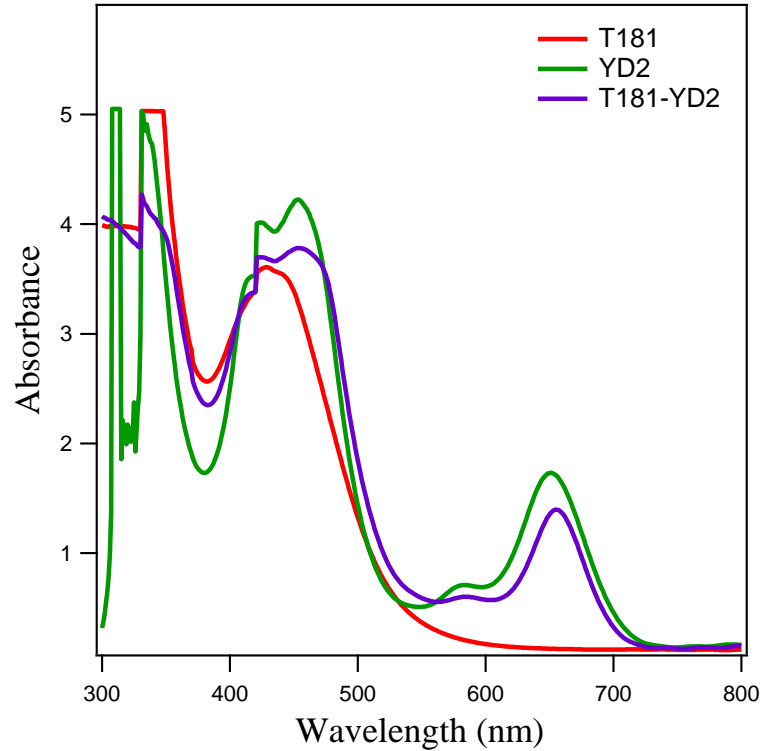
Figure 12: The absorbance spectra of TiO_2 films of T181, YD2, and T181-YD2

Later, the dye-adsorbed TiO_2 electrodes were dipped in an alkaline solution in THF:EtOH:H_2O for a couple of minutes to allow the desorption of the dye molecules. Then, the absorbance spectra of the desorbed solutions were measured as a function of wavelength in order to calculate the dye loading amounts from the maximum absorbance of the curves. The absorbance spectra of desorbed TiO_2 films of T181, YD2, and T181 mixed with YD2 are shown in Figure 13 below. Table 4 shows the dye loading amounts of T181 and YD2 in the 3 different electrodes.
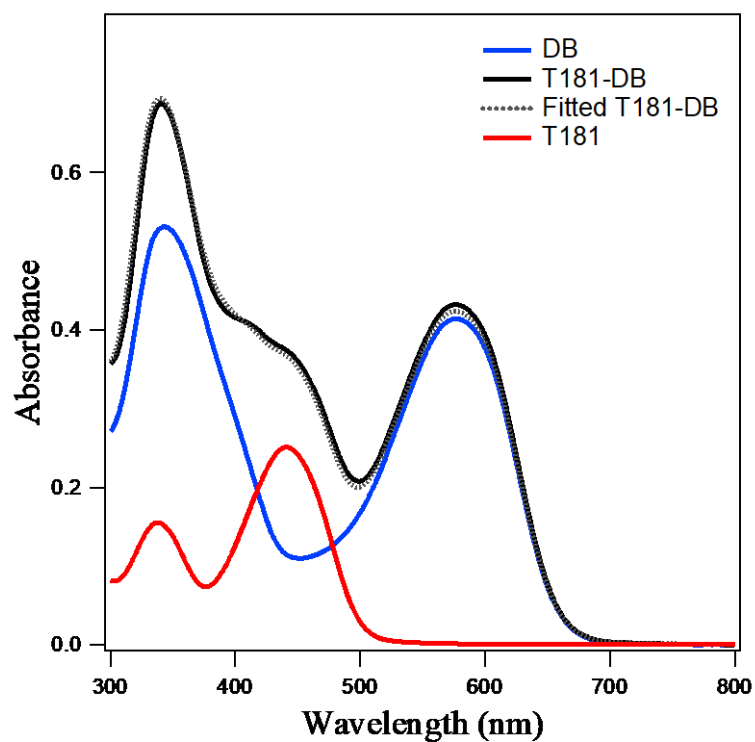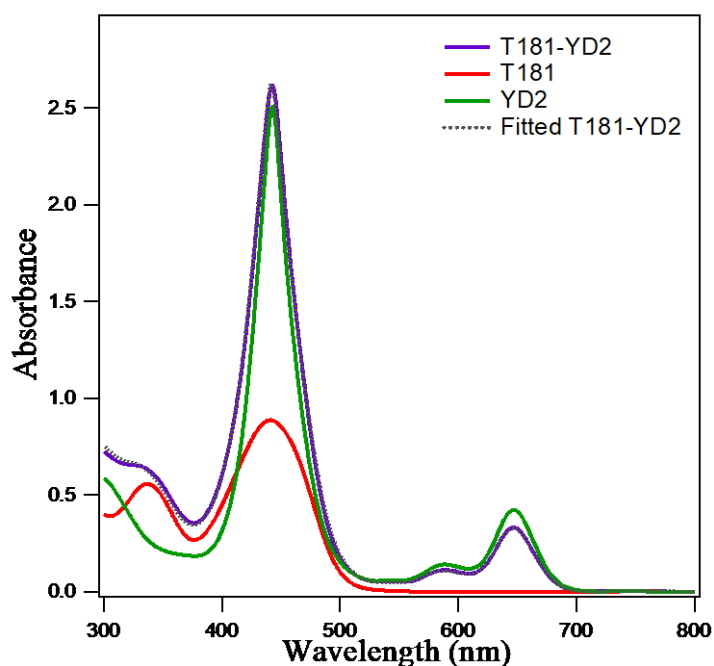
Figure 13: The absorbance spectra of desorbed TiO$_2$ films of T181, YD2, and T181-YD2

Table 4: The dye loading amount of T181 and YD2 in pure and co-sensitized TiO$_2$ films

Dye concentration in solution	n_{T181} (mol)	n_{YD2} (mol)	Total dye loading amount (mol)
T181 (0.2 mM)	2.4 ($\pm$ 0.1) x 10^{-7}	0	2.4 ($\pm$ 0.1) x 10^{-7}
YD2 (0.2 mM)	0	1.3 ($\pm$ 0.2) x 10^{-7}	1.3 ($\pm$ 0.2) x 10^{-7}
T181 (0.2 mM) + YD2 (0.2 mM)	1.8 ($\pm$ 0.1) x 10^{-7}	1.0 ($\pm$ 0.2) x 10^{-7}	2.8 ($\pm$ 0.3) x 10^{-7}
TiO$_2$ colloids 18 NR-T; TiO$_2$ film thickness= 8.0 $\pm$ 0.5 μm; TiO$_2$ electrode area= 2.56 cm^2			

To calculate the percentage of adsorption of T181 and YD2 in the co-sensitized electrode, the experimental values of the co-sensitized T181 and YD2 were fitted along with the spectra of T181 and YD2 of the desorbed solutions. The coefficients calculated

from the fitted graph were found out to be 0.752 for T181 and 0.781 for YD2. The decrease in the coefficients of YD2 and T181 to a value lower than 1 shows that the two dyes influenced each other by decreasing the dye loading amount when co-sensitized together. Furthermore, the dye loading amounts for the co-adsorbed film of T181-YD2 (1.83×10^{-7} mol of T181 and 1.00×10^{-7} mol of YD2) were less than those of T181 and YD2 when they were not co-sensitized (2.44×10^{-7} mol of T181 and 1.28×10^{-7} mol of YD2).

D. DFT Calculations:

The decrease in the dye loading amounts of the two dyes when co-sensitized together was attributed to the dyes' structural size thus, we performed density functional theory (DFT) calculations on the three dyes. Schemes 10 and 11 show the relative sizes.
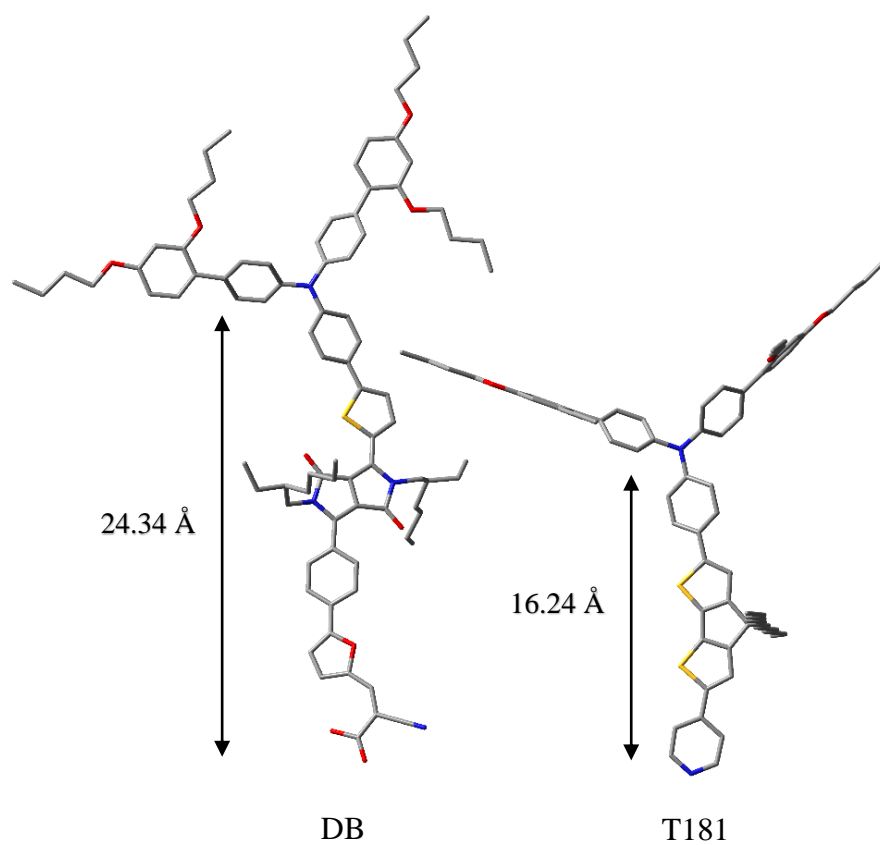
Scheme 10: The calculated relative sizes of the geometry optimized T181 and DB dyes
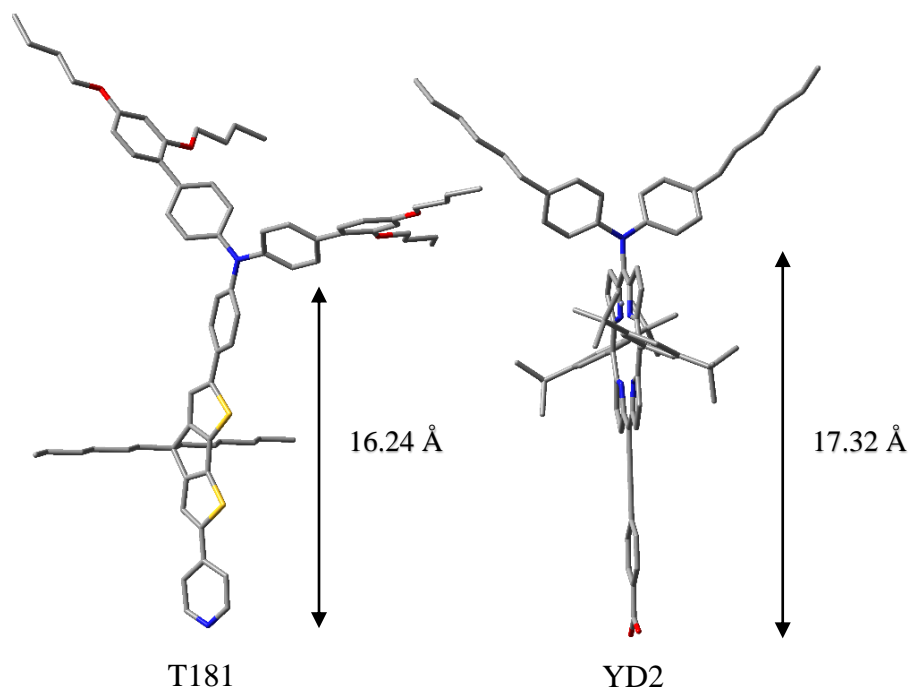
Scheme 11: The calculated relative sizes of the geometry optimized T181 and YD2 dyes

The calculated vertical distances between the N atom of the triphenylamine donor moiety to the N atom of the pyridyl moiety is 16.24 Å for T181 and the distance between the triphenylamine N atom and the O atom of the carboxylic acid moiety 24.34 Å for DB. As can be seen in Scheme 10, the bulky donor group of T181 can fit within the groove right below the DB donor group; however, this is not the case in the co-sensitized T181 and YD2, Scheme 11. The calculated vertical distance between the diphenylamine N atom and the O atom of the carboxylic acid moiety is 17.32 Å for YD2 which is very close to that of T181. Therefore, T181 and YD2 aren't able to fit together like T181 and DB. We speculate that the reason behind the lower loading of T181 in the T181-YD2 co-sensitized film might be only due to a complementary size relationship between the co-sensitized dyes, where T181 has a suitable shape and size to

fit better in the voids of the adsorbed DB dye than the YD2 dye. It is important to note here that we did not increase the DB concentration in the T181-DB film bath above 0.03 mM to increase its loading amount mainly because DB is very prone to aggregation,[149] and therefore any higher concentration would greatly and negatively affect our DSSC efficiency measurements. Based on the above results it is suggested that site selective adsorption was achieved when co-sensitizing T181 with DB or YD2.

E. Prediction of the Ideal Concentration for Co-sensitization:

Since T181 holding a pyridine anchoring group is expected to bind to the Lewis-acid sites of TiO_2, the ideal concentration that should be used in co-sensitization studies for DSSCs had to be measured in order to achieve the best photovoltaic performance from the assembled cells. Hereby, the current-voltage characteristic curves of solar cells using individual T181 and YD2 and co-sensitized T181-YD2 were studied. The working electrodes of the studied DSSCs were dipped in solutions of: 0.2 mM T181, 0.2 mM YD2, 0.2 mM YD2 + 0.1 mM T181, 0.2 mM YD2 + 0.2 mM T181, 0.2 mM YD2 + 0.3 mM T181 respectively. The current-voltage curves of the above mentioned DSSCs with I^-/I_3^- electrolyte are displayed in Figure 14 below.
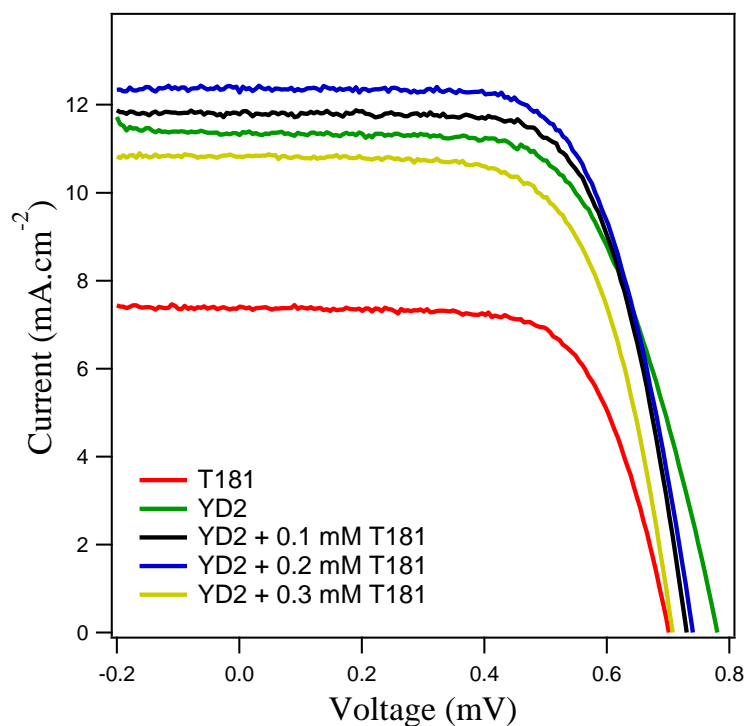
Figure 14: The current-voltage characteristic curves of YD2, T181, YD2 + 0.1 mM T181, YD2 + 0.2 mM T181, and YD2 + 0.3 mM T181 with an iodine-based electrolyte system

The advantage of co-sensitization was clearly demonstrated in the current-voltage characteristic curves. The solar cell using T181 as a sensitizer displayed a photocurrent density (J_{sc}) of 7.4 ± 0.1 mA.cm^{-2} and a value of 11.3 ± 0.1 mA.cm^{-2} for that using YD2 as a sensitizer. However, the performances of the cells using the co-sensitized T181-YD2 were significantly improved. As shown in Figure 14, the solar cell co-sensitized with a solution of 0.2 mM YD2 + 0.1 mM T181 showed a photocurrent density of a value 11.8 ± 0.1 mA.cm^{-2} higher than that of YD2 alone. Moreover, the solar cell stained in a solution of 0.2 mM YD2 + 0.2 mM T181 demonstrated the highest photocurrent density of a value 12.3 ± 0.1 mA.cm^{-2}. On the other hand, a value of 10.8 ± 0.1 mA.cm^{-2} was demonstrated for the cell stained with a solution of 0.2 mM YD2 + 0.3

mM T181 which was less than the cells with a lower concentration of the co-adsorbent T181. Based on the previous results, 0.2 mM concentration of T181 was used in the rest of the studies.

F. Co-sensitization with YD2 and DB:

After demonstrating that T181 binds to the Lewis-acid sites of the semiconductor TiO_2 by co-sensitizing it with two carboxylic acid-based dyes and acquiring the ideal concentration of T181 used for co-sensitization, dye-sensitized solar cells were fabricated in order to test the photovoltaic performance of T181 co-sensitized with DB and YD2. Two studies were performed; the first was done using an iodine-based electrolyte whereas the second using a cobalt-based electrolyte.

1. Using an Iodine-based Electrolyte System:

In our first study utilizing an iodine-based electrolyte, DSSCs were fabricated by adsorbing individual dyes T181 and YD2 having concentrations of 0.2 mM each and co-sensitized dyes T181-YD2 having the same concentrations. The photovoltaic performances of these DSSCs were studied and presented in Figure 15(a,b) and Table 5.
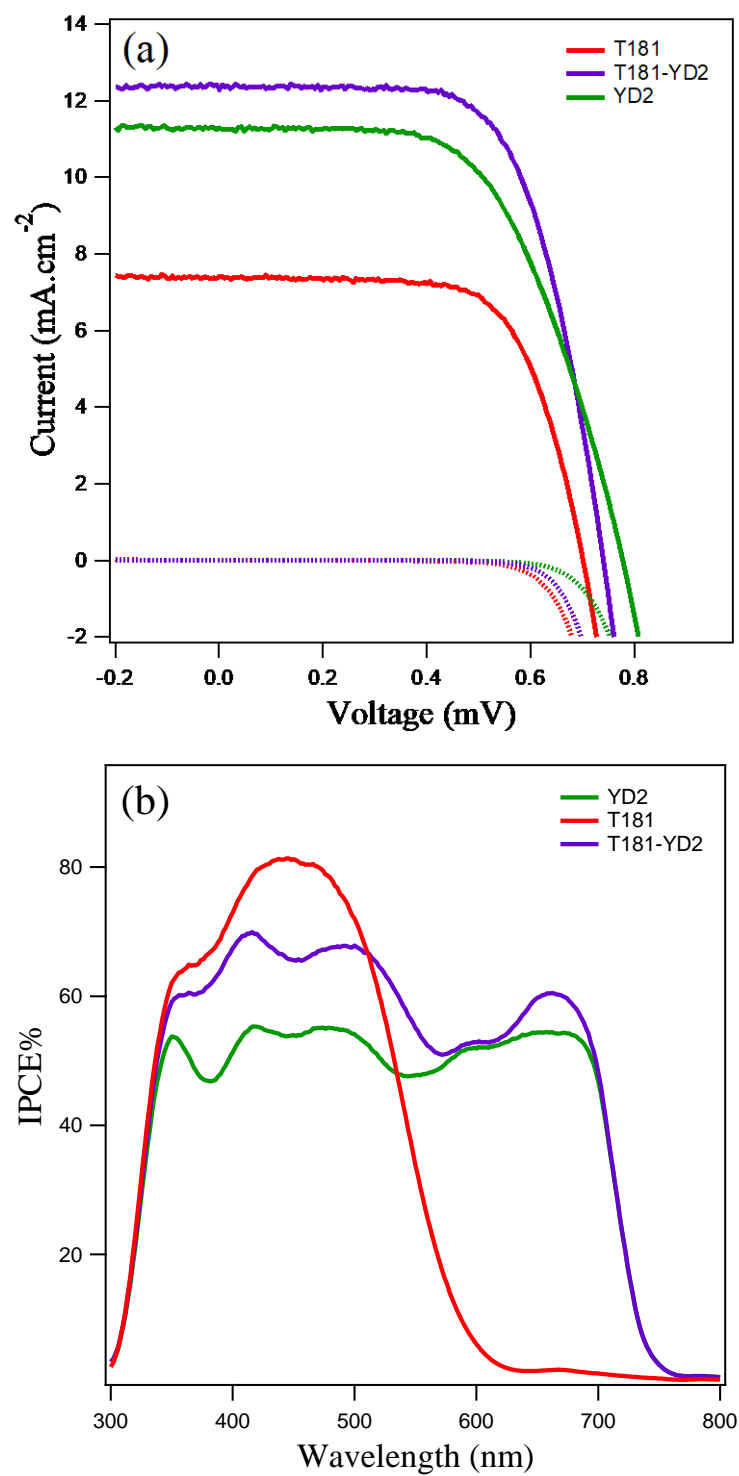
Figure 15: (a) Current density versus applied potential curves under 1000 W m^{-2} AM1.5 G illumination of DSSCs sensitized with T181 and YD2 and co-sensitized with T181-YD2 (lines) and in darkness (dotted lines). (b) Their corresponding incident photon-to-current conversion efficiency spectra

64

Table 5: Photovoltaic Performance of the T181 and YD2 DSSCs and co-sensitized T181-YD2[a]

Dye	J_{SC} (mA.cm^{-2})	V_{OC} (mV)	FF	PCE (%)
T181	7.4 (7.42)[b]	702	0.67	3.5
YD2	11.3 (11.35)[b]	776	0.60	5.2
T181-YD2	12.4 (12.89)[b]	739	0.59	5.4

[a]Measured under 100 mW.cm^{-2} simulated AM1.5 spectrum with an active area 0.5 x 0.5 cm and a black mask (0.6 x 0.6 cm); the electrolyte consisted of 2 M DMII, 0.5 M TBP, 0.1 M GuSCN, 0.05 M LiI, 0.05 M I$_2$ in ACN. [b] Integrated photocurrent (AM1.5 Global).

According to the above results, the T181-based DSSC had a power conversion efficiency of 3.5%, which was less than that of YD2 that showed a PCE% of 5.2%. The short-circuit current of the YD2-based DSSC being 11.3 mA.cm^{-2} was significantly greater than the J_{SC} of the T181-based DSSC being 7.4 mA.cm^{-2}; this was due to the limited absorption of T181 in the visible region. After co-sensitizing T181 with YD2, notable increases in the short-circuit current and power conversion efficiency were seen, as presented in Table 5. A slight increase by 3% was seen in the power conversion efficiency of the co-sensitized T181-YD2 DSSC (5.4%) compared to that of the YD2 based DSSC (5.2%). However, the V_{OC} of the co-sensitized cell was 739 mV, which was less than the V_{OC} of the YD2-based cell of 776 mV, but greater than that of the T181 based cell of 702 mV. Regarding the short-circuit currents, the co-sensitized T181-YD2 DSSC showed a J_{SC} of 12.4 mA.cm^{-2} greater than that of the YD2-based DSSC having a J_{SC} of 11.3 mA.cm^{-2}. The increase in J_{SC} was due to the complementary absorption response between T181 and YD2 which was also consistent with the IPCE% response of the co-sensitized DSSC. However, the increase in the IPCE% of the co-sensitized cell between 600 and 750 nm was probably due to a decrease in recombination processes since T181 does not absorb in this region of the spectrum.

Using the same iodine electrolyte, another co-sensitization study was done but with the T181 dye and the DB dye. DSSCs with individual T181 and DB having concentrations of 0.2 mM and 0.03 mM respectively and co-sensitized T181-DB having the same concentration as before were assembled. Their photovoltaic performances were studied and the results are presented in Figure 16 (a,b) and Table 6.
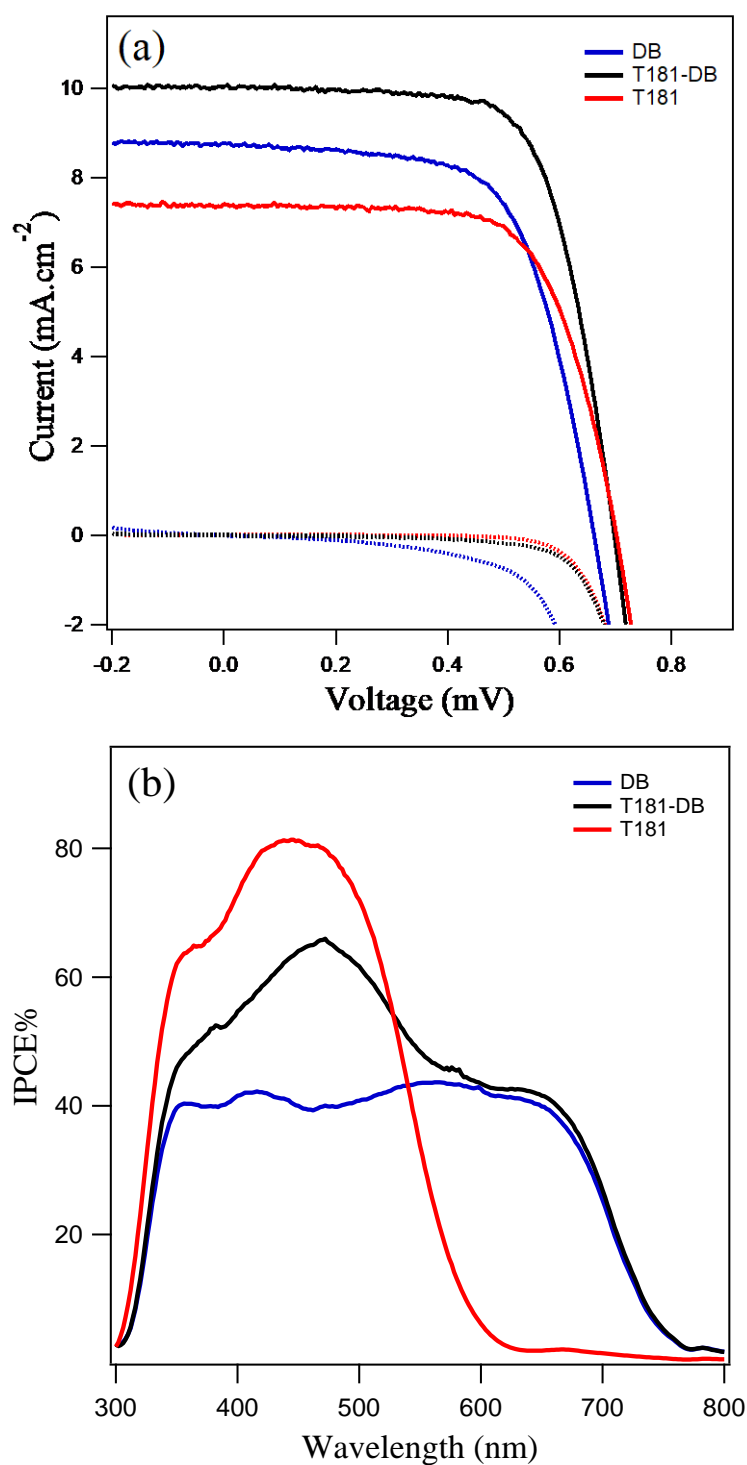
Figure 16: (a) Current density versus applied potential curves under 1000 W m^{-2} AM1.5 G illumination of DSSCs sensitized with T181 and DB and co-sensitized with T181-DB (lines) and in darkness (dotted lines). (b) Their corresponding incident photon-to-current conversion efficiency spectra

Table 6: Photovoltaic Performance of the T181 and DB DSSCs and co-sensitized T181-DB[a]

Dye	J_{SC} (mA.cm^{-2})	V_{OC} (mV)	FF	PCE (%)
T181	7.4 (7.42)[b]	702	0.67	3.5
DB	8.8 (8.73)[b]	660	0.67	3.7
T181-DB	10.0 (10.60)[b]	697	0.68	4.8

[a]Measured under 100 mW.cm^{-2} simulated AM1.5 spectrum with an active area 0.5 x 0.5 cm and a black mask (0.6 x 0.6 cm); the electrolyte consisted of 2 M DMII, 0.2 M TBP, 0.1 M GuSCN, 0.05 M LiI, 0.05 M I$_2$ in ACN. [b] Integrated photocurrent (AM1.5 Global).

The power conversion efficiency of DB (3.7%) was larger than that of T181 (3.5%). Moreover, the DB-based DSSC showed a greater short-circuit current of 8.8 mA.cm^{-2} in comparison to that of T181 of 7.4 mA.cm^{-2}. This difference in J_{SC} was due to the larger absorbance of DB in the visible region compared to the absorbance of T181. Concerning the co-sensitized T181-DB DSSC, the open-circuit voltage, short-circuit current, and power conversion efficiency were larger than those of DSSCs with individual dyes. The power conversion efficiency of the co-sensitized T181-DB cell (4.8%) was larger by 30% than that of DB (3.7%). Furthermore, the J_{SC} of the co-sensitized T181-DB DSSC was 10.0 mA.cm^{-2} larger than that of the DB-based DSSC which was 8.8 mA.cm^{-2}. This is because of the complementary absorption response between the two dyes as mirrored in the high IPCE% responses especially between 400 and 600 nm where T181 has its maximum absorption. Moreover, the T181-DB cell had a V_{OC} of 697 mV greater than the V_{OC} of the DB-based cell which was 660 mV.

2. Using a Cobalt-based Electrolyte System:

After studying the efficiencies of co-sensitizing YD2 and DB with our synthetic dye T181 using an iodine-based electrolyte, the same studies were repeated

using the same dyes but using a cobalt-based electrolyte system. As shown in Scheme 7, T181 has a structure bearing an extended linker fragment having arms connected to an oxygen atom. These fragments are responsible of increasing the steric barrier which blocks the approach of the electrolyte to the TiO_2. Such structure is expected to be effective with the cobalt-based electrolyte and the positive effect of the large alkyl groups would be more significant in this electrolyte compared to the iodine-based one. This might predictably lead to the retardation of recombination.[150,151,152] Hereby, the photovoltaic performances of DSSCs sensitized with the individual dyes T181 and YD2 having a concentration in solution of 0.2 mM each along with that of the co-sensitized dyes T181-YD2 with the same concentration as the individual dyes are presented in Figure 17 and Table 7.

Figure 17: (a) Current density versus applied potential curves under 1000 W m^{-2} AM1.5 G illumination of DSSCs sensitized with T181 and YD2 and co-sensitized with T181-YD2 (lines) and in darkness (dotted lines). (b) Their corresponding incident photon-to-current conversion efficiency spectra

Table 7: Photovoltaic Performance of the T181 and YD2 DSSCs and co-sensitized T181-YD2[a]

Dye	J_{SC} (mA.cm^{-2})	V_{OC} (mV)	FF	PCE (%)
T181	6.1 (6.0)[b]	712	0.71	3.1
YD2	6.7 (6.72)[b]	718	1.01	4.9
T181-YD2	10.3 (9.2)[b]	807	7.70	6.4

[a]Measured under 100 mW.cm^{-2} simulated AM1.5 spectrum with an active area 0.5 x 0.5 cm and a black mask (0.6 x 0.6 cm); the electrolyte consisted of 0.25 M Co(II), 0.06 M Co(III), 0.1 M LiClO$_4$ and 0.6 M TBP. [b] Integrated photocurrent (AM1.5 Global).

By referring to the above data, the power conversion efficiency of YD2 (4.9%) was greater than that of T181 (3.1%). Furthermore, T181 showed a slightly lower short-circuit current of 6.1 mA.cm^{-2} compared to that of YD2 having 6.7 mA.cm^{-2}. This slight increase for YD2 was due to the fact that YD2 had a better light absorption in the visible region than T181. However, remarkable increases in J_{SC}, V_{OC}, and PCE were seen upon the co-sensitization of T181 with YD2. As shown in Figure 17(a) and Table 7, the PCE of the co-sensitized T181-YD2 (6.4%) increased by 30% in comparison to that of YD2 alone (4.9%). Moreover, the open-circuit voltage of T181-YD2 being 807 mV was remarkably greater than that of the individual YD2 being 718 mV. With respect to the short-circuit current, the co-sensitized T181-YD2 showed a J_{SC} of 10.3 mA.cm^{-2} whereas the individual YD2 showed a J_{SC} of 6.7 mA.cm^{-2}. This result can be explained from the IPCE spectra where T181-YD2 showed a higher IPCE% when compared to YD2 alone.

In a second study using the same cobalt electrolyte, DSSCs were sensitized with individual dyes T181 and DB with a concentration of 0.2 mM and 0.03 mM,

respectively, and co-sensitized dyes T181-DB with the same concentration as the

individual dyes. The photovoltaic performances of those DSSCs were tested and

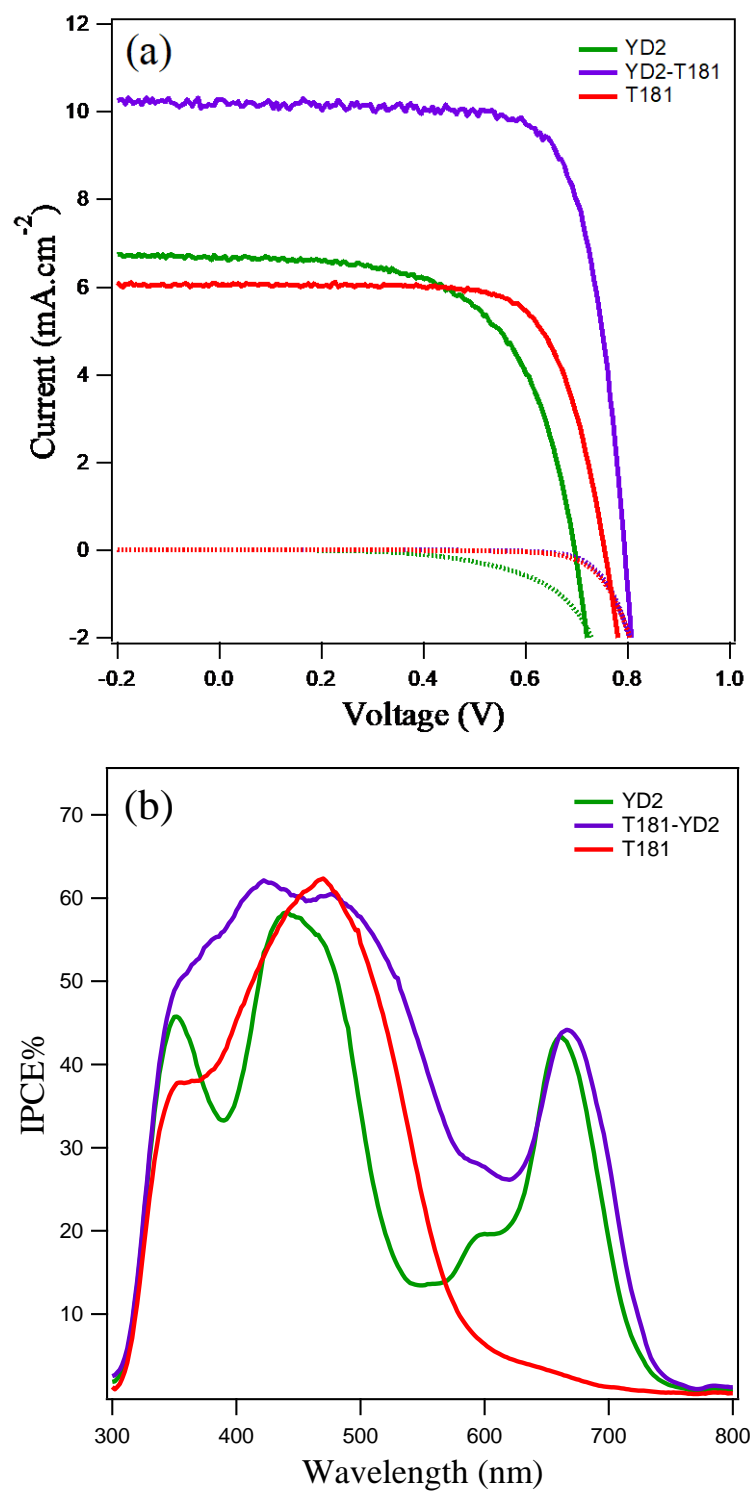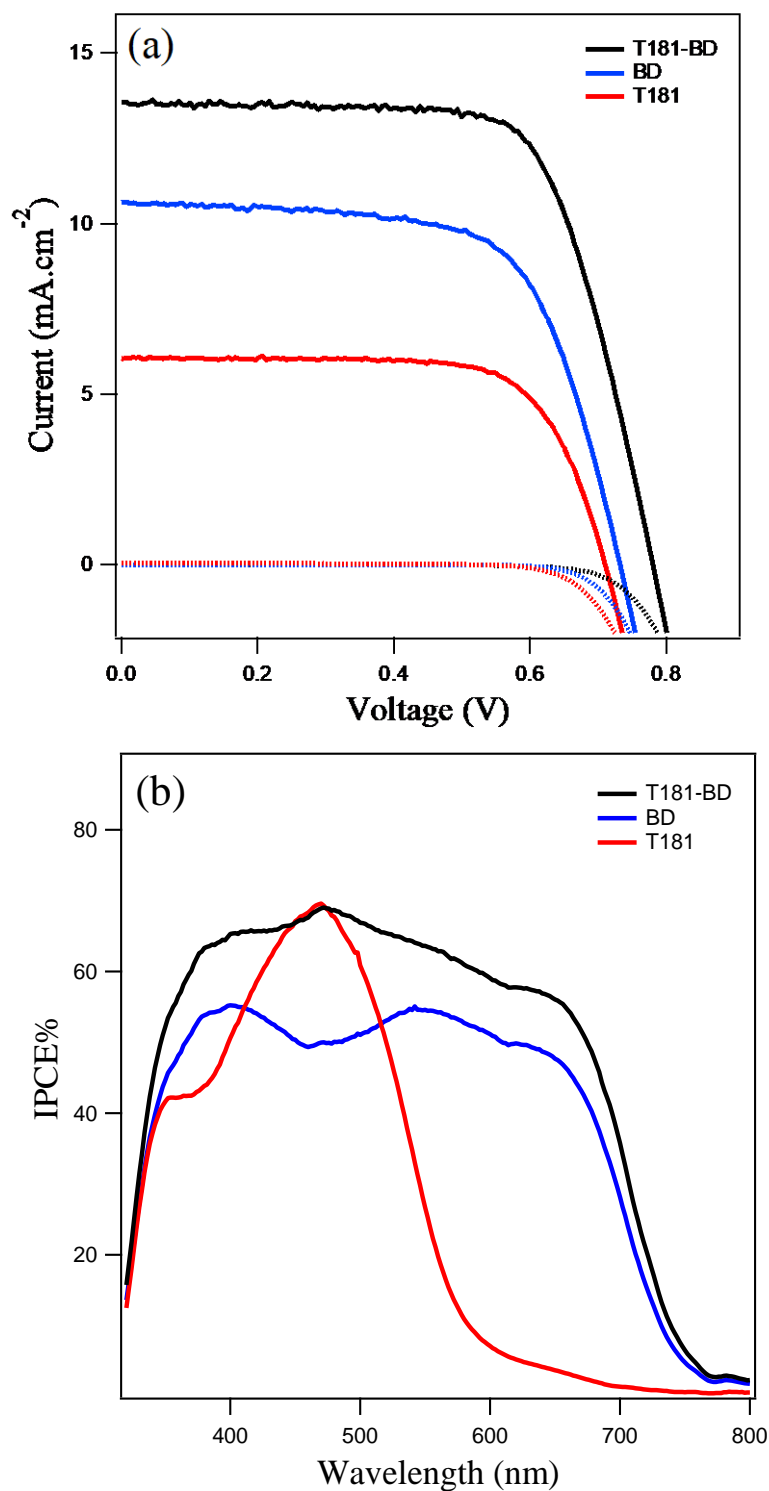presented in Figure 18 and Table 8.

Figure 18: (a) Current density versus applied potential curves under 1000 W m^{-2} AM1.5 G illumination of DSSCs sensitized with T181 and DB and co-sensitized with T181-DB (lines) and in darkness (dotted lines). (b) Their corresponding incident photon-to-current conversion efficiency spectra

Table 8: Photovoltaic Performance of the T181 and DB DSSCs and co-sensitized T181-DB[a]

Dye	J_{SC} (mA.cm^{-2})	V_{OC} (mV)	FF	PCE (%)
T181	6.1 (6.0)[b]	712	0.71	3.1
DB	10.6 (10.7)[b]	737	0.66	5.1
T181-DB	13.3 (13.0)[b]	781	0.71	7.4

[a]Measured under 100 mW.cm^{-2} simulated AM1.5 spectrum with an active area 0.5 x 0.5 cm and a black mask (0.6 x 0.6 cm); the electrolyte consisted of 0.25 M Co(II), 0.06 M Co(III), 0.1 M LiClO$_4$ and 0.2 M TBP. [b]Integrated photocurrent (AM1.5 Global).

According to the data, the DB-based DSSC had a power conversion efficiency of 5.1%, which is greater than that of T181 that showed a PCE of 3.1%. Moreover, T181 showed a much lower short-circuit current (J_{SC}) of 6.1 mA.cm^{-2} than DB which has a J_{SC} of 10.6 mA.cm^{-2}. This was due to the limited absorption of T181 in the visible region as shown in its absorption spectrum in Figure 9 and the IPCE in Figure 18(b). Upon co-sensitizing T181 with DB, remarkable increases in IPCE, J_{SC}, and V_{OC} were shown, Figure 18(a,b) and Table 8. The PCE of the co-sensitized T181-DB (7.4%) showed a 45% increase compared to that of DB alone (5.1%). The V_{OC} increased by 44 mV for the T181-DB co-sensitized DSSC when compared to that of DB alone. The increase of the J_{SC} values of the co-sensitized cell (J_{SC} = 13.3 mA.cm^{-2}) was mainly due to the complementary absorption response of T181 with the DB. This result was also consistent with the IPCE% response of the co-sensitized DSSC especially in the 400 to 600 nm region where T181 has its maximum absorption.

G. Electrochemical Impedance Spectroscopy Measurements:

For the aim of understanding the above mentioned results especially the higher V_{OC} and the high efficiencies of the co-sensitized dyes using both electrolytes,

electrochemical impedance spectroscopy (EIS) measurments were performed on all the

assembled DSSCs at open-circuit voltage at different light intensities.

1. DSSCs with the Iodine-based Electrolyte System:

The plots of the chemical capacitance (C_μ), the charge recombination

resistance (R_{CT}), and the electron lifetimes of the inidividual YD2 and T181 DSSCs and

the co-sensitized T181-YD2 DSSC using the iodine-based electrolyte are presented in
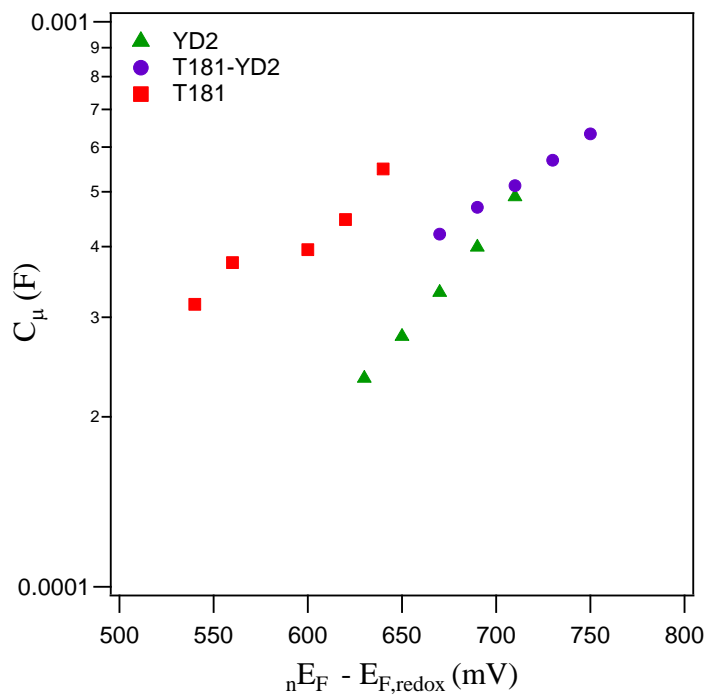
Figures 19, 20, and 21 respectively.

Figure 19: Chemical capacitance values obtained from EIS of T181, YD2, and the co-sensitized T181-YD2 DSSCs in an iodine-based electrolyte

Figure 20: Charge transfer resistance values obtained from EIS of T181, YD2, and the co-sensitized T181-YD2 DSSCs in an iodine-based electrolyte

Figure 21: Electron lifetime values obtained from EIS of T181, YD2, and the co-sensitized T181-YD2 DSSCs in an iodine-based electrolyte

From the results presented in Table 5, we have seen that the V_{OC} of the co-sensitized T181-YD2 DSSC showed a decrease compared to that of the individual YD2 based DSSC. This is compatible with the chemical capacitance values presented in Figure 19, where the T181-YD2 co-sensitized device showed a shift $\Delta(_nE_F - E_{F,redox})$ to a lower value in comparison to the YD2 sensitized device. While $E_{F,redox}$ or the redox electrolyte's Fermi level was kept the same since the same electrolyte was used in the three cells, the $_nE_F$ or the electron's quasi-Fermi energy level in the TiO_2 film was considered to be shifted downwards. This downward shift in the quasi-Fermi level of TiO_2 was attributed to the decrease in the dye loading amounts of YD2 and T181 when co-sensitized together as shown in Table 4 earlier, which resulted in lower electron

injection rates into TiO_2 hence a lower $_nE_F$ and V_{OC}. Furthermore, in Figure 20, the R_{CT} values of the T181-YD2 co-sensitized device were 37 times and 4 times higher than those of T181 and YD2, respectively. The larger R_{CT} values that correspond to lower electron recombination in the co-sensitized device were consistent with its larger short-circuit currents presented earlier, which were probably due to the blockage of the electrolyte pathway to the TiO_2 surface reducing the recombination processes. However, the recombination resistance of the T181-YD2 device was only 4 times greater than that of the YD2 device, this increase was not enough to cause an increase in the open-circuit voltage of the device. The enhancement of the short-circuit current and the recombination resistance of the co-sensitized device explained the slight increase in its conversion efficiency. Moreover, the electron lifetimes (τ_n) in the three solar cells were evaluated from the EIS experiments ($\tau_n = R_{CT}.C_\mu$) and shown in Figure 21. The τ_n values were consistent with the slower recombination processes in the T181-YD2 solar cell when compared to the YD2 based solar cell.

Furthermore, electrochemical impedance spectroscopy (EIS) measurments at open-circuit voltage at different light intensities were performed on individual T181 and DB based DSSCs and co-sensitized T181-DB DSSC with the iodine-based electrolyte. The plots of the chemical capacitance (C_μ), the charge recombination resistance (R_{CT}), and the electron lifetimes of those DSSCs assembled also in an iodine-based electrolyte are presented in Figures 22, 23, and 24 respectively.

Figure 22: Chemical capacitance values obtained from EIS of T181, DB, and the co-sensitized T181-DB DSSCs in an iodine-based electrolyte
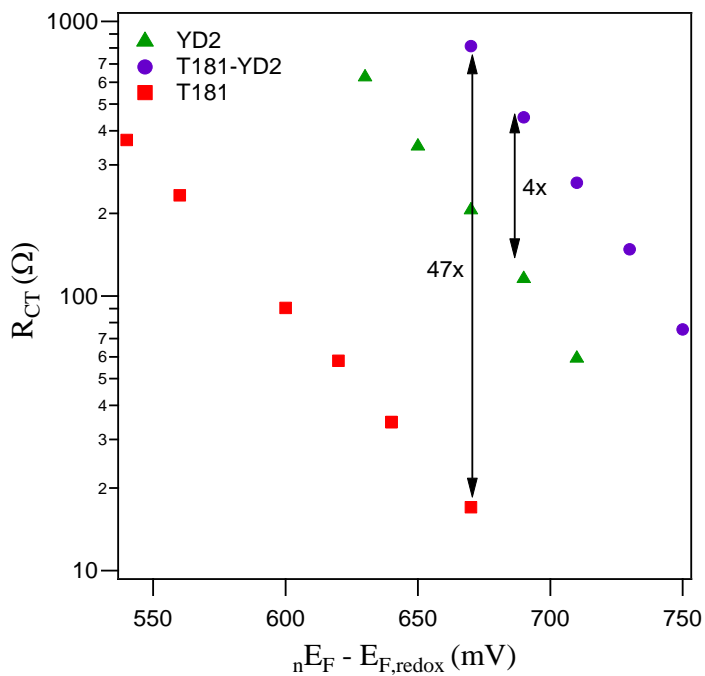

Figure 23: Charge transfer resistance values obtained from EIS of T181, DB, and the co-sensitized T181-DB DSSCs in an iodine-based electrolyte
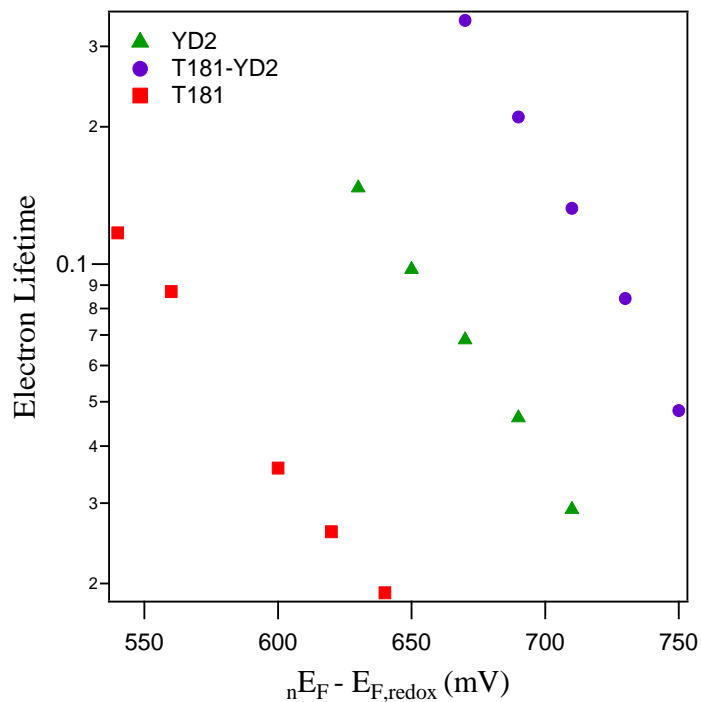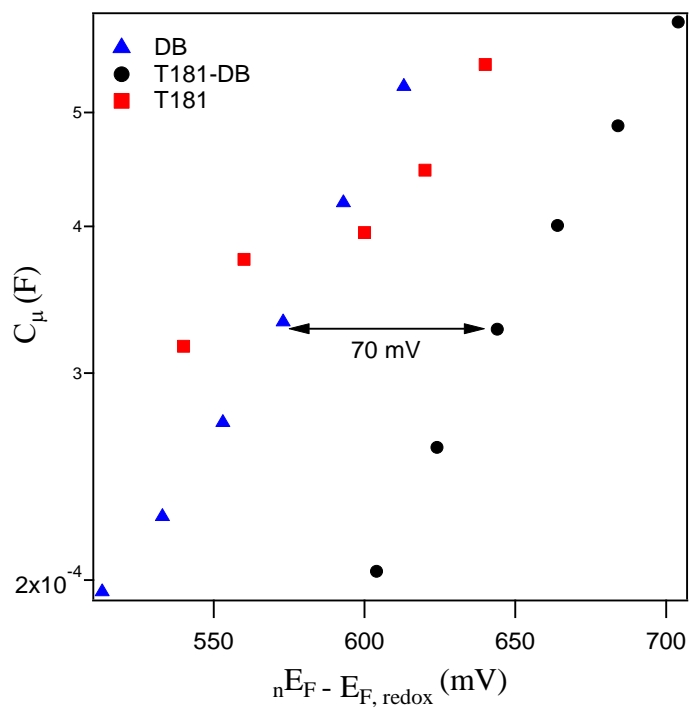
Figure 24: Electron lifetime values obtained from EIS of T181, DB, and the co-sensitized T181-DB DSSCs in an iodine-based electrolyte

From the current-voltage curves in Figure 16(a) and the values of Table 6, it was clearly seen that the open-circuit voltage of the co-sensitized T181-DB device is larger than that of the individual DB based device. This increase in V_{OC} was also depicted in the chemical capacitance curves of the devices, where the co-sensitized device showed a shift $\Delta(_nE_F - E_{F,redox})$ of approximately 70 mV higher than the DB-based device. This shift designates that the $_nE_F$ of the TiO$_2$ film was shifted upwards since the $E_{F,redox}$ was kept the same in all three devices by using the same electrolyte. The upward shift of the electrons' quasi-Fermi energy level of the TiO$_2$ film resulting from the increase in the total dye loading amount of the co-sensitized device, as shown earlier in Table 3, was the reason behind the higher V_{OC} of the co-sensitized device. Furthermore, the short-circuit current of the co-sensitized T181-DB cell also showed an

increase compared to that of the individual DB-based cell. This was explained by the charge transfer resistance values depicted in Figure 23, where the values of the T181-DB device were 30 times and 10 times larger than the values of the DB and the T181-based devices respectively. The effect of the increase of the dye loading amount in the co-sensitized cell, which prevents the approach between the electrolyte and the surface of TiO_2 was the reason behind decreasing the electron recombination rates and increasing the values of the charge transfer resistance. Moreover, the electron lifetime values shown in Figure 24 were consistent with the slower recombination processes explained above. All these factors explain the enhancement of the power conversion efficiency of the co-sensitized T181-DB cell compared to the individual dye-based cells.

2. DSSCs with the Cobalt-based Electrolyte System:

In order to explain the results of co-sensitizing YD2 and DB with T181 using a cobalt-based electrolyte system, EIS measurements were performed on the individual and co-sensitized devices assembled using the cobalt-based electrolyte system and the plots of the chemical capacitance (C_μ), the charge recombination resistance (R_{CT}), and the electron lifetimes of those DSSCs are presented in Figures 25, 26, and 27 respectively.

Figure 25: Chemical capacitance values obtained from EIS of T181, YD2, and the co-sensitized T181-YD2 DSSCs in a cobalt-based electrolyte
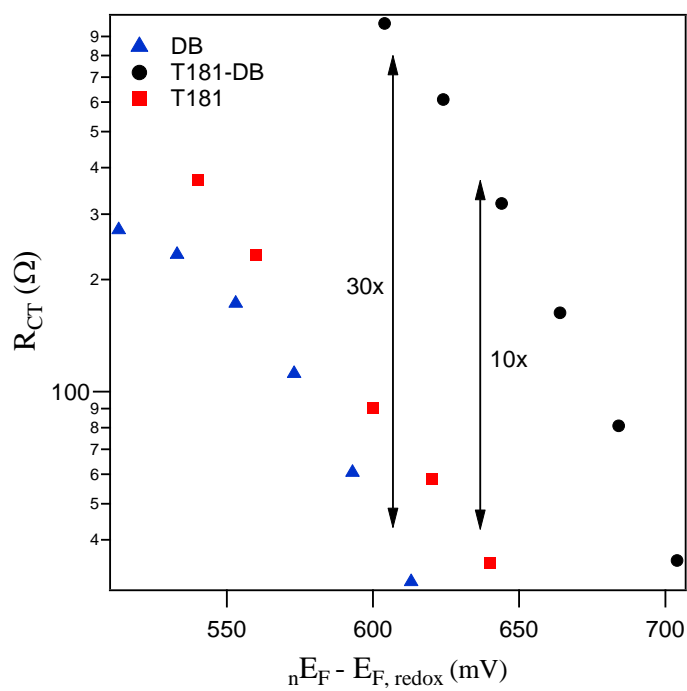

Figure 26: Charge Transfer Resistance values obtained from EIS of T181, YD2, and the co-sensitized T181-YD2 DSSCs in a cobalt-based electrolyte
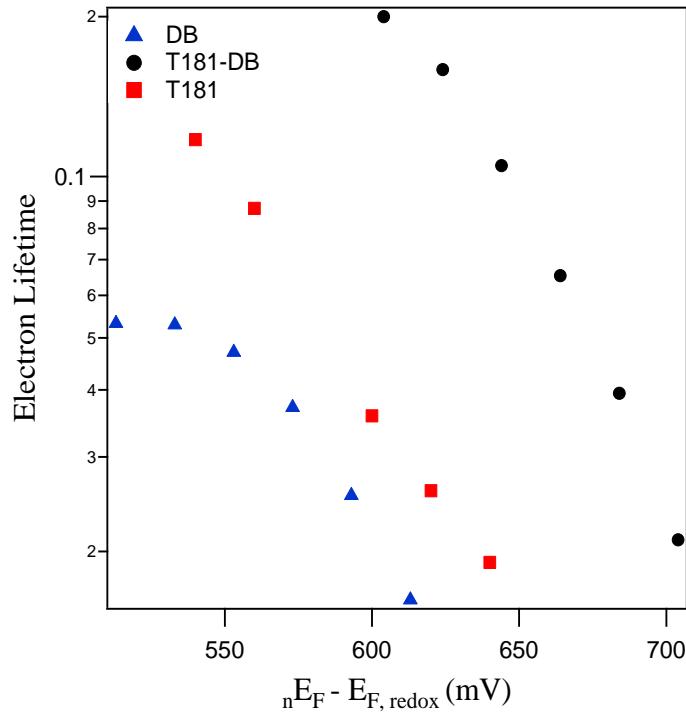
Figure 27: Electron lifetime values obtained from EIS of T181, YD2, and the co-sensitized T181-YD2 DSSCs in a cobalt-based electrolyte

From the results presented in Table 7, we have seen that the open-circuit voltage of the co-sensitized T181-YD2 was greater than that of the individual YD2 based device. This result was not clearly depicted in the values of the chemical capacitance presented in Figure 25, which did not show a significant shift in ($_nE_F$ − $E_{F,redox}$) between the co-sensitized T181-YD2 and the individual YD2-based device. However, the increase in the open-circuit voltage was explained using the charge transfer resistance values in Figure 26, where the values of the T181-YD2 device were 45 times greater than those of the YD2-based device. This considerable increase in R_{CT} indicates the large regression in the recombination rates of the co-sensitized device compared to the YD2 based device, which was due to the increase in the total dye loading amount of the co-sensitized device. The high regression in the recombination rates of the co-sensitized cell lead to an increase in the open-circuit voltage of the

device. Moreover, the lower electron recombination caused a higher power conversion efficiency and a higher short-circuit current of the device compared to the YD2-based device. Furthermore, the electron lifetime values of Figure 27 were consistent with the slower recombination processes seen by the R_{CT} values of the co-sensitized T181-YD2 solar cell.

In the second study using the same cobalt-based electrolyte system where T181 was co-sensitized with DB, the EIS measurements of the DSSCs were performed and the values of C_μ, R_{CT}, and the electron lifetimes of those DSSCs are presented in Figures 28, 29, and 30 respectively.
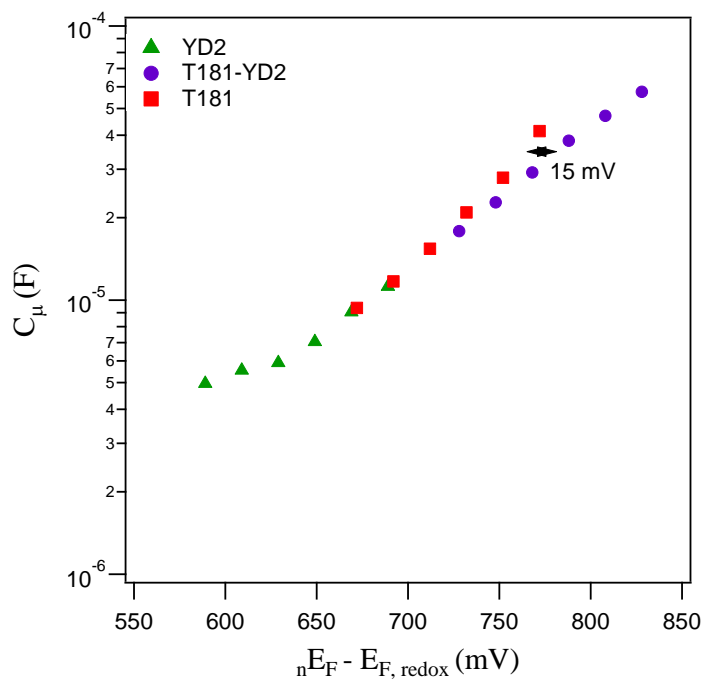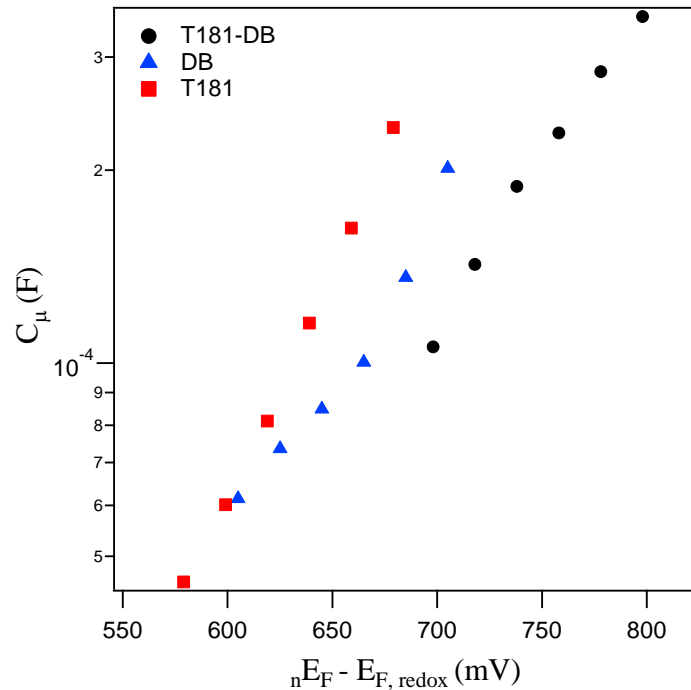

Figure 28: Chemical capacitance values obtained from EIS of T181, DB, and the co-sensitized T181-DB DSSCs in a cobalt-based electrolyte
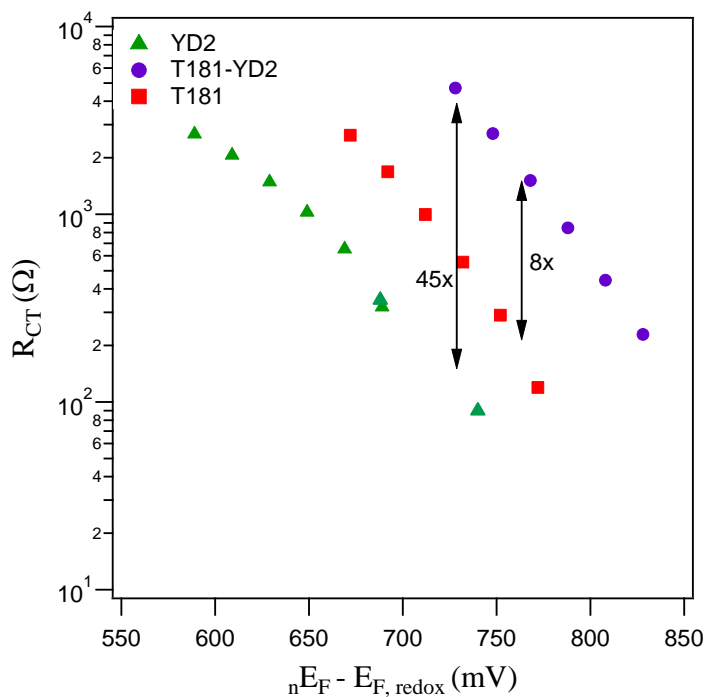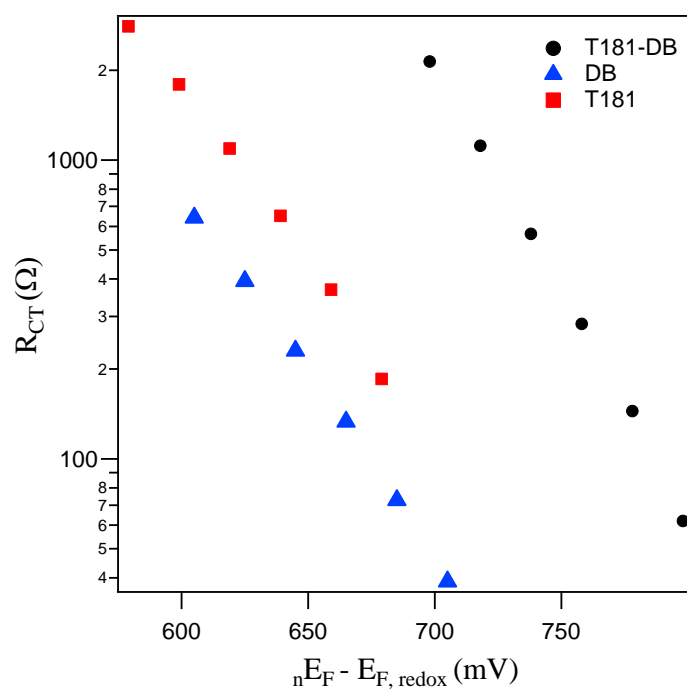
Figure 29: Charge transfer resistance values obtained from EIS of T181, YD2, and the co-sensitized T181-YD2 DSSCs in a cobalt-based electrolyte
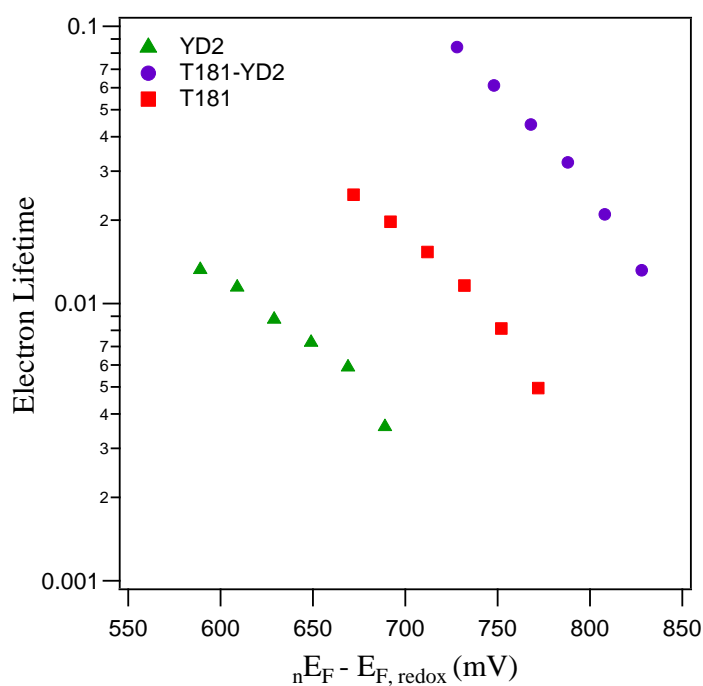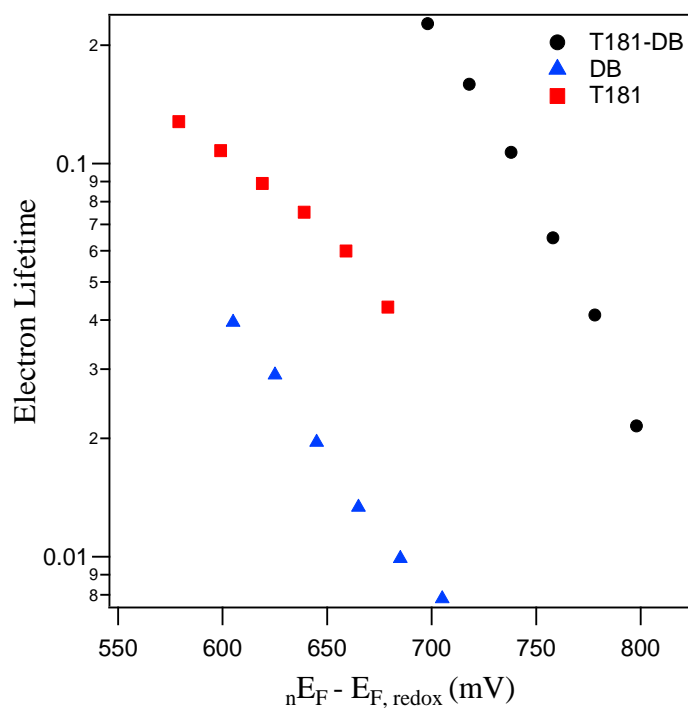

Figure 30: Electron lifetime values obtained from EIS of T181, YD2, and the co-sensitized T181-YD2 DSSCs in a cobalt-based electrolyte

From the results shown in Figure 28 of the chemical capacitance values, the T181-DB co-sensitized device showed a shift of 40-50 mV approximately towards a higher value in the ($_nE_F - E_{F,redox}$). This upward shift could be a reason for the increase in the V_{OC} of the co-sensitized device compared to the DB-based device. The above mentioned higher voltage was due to the larger dye coverage on the surface of TiO_2 which resulted in higher electron injection rates into TiO_2 and subsequently, a higher electron quasi-Fermi energy level $_nE_F$ and a larger open-circuit voltage. Futhermore, in Figure 29, the charge transfer resistance values of the co-sensitized T181-DB cell were significantly higher than those of the individual DB based cell indicating lower electron recombination rates probably due to the prevention of the approach between the electrolyte and the surface of TiO_2. The upward shift in $_nE_F$ and the decrease in recombination rates were consistent with the high open-circuit voltage and short-circuit current of the co-sensitized device. In addition, the high electron lifetimes of the T181-DB solar cell depicted in Figure 30 were also in consistency with the slow recombination processes explained above.

CHAPTER IV

CONCLUSION

In conclusion, we were successful in synthesizing two dyes T181 and T182 having pyridine and pyridine oxide anchoring groups, respectively. After proving that T181 binds to the Lewis-acid sites of TiO_2 which was not the case with T182; T181 was effectively co-sensitized with carboxylic acid-based dyes YD2 and DB in fully operating DSSCs using iodine and cobalt-based electrolyte systems. The dye loading measurements of T181 with DB clearly showed that the two dyes do not compete on the same adsorption site since the total dye loading amount was about the sum of the amounts of the two dyes in the individual films. However, the total dye loading amount of T181 and YD2 showed a decrease from the sum of the two dyes in the individual films, which was explained by the structure-size effect on the dye loadings of T181 and YD2, where YD2 and T181 have similar structural dimensions. Moreover, the photovoltaic performances of the co-sensitized T181-YD2 and T181-DB liquid DSSCs were enhanced in both electrolyte systems in comparison to the individual YD2 and DB DSSCs. However, better photovoltage and photocurrent enhancements were seen for co-sensitized DSSCs assembled with the cobalt-based electrolyte system since the structure of T181 bearing an extended linker fragment is more effective with the cobalt-based electrolyte, where the positive effect of the large alkyl groups would be more significant compared to an iodine-based electrolyte. Furthermore, the electrochemical impedance spectroscopy measurements of the individual and co-sensitized DSSCs in both electrolyte systems were consistent with the results seen. The EIS experiments

explained the reason behind the increases of V_{OCS} and I_{SCS}, that were due to large decreases in recombination processes and E_F shifts towards higher values. As a final conclusion, the method of co-sensitization of carboxylic acid and pyridine-based dyes proved to be a successful strategy to increase light absorption, decrease recombination losses, and enhance the performance of dye sensitized solar cells.
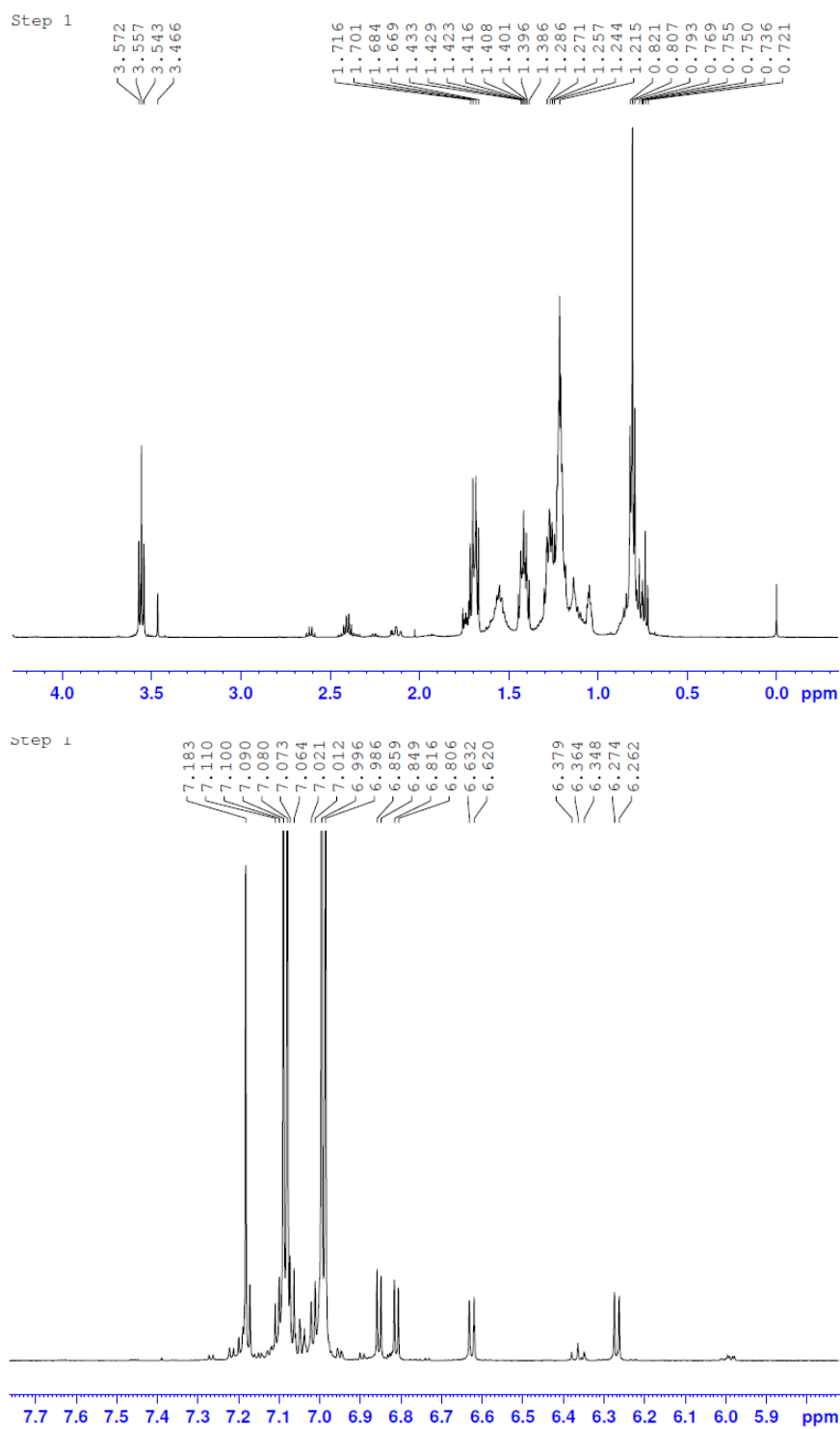
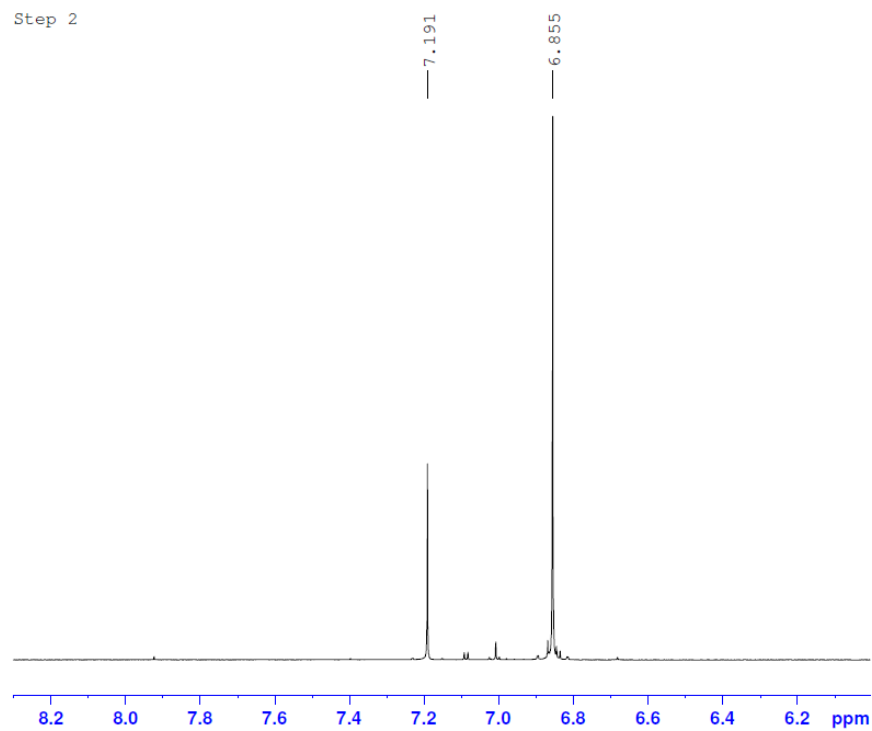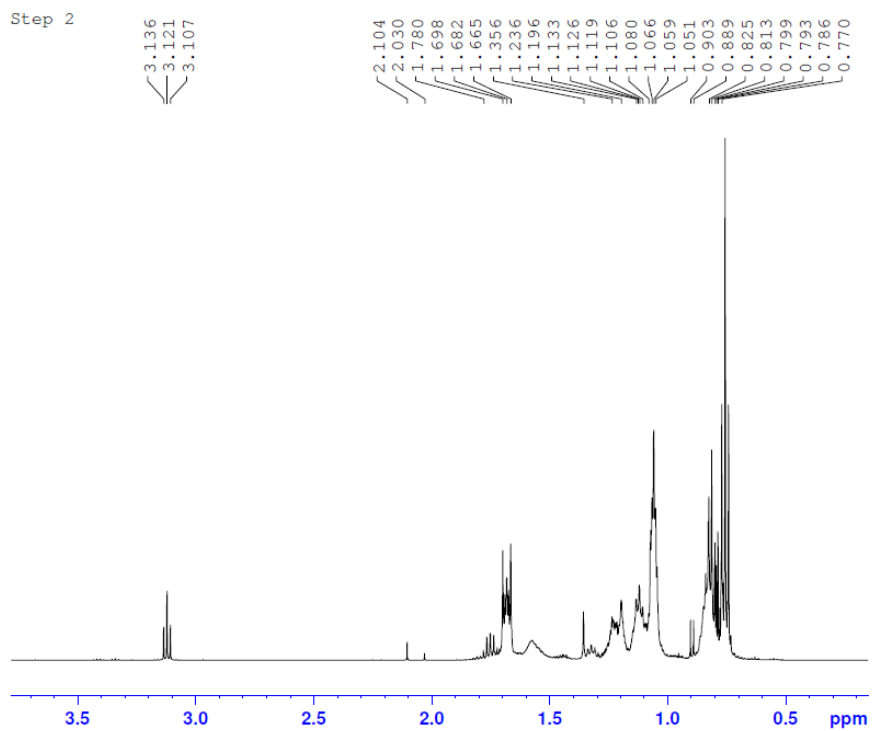**Figure 31S:** ^{1}H NMR of 4-dihexyl-4H-cyclopenta[2,1-b:3,4-b']dithiophene

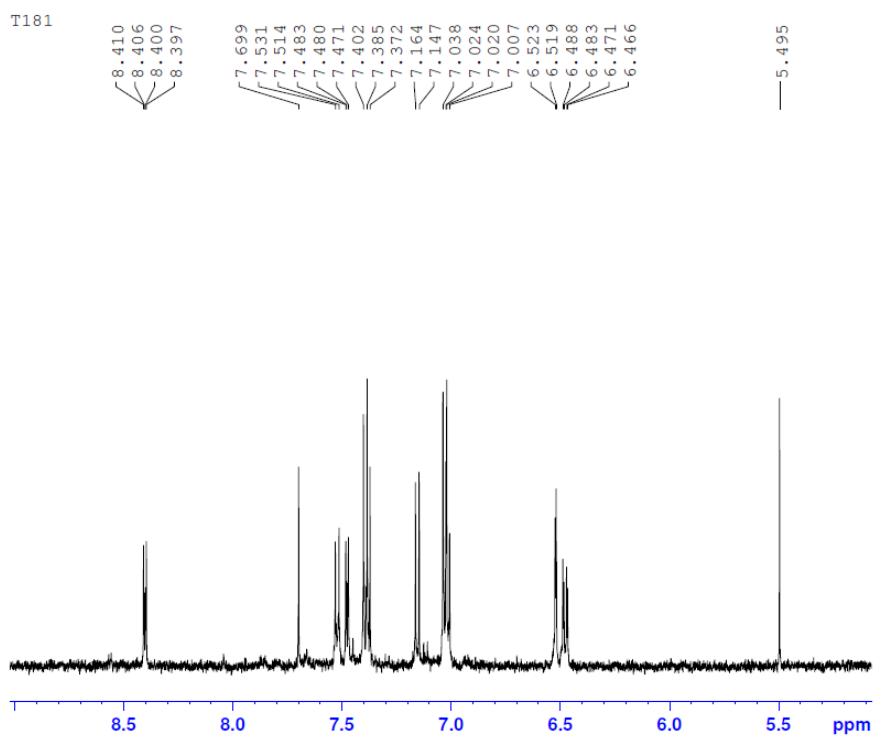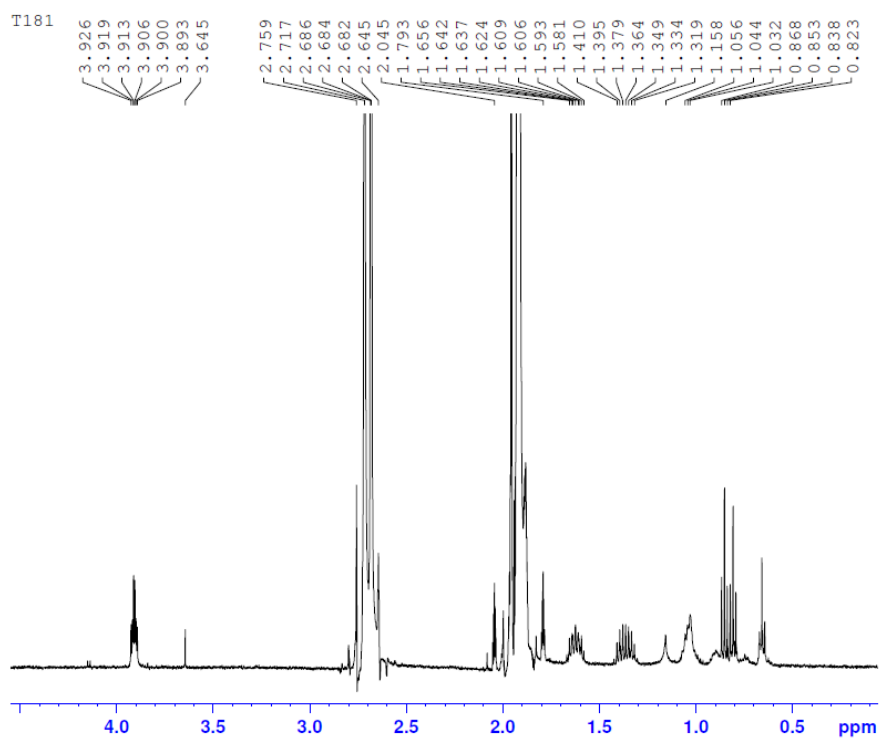**Figure 32S:** ¹H NMR of 2,6-dibromo-4,4-dihexyl-4H-cyclopenta[2,1-b:3,4-b']dithiophene
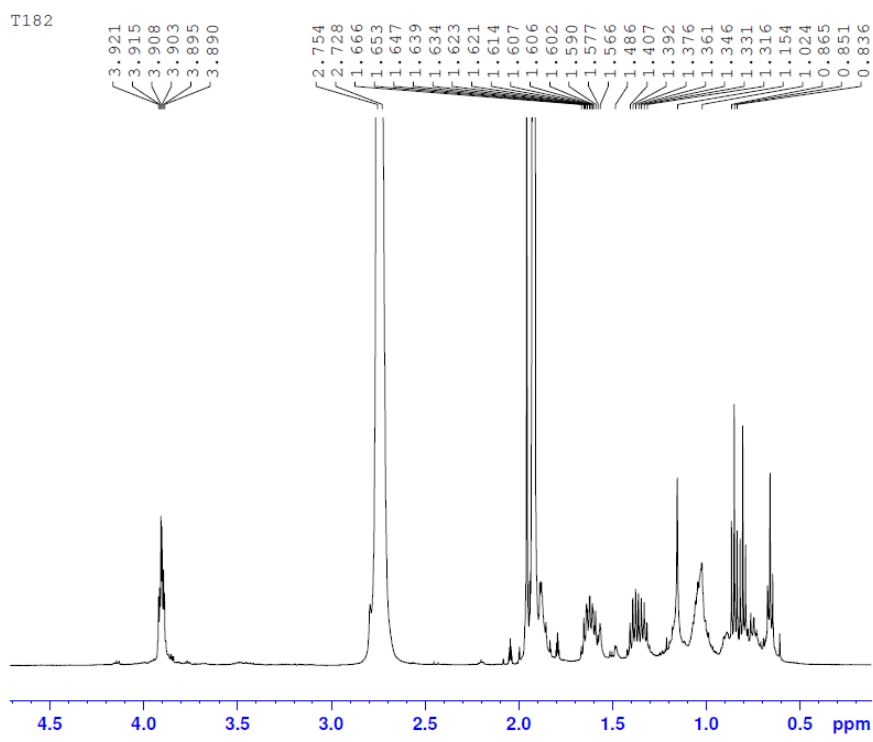
Figure 33S: ^{1}H NMR of T181 dye
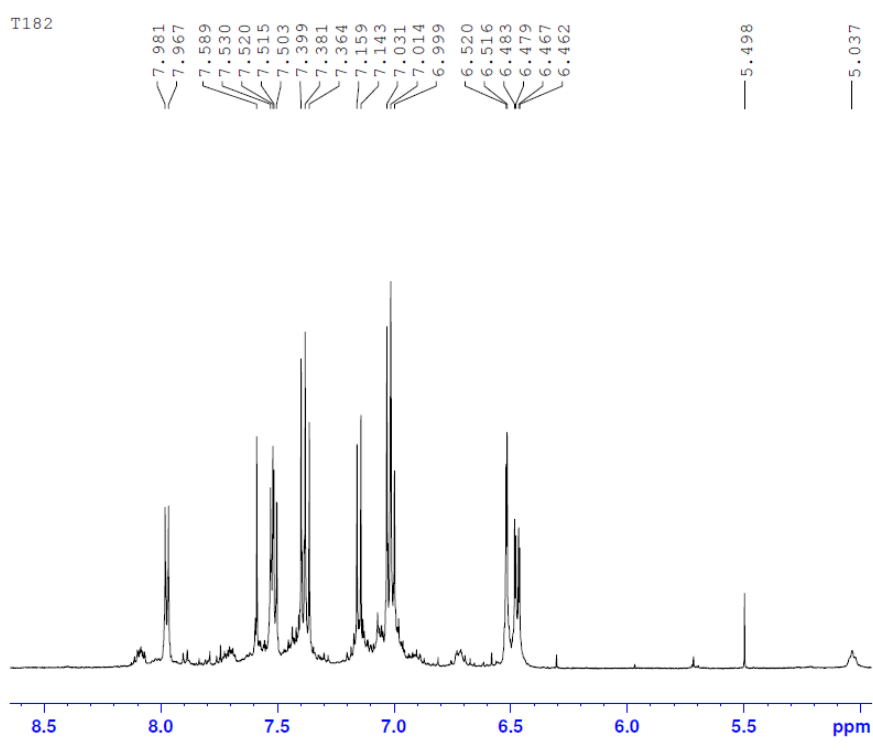
T182

Figure 34S: ^{1}H NMR of T182 dye
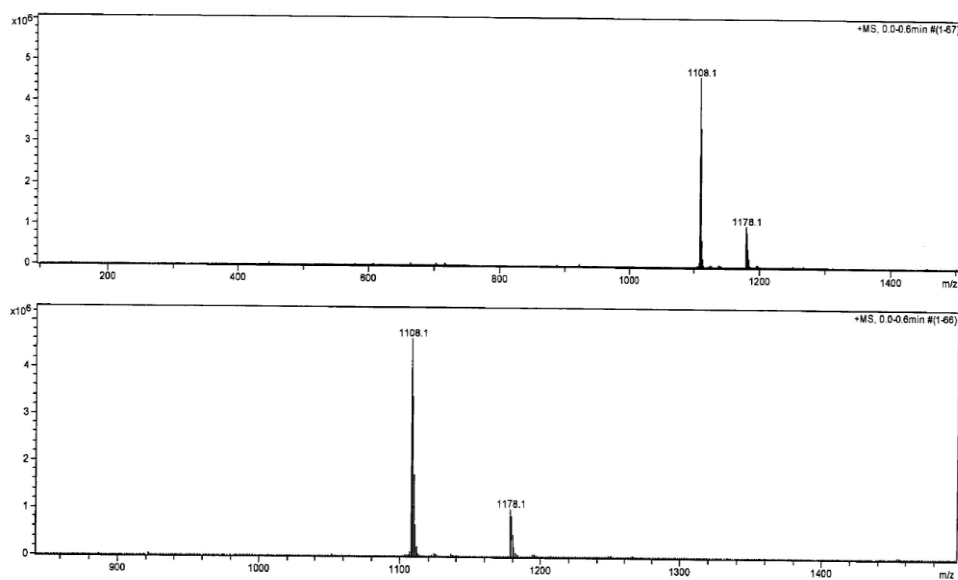
Figure 35S: Mass Spectroscopy of T181

Figure 36S: Mass Spectrometry of T182

REFERENCES

1. Dresselhaus, M.; Thomas, I., Alternative energy technologies. *Nature* **2001,** *414* (6861), 332.
2. Twidell, J.; Weir, T., *Renewable energy resources*. Routledge: 2015.
3. Johansson, T. B.; Burnham, L., *Renewable energy: sources for fuels and electricity*. Island press: 1993.
4. Asif, M.; Muneer, T., Energy supply, its demand and security issues for developed and emerging economies. *Renew. Sust. Energ. Rev.* **2007,** *11* (7), 1388-1413.
5. Uno, K., Energy Demand and Supply. In *Environmental Options: Accounting for Sustainability*, Springer: 1995; pp 49-107.
6. Quaschning, V., *Understanding renewable energy systems*. Routledge: 2016.
7. Lewis, N. S., Toward cost-effective solar energy use. *science* **2007,** *315* (5813), 798-801.
8. Myers, D. R., *Solar radiation: practical modeling for renewable energy applications*. CRC Press: 2017.
9. Herzog, A. V.; Lipman, T. E.; Kammen, D. M., Renewable energy sources. *Encyclopedia of Life Support Systems (EOLSS). Forerunner Volume-'Perspectives and Overview of Life Support Systems and Sustainable Development* **2001.**
10. Schiermeier, Q.; Tollefson, J.; Scully, T.; Witze, A.; Morton, O., Energy alternatives: Electricity without carbon. *Nature News* **2008,** *454* (7206), 816-823.
11. Hoffmann, W., PV solar electricity industry: Market growth and perspective. *Sol. Energy Mater Sol. Cells* **2006,** *90* (18), 3285-3311.
12. Reichelstein, S.; Yorston, M., The prospects for cost competitive solar PV power. *Energy Policy* **2013,** *55*, 117-127.
13. Jäger-Waldau, A., Snapshot of Photovoltaics—March 2017. *Sustainability* **2017,** *9* (5), 783.
14. Chapin, D. M.; Fuller, C.; Pearson, G., A new silicon p-n junction photocell for converting solar radiation into electrical power. *J. Appl. Phys.* **1954,** *25* (5), 676-677.
15. Pizzini, S.; Acciarri, M.; Binetti, S., From electronic grade to solar grade silicon: chances and challenges in photovoltaics. *Phys. Status Solidi A* **2005,** *202* (15), 2928-2942.
16. Dhere, N. G., Toward GW/year of CIGS production within the next decade. *Sol. Energy Mater Sol. Cells* **2007,** *91* (15), 1376-1382.
17. Shockley, W., The Theory of p-n Junctions in Semiconductors and p-n Junction Transistors. *Bell Labs Tech J.* **1949,** *28* (3), 435-489.
18. Cusano, D., CdTe solar cells and photovoltaic heterojunctions in II–VI compounds. *Solid-State Electron.* **1963,** *6* (3), 217-232.
19. Carlson, D. E.; Wronski, C. R., Amorphous silicon solar cell. *Appl. Phys. Lett.* **1976,** *28* (11), 671-673.
20. Dimmler, B.; Schock, H., Scaling-up of CIS technology for thin-film solar modules. *Progress in Photovoltaics: Research and Applications* **1996,** *4* (6), 425-433.

21. Green, M. A.; Basore, P.; Chang, N.; Clugston, D.; Egan, R.; Evans, R.; Hogg, D.; Jarnason, S.; Keevers, M.; Lasswell, P., Crystalline silicon on glass (CSG) thin-film solar cell modules. *Solar energy* **2004,** *77* (6), 857-863.

22. Goetzberger, A.; Hebling, C.; Schock, H.-W., Photovoltaic materials, history, status and outlook. *Mater Sci Eng R Rep.* **2003,** *40* (1), 1-46.

23. Green, M., Recent developments in photovoltaics. *Solar energy* **2004,** *76* (1), 3-8.

24. Green, M. A., *Third generation photovoltaics*. Springer: 2006.

25. Conibeer, G.; Green, M.; Corkish, R.; Cho, Y.; Cho, E.-C.; Jiang, C.-W.; Fangsuwannarak, T.; Pink, E.; Huang, Y.; Puzzer, T., Silicon nanostructures for third generation photovoltaic solar cells. *Thin Solid Films* **2006,** *511*, 654-662.

26. Tulloch, G. E., Light and energy—dye solar cells for the 21st century. *J. Photochem. Photobiol., A* **2004,** *164* (1), 209-219.

27. Caramori, S.; Cristino, V.; Boaretto, R.; Argazzi, R.; Bignozzi, C. A.; Di Carlo, A., New components for dye-sensitized solar cells. *Int. J. Photoenergy.* **2010,** *2010*.

28. Grätzel, M., Solar energy conversion by dye-sensitized photovoltaic cells. *Inorg. Chem.* **2005,** *44* (20), 6841-6851.

29. O'regan, B.; Grätzel, M., A low-cost, high-efficiency solar cell based on dye-sensitized colloidal TiO 2 films. *Nature* **1991,** *353* (6346), 737-740.

30. Green, M. A.; Emery, K.; Hishikawa, Y.; Warta, W.; Dunlop, E. D., Solar cell efficiency tables (Version 45). *Progress in photovoltaics: research and applications* **2015,** *23* (1), 1-9.

31. Listorti, A.; O'Regan, B.; Durrant, J. R., Electron transfer dynamics in dye-sensitized solar cells. *Chem. Mater.* **2011,** *23* (15), 3381-3399.

32. O'Regan, B. C.; Durrant, J. R., Kinetic and energetic paradigms for dye-sensitized solar cells: moving from the ideal to the real. *Acc. Chem. Res.* **2009,** *42* (11), 1799-1808.

33. Hagfeldt, A.; Boschloo, G.; Lindström, H.; Figgemeier, E.; Holmberg, A.; Aranyos, V.; Magnusson, E.; Malmqvist, L., A system approach to molecular solar cells. *Coord. Chem. Rev.* **2004,** *248* (13), 1501-1509.

34. Anderson, N. A.; Lian, T., Ultrafast electron transfer at the molecule-semiconductor nanoparticle interface. *Annu. Rev. Phys. Chem.* **2005,** *56*, 491-519.

35. Anderson, N. A.; Lian, T., Ultrafast electron injection from metal polypyridyl complexes to metal-oxide nanocrystalline thin films. *Coord. Chem. Rev.* **2004,** *248* (13), 1231-1246.

36. Durrant, J. R.; Haque, S. A.; Palomares, E., Photochemical energy conversion: from molecular dyads to solar cells. *Chem. Commun.* **2006,** (31), 3279-3289.

37. Kallioinen, J.; Benkö, G.; Sundström, V.; Korppi-Tommola, J. E.; Yartsev, A. P., Electron transfer from the singlet and triplet excited states of Ru (dcbpy) 2 (NCS) 2 into nanocrystalline TiO2 thin films. *J. Phys. Chem. B* **2002,** *106* (17), 4396-4404.

38. Asbury, J. B.; Anderson, N. A.; Hao, E.; Ai, X.; Lian, T., Parameters affecting electron injection dynamics from ruthenium dyes to titanium dioxide nanocrystalline thin film. *J. Phys. Chem. B* **2003,** *107* (30), 7376-7386.

39. Kelly, C. A.; Farzad, F.; Thompson, D. W.; Stipkala, J. M.; Meyer, G. J., Cation-controlled interfacial charge injection in sensitized nanocrystalline TiO2. *Langmuir* **1999,** *15* (20), 7047-7054.

40. Tachibana, Y.; Nazeeruddin, M. K.; Grätzel, M.; Klug, D. R.; Durrant, J. R., Electron injection kinetics for the nanocrystalline TiO 2 films sensitised with the dye (Bu 4 N) 2 Ru (dcbpyH) 2 (NCS) 2. *Chem. Phys.* **2002,** *285* (1), 127-132.

41. Montanari, I.; Nelson, J.; Durrant, J. R., Iodide electron transfer kinetics in dye-sensitized nanocrystalline TiO2 films. *J. Phys. Chem. B* **2002,** *106* (47), 12203-12210.

42. Bisquert, J.; Mora-Seró, I., Simulation of steady-state characteristics of dye-sensitized solar cells and the interpretation of the diffusion length. *J. Phys. Chem. Lett.* **2009,** *1* (1), 450-456.

43. Solbrand, A.; Lindström, H.; Rensmo, H.; Hagfeldt, A.; Lindquist, S.-E.; Södergren, S., Electron transport in the nanostructured TiO2− electrolyte system studied with time-resolved photocurrents. *J. Phys. Chem. B* **1997,** *101* (14), 2514-2518.

44. Anderson, A. Y.; Barnes, P. R.; Durrant, J. R.; O'Regan, B. C., Quantifying regeneration in dye-sensitized solar cells. *J. Phys. Chem. C* **2011,** *115* (5), 2439-2447.

45. Onicha, A. C.; Castellano, F. N., Electrolyte-Dependent Photovoltaic Responses in Dye-Sensitized Solar Cells Based on an Osmium (II) Dye of Mixed Denticity. *J. Phys. Chem. C* **2010,** *114* (14), 6831-6840.

46. Upadhyaya, H. M.; Hirata, N.; Haque, S. A.; de Paoli, M.-A.; Durrant, J. R., Kinetic competition in flexible dye sensitised solar cells employing a series of polymer electrolytes. *Chem. Commun.* **2006,** (8), 877-879.

47. Pelet, S.; Moser, J.-E.; Grätzel, M., Cooperative effect of adsorbed cations and iodide on the interception of back electron transfer in the dye sensitization of nanocrystalline TiO2. *J. Phys. Chem. B* **2000,** *104* (8), 1791-1795.

48. Kroeze, J. E.; Hirata, N.; Koops, S.; Nazeeruddin, M. K.; Schmidt-Mende, L.; Grätzel, M.; Durrant, J. R., Alkyl chain barriers for kinetic optimization in dye-sensitized solar cells. *J. Am. Chem. Soc.* **2006,** *128* (50), 16376-16383.

49. Alebbi, M.; Bignozzi, C. A.; Heimer, T. A.; Hasselmann, G. M.; Meyer, G. J., The limiting role of iodide oxidation in cis-Os (dcb) 2 (CN) 2/TiO2 photoelectrochemical cells. *J. Phys. Chem. B* **1998,** *102* (39), 7577-7581.

50. Tatay, S.; Haque, S. A.; O'Regan, B.; Durrant, J. R.; Verhees, W.; Kroon, J.; Vidal-Ferran, A.; Gaviña, P.; Palomares, E., Kinetic competition in liquid electrolyte and solid-state cyanine dye sensitized solar cells. *J. Mater. Chem.* **2007,** *17* (29), 3037-3044.

51. Kuciauskas, D.; Freund, M. S.; Gray, H. B.; Winkler, J. R.; Lewis, N. S., Electron transfer dynamics in nanocrystalline titanium dioxide solar cells sensitized with ruthenium or osmium polypyridyl complexes. *J. Phys. Chem. B* **2001,** *105* (2), 392-403.

52. O'Regan, B.; Moser, J.; Anderson, M.; Graetzel, M., Vectorial electron injection into transparent semiconductor membranes and electric field effects on the dynamics of light-induced charge separation. *J. Phys. Chem.* **1990,** *94* (24), 8720-8726.

53. Kopidakis, N.; Schiff, E.; Park, N.-G.; Van de Lagemaat, J.; Frank, A., Ambipolar diffusion of photocarriers in electrolyte-filled, nanoporous TiO2. *J. Phys. Chem. B* **2000,** *104* (16), 3930-3936.

54. Cao, F.; Oskam, G.; Meyer, G. J.; Searson, P. C., Electron transport in porous nanocrystalline TiO2 photoelectrochemical cells. *J. Phys. Chem.* **1996,** *100* (42), 17021-17027.

55. Kopidakis, N.; Neale, N.; Zhu, K.; Van De Lagemaat, J.; Frank, A., Spatial location of transport-limiting traps in Ti O 2 nanoparticle films in dye-sensitized solar cells. *Appl. Phys. Lett.* **2005,** *87* (20), 202106.

56. Zhu, K.; Kopidakis, N.; Neale, N. R.; van de Lagemaat, J.; Frank, A. J., Influence of surface area on charge transport and recombination in dye-sensitized TiO2 solar cells. *J. Phys. Chem. B* **2006,** *110* (50), 25174-25180.

57. Kopidakis, N.; Benkstein, K. D.; van de Lagemaat, J.; Frank, A. J., Transport-limited recombination of photocarriers in dye-sensitized nanocrystalline TiO2 solar cells. *J. Phys. Chem. B* **2003,** *107* (41), 11307-11315.

58. Papageorgiou, N.; Maier, W.; Grätzel, M., An iodine/triiodide reduction electrocatalyst for aqueous and organic media. *J. Electrochem. Soc.* **1997,** *144* (3), 876-884.

59. Lan, J.-L.; Wang, Y.-Y.; Wan, C.-C.; Wei, T.-C.; Feng, H.-P.; Peng, C.; Cheng, H.-P.; Chang, Y.-H.; Hsu, W.-C., The simple and easy way to manufacture counter electrode for dye-sensitized solar cells. *Curr. Appl. Phys.* **2010,** *10* (2), S168-S171.

60. Mukherjee, S.; Ramalingam, B.; Griggs, L.; Hamm, S.; Baker, G. A.; Fraundorf, P.; Sengupta, S.; Gangopadhyay, S., Ultrafine sputter-deposited Pt nanoparticles for triiodide reduction in dye-sensitized solar cells: impact of nanoparticle size, crystallinity and surface coverage on catalytic activity. *Nanotechnology* **2012,** *23* (48), 485405.

61. Barzykin, A.; Tachiya, M., Mechanism of charge recombination in dye-sensitized nanocrystalline semiconductors: random flight model. *J. Phys. Chem. B* **2002,** *106* (17), 4356-4363.

62. Haque, S. A.; Tachibana, Y.; Willis, R. L.; Moser, J. E.; Grätzel, M.; Klug, D. R.; Durrant, J. R., Parameters influencing charge recombination kinetics in dye-sensitized nanocrystalline titanium dioxide films. *J. Phys. Chem. B* **2000,** *104* (3), 538-547.

63. Katoh, R.; Furube, A.; Barzykin, A. V.; Arakawa, H.; Tachiya, M., Kinetics and mechanism of electron injection and charge recombination in dye-sensitized nanocrystalline semiconductors. *Coord. Chem. Rev.* **2004,** *248* (13), 1195-1213.

64. Haque, S. A.; Tachibana, Y.; Klug, D. R.; Durrant, J. R., Charge recombination kinetics in dye-sensitized nanocrystalline titanium dioxide films under externally applied bias. *J. Phys. Chem. B* **1998,** *102* (10), 1745-1749.

65. Ardo, S.; Meyer, G. J., Photodriven heterogeneous charge transfer with transition-metal compounds anchored to TiO 2 semiconductor surfaces. *Chem. Soc. Rev.* **2009,** *38* (1), 115-164.

66. Clifford, J. N.; Palomares, E.; Nazeeruddin, M. K.; Grätzel, M.; Nelson, J.; Li, X.; Long, N. J.; Durrant, J. R., Molecular control of recombination dynamics in dye-sensitized nanocrystalline TiO2 films: Free energy vs distance dependence. *J. Am. Chem. Soc.* **2004,** *126* (16), 5225-5233.

67. Schlichthörl, G.; Huang, S.; Sprague, J.; Frank, A., Band edge movement and recombination kinetics in dye-sensitized nanocrystalline TiO2 solar cells: a study by intensity modulated photovoltage spectroscopy. *J. Phys. Chem. B* **1997,** *101* (41), 8141-8155.

68. Cameron, P. J.; Peter, L. M.; Hore, S., How important is the back reaction of electrons via the substrate in dye-sensitized nanocrystalline solar cells? *J. Phys. Chem. B* **2005,** *109* (2), 930-936.

69. Huang, S.; Schlichthörl, G.; Nozik, A.; Grätzel, M.; Frank, A., Charge recombination in dye-sensitized nanocrystalline TiO2 solar cells. *J. Phys. Chem. B* **1997,** *101* (14), 2576-2582.

70. Liu, Y.; Hagfeldt, A.; Xiao, X.-R.; Lindquist, S.-E., Investigation of influence of redox species on the interfacial energetics of a dye-sensitized nanoporous TiO 2 solar cell. *Sol. Energy Mater Sol. Cells* **1998,** *55* (3), 267-281.

71. Boschloo, G.; Häggman, L.; Hagfeldt, A., Quantification of the effect of 4-tert-butylpyridine addition to I-/I3-redox electrolytes in dye-sensitized nanostructured TiO2 solar cells. *J. Phys. Chem. B* **2006,** *110* (26), 13144-13150.

72. Nakade, S.; Kanzaki, T.; Kubo, W.; Kitamura, T.; Wada, Y.; Yanagida, S., Role of electrolytes on charge recombination in dye-sensitized tio2 solar cell (1): the case of solar cells using the I-/I3-redox couple. *J. Phys. Chem. B* **2005,** *109* (8), 3480-3487.

73. Zhang, Z.; Evans, N.; Zakeeruddin, S. M.; Humphry-Baker, R.; Grätzel, M., Effects of ω-guanidinoalkyl acids as coadsorbents in dye-sensitized solar cells. *J. Phys. Chem. C* **2007,** *111* (1), 398-403.

74. Mori, S. N.; Kubo, W.; Kanzaki, T.; Masaki, N.; Wada, Y.; Yanagida, S., Investigation of the effect of alkyl chain length on charge transfer at TiO2/dye/electrolyte interface. *J. Phys. Chem. C* **2007,** *111* (8), 3522-3527.

75. O'Regan, B. C.; López-Duarte, I.; Martínez-Díaz, M. V.; Forneli, A.; Albero, J.; Morandeira, A.; Palomares, E.; Torres, T.; Durrant, J. R., Catalysis of recombination and its limitation on open circuit voltage for dye sensitized photovoltaic cells using phthalocyanine dyes. *J. Am. Chem. Soc.* **2008,** *130* (10), 2906-2907.

76. Kalyanasundaram, K., *Dye-sensitized solar cells*. EPFL press: 2010.

77. Gonçalves, L. M.; de Zea Bermudez, V.; Ribeiro, H. A.; Mendes, A. M., Dye-sensitized solar cells: A safe bet for the future. *Energy Environ. Sci.* **2008,** *1* (6), 655-667.

78. Grätzel, M., Recent advances in sensitized mesoscopic solar cells. *Acc. Chem. Res.* **2009,** *42* (11), 1788-1798.

79. Wu, J.; Lan, Z.; Hao, S.; Li, P.; Lin, J.; Huang, M.; Fang, L.; Huang, Y., Progress on the electrolytes for dye-sensitized solar cells. *Pure Appl. Chem.* **2008,** *80* (11), 2241-2258.

80. Privalov, T.; Boschloo, G.; Hagfeldt, A.; Svensson, P. H.; Kloo, L., A study of the interactions between I−/I3− redox mediators and organometallic sensitizing dyes in solar cells. *J. Phys. Chem. C* **2008,** *113* (2), 783-790.

81. Ferber, J.; Stangl, R.; Luther, J., An electrical model of the dye-sensitized solar cell. *Sol. Energy Mater Sol. Cells* **1998,** *53* (1), 29-54.

82. Schiffmann, F.; VandeVondele, J.; Hutter, J.; Urakawa, A.; Wirz, R.; Baiker, A., An atomistic picture of the regeneration process in dye sensitized solar cells. *Proc. Natl. Acad. Sci.* **2010,** *107* (11), 4830-4833.

83. Yu, Z.; Vlachopoulos, N.; Gorlov, M.; Kloo, L., Liquid electrolytes for dye-sensitized solar cells. *Dalton Trans.* **2011,** *40* (40), 10289-10303.

84. Snaith, H. J.; Schmidt-Mende, L., Advances in liquid-electrolyte and solid-state dye-sensitized solar cells. *Adv. Mater.* **2007,** *19* (20), 3187-3200.

85. Wu, J.; Lan, Z.; Lin, J.; Huang, M.; Li, P., Effect of solvents in liquid electrolyte on the photovoltaic performance of dye-sensitized solar cells. *J. Power Sources* **2007,** *173* (1), 585-591.

86. Fukui, A.; Komiya, R.; Yamanaka, R.; Islam, A.; Han, L., Effect of a redox electrolyte in mixed solvents on the photovoltaic performance of a dye-sensitized solar cell. *Sol. Energy Mater Sol. Cells* **2006,** *90* (5), 649-658.

87. Wang, M.; Grätzel, C.; Zakeeruddin, S. M.; Grätzel, M., Recent developments in redox electrolytes for dye-sensitized solar cells. *Energy Environ. Sci.* **2012,** *5* (11), 9394-9405.

88. Lee, K.-M.; Suryanarayanan, V.; Ho, K.-C., Influences of different TiO 2 morphologies and solvents on the photovoltaic performance of dye-sensitized solar cells. *J. Power Sources* **2009,** *188* (2), 635-641.

89. Gorlov, M.; Kloo, L., Ionic liquid electrolytes for dye-sensitized solar cells. *Dalton Trans.* **2008,** (20), 2655-2666.

90. Kawano, R.; Matsui, H.; Matsuyama, C.; Sato, A.; Susan, M. A. B. H.; Tanabe, N.; Watanabe, M., High performance dye-sensitized solar cells using ionic liquids as their electrolytes. *J. Photochem. Photobiol., A* **2004,** *164* (1), 87-92.

91. Fredin, K.; Gorlov, M.; Pettersson, H.; Hagfeldt, A.; Kloo, L.; Boschloo, G., On the influence of anions in binary ionic liquid electrolytes for monolithic dye-sensitized solar cells. *J. Phys. Chem. C* **2007,** *111* (35), 13261-13266.

92. Son, K. M.; Kang, M. G.; Vittal, R.; Lee, J.; Kim, K.-J., Effects of substituents of imidazolium cations on the performance of dye-sensitized TiO2 solar cells. *J. Appl. Electrochem.* **2008,** *38* (12), 1647-1652.

93. Wachter, P.; Zistler, M.; Schreiner, C.; Berginc, M.; Krašovec, U. O.; Gerhard, D.; Wasserscheid, P.; Hinsch, A.; Gores, H. J., Characterisation of DSSC-electrolytes based on 1-ethyl-3-methylimidazolium dicyanamide: Measurement of triiodide diffusion coefficient, viscosity, and photovoltaic performance. *J. Photochem. Photobiol., A* **2008,** *197* (1), 25-33.

94. Wang, P.; Wenger, B.; Humphry-Baker, R.; Moser, J.-E.; Teuscher, J.; Kantlehner, W.; Mezger, J.; Stoyanov, E. V.; Zakeeruddin, S. M.; Grätzel, M., Charge separation and efficient light energy conversion in sensitized mesoscopic solar cells based on binary ionic liquids. *J. Am. Chem. Soc.* **2005,** *127* (18), 6850-6856.

95. Ejigu, A.; Lovelock, K. R.; Licence, P.; Walsh, D. A., Iodide/triiodide electrochemistry in ionic liquids: Effect of viscosity on mass transport, voltammetry and scanning electrochemical microscopy. *Electrochimica Acta* **2011,** *56* (28), 10313-10320.

96. Rogers, R. D.; Seddon, K. R., Ionic liquids--solvents of the future? *Science* **2003,** *302* (5646), 792-793.

97. Hamann, T. W.; Ondersma, J. W., Dye-sensitized solar cell redox shuttles. *Energy Environ. Sci.* **2011,** *4* (2), 370-381.

98. Boschloo, G.; Hagfeldt, A., Characteristics of the iodide/triiodide redox mediator in dye-sensitized solar cells. *Acc. Chem. Res.* **2009,** *42* (11), 1819-1826.

99. Datta, J.; Bhattacharya, A.; Kundu, K. K., Relative Standard Electrode Potentials of I3−/I−, I2/I3−, and I2/I− Redox Couples and the Related Formation Constants of I3− in Some Pure and Mixed Dipolar Aprotic Solvents. *Bull. Chem. Soc. Jpn.* **1988,** *61* (5), 1735-1742.

100. Kawano, R.; Watanabe, M., Equilibrium potentials and charge transport of an I−/I 3− redox couple in an ionic liquid. *Chem. Commun.* **2003,** (3), 330-331.

101. Daeneke, T.; Mozer, A. J.; Uemura, Y.; Makuta, S.; Fekete, M.; Tachibana, Y.; Koumura, N.; Bach, U.; Spiccia, L., Dye regeneration kinetics in dye-sensitized solar cells. *J. Am. Chem. Soc.* **2012,** *134* (41), 16925-16928.

102. Papageorgiou, N.; Grätzel, M.; Infelta, P., On the relevance of mass transport in thin layer nanocrystalline photoelectrochemical solar cells. *Sol. Energy Mater Sol. Cells* **1996,** *44* (4), 405-438.

103. Yu, Q.; Wang, Y.; Yi, Z.; Zu, N.; Zhang, J.; Zhang, M.; Wang, P., High-efficiency dye-sensitized solar cells: the influence of lithium ions on exciton dissociation, charge recombination, and surface states. *ACS nano* **2010,** *4* (10), 6032-6038.

104. Frank, A. J.; Kopidakis, N.; van de Lagemaat, J., Electrons in nanostructured TiO 2 solar cells: transport, recombination and photovoltaic properties. *Coord. Chem. Rev.* **2004,** *248* (13), 1165-1179.

105. Wang, H.; Bell, J.; Desilvestro, J.; Bertoz, M.; Evans, G., Effect of inorganic iodides on performance of dye-sensitized solar cells. *J. Phys. Chem. C* **2007,** *111* (41), 15125-15131.

106. Cong, J.; Yang, X.; Kloo, L.; Sun, L., Iodine/iodide-free redox shuttles for liquid electrolyte-based dye-sensitized solar cells. *Energy Environ. Sci.* **2012,** *5* (11), 9180-9194.

107. Tian, H.; Sun, L., Iodine-free redox couples for dye-sensitized solar cells. *J. Mater. Chem.* **2011,** *21* (29), 10592-10601.

108. Yella, A.; Lee, H.-W.; Tsao, H. N.; Yi, C.; Chandiran, A. K.; Nazeeruddin, M. K.; Diau, E. W.-G.; Yeh, C.-Y.; Zakeeruddin, S. M.; Grätzel, M., Porphyrin-sensitized solar cells with cobalt (II/III)–based redox electrolyte exceed 12 percent efficiency. *science* **2011,** *334* (6056), 629-634.

109. Nelson, J. J.; Amick, T. J.; Elliott, C. M., Mass transport of polypyridyl cobalt complexes in dye-sensitized solar cells with mesoporous TiO2 photoanodes. *J. Phys. Chem. C* **2008,** *112* (46), 18255-18263.

110. Cameron, P. J.; Peter, L. M.; Zakeeruddin, S. M.; Grätzel, M., Electrochemical studies of the Co (III)/Co (II)(dbbip) 2 redox couple as a mediator for dye-sensitized nanocrystalline solar cells. *Coord. Chem. Rev.* **2004,** *248* (13), 1447-1453.

111. Yum, J.-H.; Baranoff, E.; Kessler, F.; Moehl, T.; Ahmad, S.; Bessho, T.; Marchioro, A.; Ghadiri, E.; Moser, J.-E.; Yi, C., A cobalt complex redox shuttle for dye-sensitized solar cells with high open-circuit potentials. *Nat. Commun.* **2012,** *3*, 631.

112. Mathew, S.; Yella, A.; Gao, P.; Humphry-Baker, R.; Curchod, B. F.; Ashari-Astani, N.; Tavernelli, I.; Rothlisberger, U.; Nazeeruddin, M. K.; Grätzel, M., Dye-sensitized solar cells with 13% efficiency achieved through the molecular engineering of porphyrin sensitizers. *Nat. Chem.* **2014,** *6* (3), 242-247.

113. Song, H.; Liu, Q.; Xie, Y., Porphyrin-sensitized solar cells: systematic molecular optimization, coadsorption and cosensitization. *Chem. Commun.* **2018.**

114. Wang, M.; Chamberland, N.; Breau, L.; Moser, J.-E.; Humphry-Baker, R.; Marsan, B.; Zakeeruddin, S. M.; Grätzel, M., An organic redox electrolyte to rival triiodide/iodide in dye-sensitized solar cells. *Nat. Chem.* **2010,** *2* (5), 385-389.

115. Burschka, J.; Brault, V.; Ahmad, S.; Breau, L.; Nazeeruddin, M. K.; Marsan, B.; Zakeeruddin, S. M.; Grätzel, M., Influence of the counter electrode on the photovoltaic performance of dye-sensitized solar cells using a disulfide/thiolate redox electrolyte. *Energy Environ. Sci.* **2012,** *5* (3), 6089-6097.

116. Bai, Y.; Yu, Q.; Cai, N.; Wang, Y.; Zhang, M.; Wang, P., High-efficiency organic dye-sensitized mesoscopic solar cells with a copper redox shuttle. *Chem. Commun.* **2011,** *47* (15), 4376-4378.

117. Kambe, S.; Nakade, S.; Kitamura, T.; Wada, Y.; Yanagida, S., Influence of the electrolytes on electron transport in mesoporous TiO2− electrolyte systems. *J. Phys. Chem. B* **2002,** *106* (11), 2967-2972.

118. Nazeeruddin, M. K.; Kay, A.; Rodicio, I.; Humphry-Baker, R.; Müller, E.; Liska, P.; Vlachopoulos, N.; Grätzel, M., Conversion of light to electricity by cis-X2bis (2, 2'-bipyridyl-4, 4'-dicarboxylate) ruthenium (II) charge-transfer sensitizers (X= Cl-, Br-, I-, CN-, and SCN-) on nanocrystalline titanium dioxide electrodes. *J. Am. Chem. Soc.* **1993,** *115* (14), 6382-6390.

119. Bella, F.; Sacco, A.; Pugliese, D.; Laurenti, M.; Bianco, S., Additives and salts for dye-sensitized solar cells electrolytes: what is the best choice? *J. Power Sources* **2014,** *264*, 333-343.

120. Kusama, H.; Arakawa, H., Influence of benzimidazole additives in electrolytic solution on dye-sensitized solar cell performance. *J. Photochem. Photobiol., A* **2004,** *162* (2), 441-448.

121. Kusama, H.; Arakawa, H., Influence of alkylaminopyridine additives in electrolytes on dye-sensitized solar cell performance. *Sol. Energy Mater Sol. Cells* **2004,** *81* (1), 87-99.

122. Kusama, H.; Konishi, Y.; Sugihara, H.; Arakawa, H., Influence of alkylpyridine additives in electrolyte solution on the performance of dye-sensitized solar cell. *Sol. Energy Mater Sol. Cells* **2003,** *80* (2), 167-179.

123. Shi, C.; Dai, S.; Wang, K.; Pan, X.; Kong, F.; Hu, L., The adsorption of 4-tert-butylpyridine on the nanocrystalline TiO 2 and Raman spectra of dye-sensitized solar cells in situ. *Vib. Spectro.* **2005,** *39* (1), 99-105.

124. Watson, D. F.; Meyer, G. J., Cation effects in nanocrystalline solar cells. *Coord. Chem. Rev.* **2004,** *248* (13), 1391-1406.

125. Zhang, C.; Huang, Y.; Huo, Z.; Chen, S.; Dai, S., Photoelectrochemical effects of guanidinium thiocyanate on dye-sensitized solar cell performance and stability. *J. Phys. Chem. C* **2009,** *113* (52), 21779-21783.

126. Kopidakis, N.; Neale, N. R.; Frank, A. J., Effect of an adsorbent on recombination and band-edge movement in dye-sensitized TiO2 solar cells: evidence for surface passivation. *J. Phys. Chem. B* **2006,** *110* (25), 12485-12489.

127. Haque, S. A.; Palomares, E.; Cho, B. M.; Green, A. N.; Hirata, N.; Klug, D. R.; Durrant, J. R., Charge separation versus recombination in dye-sensitized nanocrystalline solar cells: the minimization of kinetic redundancy. *J. Am. Chem. Soc.* **2005,** *127* (10), 3456-3462.

128. Koops, S. E.; O'Regan, B. C.; Barnes, P. R.; Durrant, J. R., Parameters influencing the efficiency of electron injection in dye-sensitized solar cells. *J. Am. Chem. Soc.* **2009,** *131* (13), 4808-4818.

129. Clifford, J. N.; Martínez-Ferrero, E.; Viterisi, A.; Palomares, E., Sensitizer molecular structure-device efficiency relationship in dye sensitized solar cells. *Chem. Soc. Rev.* **2011,** *40* (3), 1635-1646.

130. Yen, Y.-S.; Chou, H.-H.; Chen, Y.-C.; Hsu, C.-Y.; Lin, J. T., Recent developments in molecule-based organic materials for dye-sensitized solar cells. *J. Mater. Chem.* **2012,** *22* (18), 8734-8747.

131. Mishra, A.; Fischer, M. K.; Bäuerle, P., Metal-free organic dyes for dye-sensitized solar cells: From structure: Property relationships to design rules. *Angew. Chem. Int. Ed.* **2009,** *48* (14), 2474-2499.

132. Wiberg, J.; Marinado, T.; Hagberg, D. P.; Sun, L.; Hagfeldt, A.; Albinsson, B., Effect of anchoring group on electron injection and recombination dynamics in organic dye-sensitized solar cells. *J. Phys. Chem. C* **2009,** *113* (9), 3881-3886.

133. Haid, S.; Marszalek, M.; Mishra, A.; Wielopolski, M.; Teuscher, J.; Moser, J. E.; Humphry-Baker, R.; Zakeeruddin, S. M.; Grätzel, M.; Bäuerle, P., Significant Improvement of Dye-Sensitized Solar Cell Performance by Small Structural Modification in π-Conjugated Donor–Acceptor Dyes. *Adv. Funct. Mater.* **2012,** *22* (6), 1291-1302.

134. Ooyama, Y.; Shimada, Y.; Kagawa, Y.; Yamada, Y.; Imae, I.; Komaguchi, K.; Harima, Y., Synthesis of new-type donor–acceptor π-conjugated benzofuro [2, 3-c] oxazolo [4, 5-a] carbazole fluorescent dyes and their photovoltaic performances of dye-sensitized solar cells. *Tetrahedron Lett.* **2007,** *48* (52), 9167-9170.

135. Ooyama, Y.; Inoue, S.; Nagano, T.; Kushimoto, K.; Ohshita, J.; Imae, I.; Komaguchi, K.; Harima, Y., Dye-Sensitized Solar Cells Based On Donor–Acceptor π-Conjugated Fluorescent Dyes with a Pyridine Ring as an Electron-Withdrawing Anchoring Group. *Angew. Chem.* **2011,** *123* (32), 7567-7571.

136. Harima, Y.; Fujita, T.; Kano, Y.; Imae, I.; Komaguchi, K.; Ooyama, Y.; Ohshita, J., Lewis-acid sites of TiO2 surface for adsorption of organic dye having pyridyl group as anchoring unit. *J. Phys. Chem. C* **2013,** *117* (32), 16364-16370.

137. Ooyama, Y.; Nagano, T.; Inoue, S.; Imae, I.; Komaguchi, K.; Ohshita, J.; Harima, Y., Dye-Sensitized Solar Cells Based on Donor-π-Acceptor Fluorescent Dyes with a Pyridine Ring as an Electron-Withdrawing-Injecting Anchoring Group. *Chem. Eur. J.* **2011,** *17* (52), 14837-14843.

138. Zhang, M.-D.; Xie, H.-X.; Ju, X.-H.; Qin, L.; Yang, Q.-X.; Zheng, H.-G.; Zhou, X.-F., DD-π-A organic dyes containing 4, 4′-di (2-thienyl) triphenylamine moiety for efficient dye-sensitized solar cells. *Phys. Chem. Chem. Phys.* **2013,** *15* (2), 634-641.

139. Péchy, P.; Rotzinger, F. P.; Nazeeruddin, M. K.; Kohle, O.; Zakeeruddin, S. M.; Humphry-Baker, R.; Grätzel, M., Preparation of phosphonated polypyridyl ligands to anchor transition-metal complexes on oxide surfaces: application for the conversion of light to electricity with nanocrystalline TiO 2 films. *J. Chem. Soc., Chem. Commun.* **1995,** (1), 65-66.

140. Guerrero, G.; Alauzun, J. G.; Granier, M.; Laurencin, D.; Mutin, P. H., Phosphonate coupling molecules for the control of surface/interface properties and the synthesis of nanomaterials. *Dalton Trans.* **2013,** *42* (35), 12569-12585.

141. Zabri, H.; Gillaizeau, I.; Bignozzi, C. A.; Caramori, S.; Charlot, M.-F.; Cano-Boquera, J.; Odobel, F., Synthesis and comprehensive characterizations of new cis-RuL2X2 (X= Cl, CN, and NCS) sensitizers for nanocrystalline tio2 solar cell using bis-phosphonated bipyridine ligands (L). *Inorg. Chem.* **2003,** *42* (21), 6655-6666.

142. Pujari, S. P.; Scheres, L.; Marcelis, A.; Zuilhof, H., Covalent surface modification of oxide surfaces. *Angew. Chem. Int. Ed.* **2014,** *53* (25), 6322-6356.

143. Wang, L.; Yang, X.; Li, S.; Cheng, M.; Sun, L., A new type of organic sensitizers with pyridine-N-oxide as the anchoring group for dye-sensitized solar cells. *RSC Adv.* **2013,** *3* (33), 13677-13680.

144. Zhang, L.; Cole, J. M., Anchoring groups for dye-sensitized solar cells. *ACS Appl. Mater. Interfaces* **2015,** *7* (6), 3427-3455.

145. Shibayama, N.; Ozawa, H.; Ooyama, Y.; Arakawa, H., Highly Efficient Cosensitized Plastic-Substrate Dye-Sensitized Solar Cells with Black Dye and Pyridine-Anchor Organic Dye. *Bull. Chem. Soc. Jpn.* **2014,** *88* (2), 366-374.

146. Shibayama, N.; Ozawa, H.; Abe, M.; Ooyama, Y.; Arakawa, H., A new cosensitization method using the Lewis acid sites of a TiO 2 photoelectrode for dye-sensitized solar cells. *Chem. Commun.* **2014,** *50* (48), 6398-6401.

147. Frisch, M.; Trucks, G.; Schlegel, H.; Scuseria, G.; Robb, M.; Cheeseman, J.; Montgomery Jr, J.; Vreven, T.; Kudin, K.; Burant, J., gaussian 03, Gaussian. *Inc., Pittsburgh, PA* **2003,** *2003*.

148. Cossi, M.; Barone, V., Time-dependent density functional theory for molecules in liquid solutions. *J. Chem. Phys.* **2001,** *115* (10), 4708-4717.

149. Aung, S. H.; Hao, Y.; Oo, T. Z.; Boschloo, G., 2-(4-Butoxyphenyl)-N-hydroxyacetamide: An Efficient Preadsorber for Dye-Sensitized Solar Cells. *ACS Omega* **2017,** *2* (5), 1820-1825.

150. Murakami, T. N.; Koumura, N.; Uchiyama, T.; Uemura, Y.; Obuchi, K.; Masaki, N.; Kimura, M.; Mori, S., Recombination inhibitive structure of organic dyes for cobalt complex redox electrolytes in dye-sensitised solar cells. *J. Mater. Chem. A* **2013,** *1* (3), 792-798.

151. Ellis, H.; Eriksson, S. K.; Feldt, S. M.; Gabrielsson, E.; Lohse, P. W.; Lindblad, R.; Sun, L.; Rensmo, H. k.; Boschloo, G.; Hagfeldt, A., Linker unit modification of triphenylamine-based organic dyes for efficient cobalt mediated dye-sensitized solar cells. *J. Phys. Chem. C* **2013,** *117* (41), 21029-21036.

152. Cao, Y.; Cai, N.; Wang, Y.; Li, R.; Yuan, Y.; Wang, P., Modulating the assembly of organic dye molecules on titania nanocrystals via alkyl chain elongation for efficient mesoscopic cobalt solar cells. *Phys. Chem. Chem. Phys.* **2012,** *14* (23), 8282-8286.